TECHNISCHE UNIVERSITÄT WIEN
Vienna University of Technology

IUPUI

Master Thesis

Effect of anti-resorptive treatments on material properties and damage behavior of individual trabeculae of bone

Andreas Grabos
Mat. Nr.: 1125146

Supervisors at TU-Wien, Institute of Lightweight Design and Structural Biomechanics:

Univ.Prof. Dr. Philipp Thurner

Dipl.-Ing. Martin Frank

Supervisor at IUPUI, Department of Anatomy and Cell Biology:

Dr. Matthew Allen

September 26, 2019, Vienna

Die approbierte gedruckte Originalversion dieser Diplomarbeit ist an der TU Wien Bibliothek verfügbar.
The approved original version of this thesis is available in print at TU Wien Bibliothek.

TU Bibliothek Your knowledge hub WIEN

Affidavit

I declare in lieu of oath, that I wrote this thesis and performed the associated research myself, using only literature cited in this volume.

Vienna, October 2019

Andreas Grabos

Die approbierte gedruckte Originalversion dieser Diplomarbeit ist an der TU Wien Bibliothek verfügbar.
The approved original version of this thesis is available in print at TU Wien Bibliothek.

Acknowledgement

Firstly, I would like to express my sincere gratitude to my supervisors at the TU Wien, Univ.Prof. Dr. Philipp Thurner and Dipl.-Ing. Martin Frank for their continuous support, patience and encouragement.
A special thanks goes to Dipl.-Ing. Martin Frank for providing his Python scripts, which were necessary to assess mechanical data from the tensile tests performed and his support therewith and for everything I have learned from him during this research project.

My sincere thanks also goes to my supervisor at my American host university UIPUI, Dr. Matthew Allen and his coworkers for all their efforts before, during and after my stay. It was fantastic to have the opportunity to work in their facilities.

Furthermore, I want to thank all my supervisors of both universities for their support during my scholarship application that made it possible to do research abroad and learn from experts in a completely new environment that made me grow not only academically but also as a person.

Most importantly, none of this could have happened without my family. I have to express my very profound gratitude to my family for providing me with unfailing support, love and encouragement throughout my years of study and through the process of researching and writing this thesis. This accomplishment would not have been possible without them.

Die approbierte gedruckte Originalversion dieser Diplomarbeit ist an der TU Wien Bibliothek verfügbar.
The approved original version of this thesis is available in print at TU Wien Bibliothek.

Kurzfassung

Das Ziel dieser wissenschaftlichen Arbeit ist die Beantwortung der Frage, ob anti-resorptive Medikamente einen Effekt auf die Materialeigenschaften und das mikroskopische Schädigungsverhalten individueller Knochentrabekel haben. Um dieses Ziel zu erreichen wurde eine Kombination von Materialien und Expertise, verfügbar durch die Laboratorien der gelisteten Betreuer an der TU Wien, Purdue Universität und der Indiana University School of Medicine, genutzt. Individuelle Trabekel wurden aus Wirbelkörpern von Hunden entnommen, denen für 1 Jahr klinisch relevante Dosen von Alendronat (0.2 mg/kg/day) oder Raloxifen (0.5 mg/kg/day) oral verabreicht wurden. Diese Proben wurden aufgrund von Daten früherer Studien verwendet, die nahelegen, dass Raloxifen auf Gewebeebene fundamental unterschiedliche Effekte im Vergleich zu Alendronat hervorruft. Zusätzlich wurden individuelle Trabekel von Wirbelkörpern unbehandelter Hunde als Kontrollgruppe verwendet.

Materialeigenschaften wurden durch weggesteuerte Zugversuche ermittelt wobei die Dehnungsmessung optisch erfolgte. Deformationen der Tabekel wurde durch Digital Image Correlation (DIC) ermittelt und Spannungs-Dehnungsdiagramme mit Hilfe von Python Skripten erstellt. Mikroschaden wurde sowohl durch histologische Mikroskopie in Kombination mit dem Färbemittel Fuchsin als auch durch Mikro-CT unter Nutzung des Kontrastmittels Barium Sulfat untersucht. Die Ergebnisse zeigen eine Erhöhung der Festigkeit und des Zugmoduls für Trabekel von Raloxifen und Alendronat behandelten Proben. Es wurden keine signifikanten Unterschiede in der Akkumulation von Mikroschaden festgestellt. Raloxifen veränderte die Materialeigenschaften relativ unabhängig von der Knochenmineraldichte. Im Gegensatz hierzu wies Alendronat eine deutliche Abhängigkeit auf, was darauf hindeutet, dass diese Medikamente die Knochenmatrix auf eine unterschiedliche Weise verändern.

Die approbierte gedruckte Originalversion dieser Diplomarbeit ist an der TU Wien Bibliothek verfügbar.
The approved original version of this thesis is available in print at TU Wien Bibliothek.
TU Bibliothek Your knowledge hub WIEN

Abstract

The goal of this research project was to determine whether anti-resorptive treatments have an effect on material properties and microscopic damage behavior of individual bone trabeculae. To achieve this goal, a combination of materials and expertise available through the laboratories of the listed supervisors at TU-Wien, Purdue University and the Indiana University School of Medicine, were used.

Individual trabeculae were harvested from vertebrae of dogs treated orally for 12 months with clinically relevant doses of alendronate (0.2 mg/kg/day) or raloxifene (0.5 mg/kg/day). These samples were investigated as previous data suggested that raloxifene may produce fundamentally different effects at the tissue level compared to bisphosphonates. Additionally, individual trabeculae from vertebrae of dogs without any treatment were used as a control group. Material properties were determined by camera recorded displacement-controlled tensile tests. Deformations of the trabeculae were measured by digital image correlation (DIC), and stress-strain-curves were created using Python scripts. Microdamage was then investigated using histological microscopy as well as micro-CT scans in combination with basic fuchsin staining and the contrast agent barium sulfate respectively.

Results showed an overall increase of maximum stress and Young's modulus for both, raloxifene and alendronate-treated specimens. No significant difference in microdamage accumulation was found between the groups. Raloxifene changed the material properties, which indicates a reduction of the fracture risk, relatively independent of bone mineral density. This is contrasted by alendronate, which showed a higher dependency thereof, and thus these treatments are suspected to alter the bone matrix in a fundamentally different way.

Die approbierte gedruckte Originalversion dieser Diplomarbeit ist an der TU Wien Bibliothek verfügbar.
The approved original version of this thesis is available in print at TU Wien Bibliothek.
TU Bibliothek Your knowledge hub WIEN

Contents

1 Introduction **1**

1.1 Motivation 1

1.2 Research Problem 2

1.3 Thesis Structure 3

2 Biological and Pharmaceutical Background **5**

2.1 Bone Tissue 5

2.2 Cancellous Bone versus Cortical Bone 7

2.3 Bone Quality and Bone mineral density 10

2.4 Microdamage 12

2.5 Modeling and Remodeling 15

2.6 Osteoporosis 19

2.7 Pharmaceutical Treatments for Osteoporosis 21

3 Methodological Background **23**

3.1 Mechanical testing of Bone 23

3.2 Assessment of Microdamage 25

3.2.1 Microcrack Staining 26

3.2.2 Confocal Laser Scanning Microscopy (CLSM) 27

3.2.3 Micro-computed Tomography (micro-CT) 29

4 Materials and Methods **30**

4.1 Materials 30

4.2 Sample Preparation 31

4.2.1 Sectioning of Vertebrae 31

4.2.2 Excising of Single Trabeculae 33

4.2.3 Micro-CT-Imaging and Measurement of Trabeculae 35

4.2.4 Embedding of Trabeculae 36

4.2.5 Application of the Speckle Pattern 39

Die approbierte gedruckte Originalversion dieser Diplomarbeit ist an der TU Wien Bibliothek verfügbar.
The approved original version of this thesis is available in print at TU Wien Bibliothek.
TU Bibliothek Your knowledge hub WIEN

4.3 Mechanical Testing of Individual Trabeculae 40
4.3.1 Setup 40
4.3.2 Stop Criterion 43
4.3.3 Test Procedure 44
4.4 Analysis of Mechanical Test-Data 47
4.4.1 Strain Determination 47
4.4.2 Stress Determination 49
4.4.3 Material Properties Determination 49
4.5 Labeling of microscopic damage 51
4.5.1 Basic Fuchsin 51
4.5.2 Barium Sulfate 53
4.6 Micro-CT-Imaging 56
4.7 CLSM Imaging 56
4.7.1 Sample Preparation and Setup 57
4.7.2 CLSM Procedure 58
4.8 Analysis of CLSM Image-Data 59
4.9 Statistical Analysis 61

5 Results **62**
5.1 Material Properties 63
5.2 Microdamage 78
5.2.1 CLSM 78
5.2.2 Micro-CT 83

6 Discussion **84**
6.1 Materials 84
6.2 Methods 85
6.3 Results 88

7 Conclusion and Outlook **97**

Die approbierte gedruckte Originalversion dieser Diplomarbeit ist an der TU Wien Bibliothek verfügbar.
The approved original version of this thesis is available in print at TU Wien Bibliothek.
TU Bibliothek Your knowledge hub WIEN

8 Appendix **99**

8.1 3D Registration for Barium Staining Protocol: 99

8.2 CTAn Threshold Protocol 100

8.3 Skyscan micrsoCT Settings 101

8.4 NRecon Reconstruction Settings 103

References **113**

Die approbierte gedruckte Originalversion dieser Diplomarbeit ist an der TU Wien Bibliothek verfügbar.
The approved original version of this thesis is available in print at TU Wien Bibliothek.

1 Introduction

1.1 Motivation

Fractures linked to osteoporosis constitute a major concern in an aging population. Current clinical practice relies on areal bone mineral density (aBMD, i.e. bone quantity) as an indicator of fracture risk, yet it is becoming increasingly clear that aBMD has poor predictive ability on an individual basis. It has been demonstrated that not only bone quantity, which consists of density and size, but also bone quality (summarizing bone microarchitecture, microdamage accumulation, hydration, collagen quality and other tissue properties) has significant effects on bone fracture and failure. Nevertheless, the most abundant and used therapeutic agents for treating osteoporosis to prevent new or additional fractures in an individual, are still based solely on the paradigm that aBMD is the measuring stick that should be used to assess efficacy of reducing fracture risk. These medications are almost all of anti-resorptive character, i.e. they impede the action of osteoclast cells, which are in charge of resorbing bone. In principle, this therapy is effective, nevertheless adverse effects such as atypical femoral fractures and osteonecrosis of the jaw have been encountered. [8] Consequently, many patients who could benefit from this therapy refuse these treatments. Even if such adverse effects are rare, they warrant a deeper investigation of the effects of anti-resorptive treatments on bone tissue beyond the intended effect of impeding osteoclast activity.

In this context, this project is focused on the questions of how anti-resorptives influence the mechanical properties of trabecular bone at the tissue and material level, and how this is linked to damage formation.

Die approbierte gedruckte Originalversion dieser Diplomarbeit ist an der TU Wien Bibliothek verfügbar.
The approved original version of this thesis is available in print at TU Wien Bibliothek.
TU Bibliothek Your knowledge hub WIEN

1.2 Research Problem

The average global socio-economic financial burden for treatment of osteoporosis-related fractures is projected to reach 100 Billion US$ by mid-century. The International Osteoporosis Foundation estimates that osteoporotic fractures occur worldwide every 3 seconds, which sums up to almost 25000 fractures per day or 9 million per year. [31] These are, among others, comprised of an estimated 1.6 million hip, 1.7 million forearm and 1.4 million clinical (symptomatic) vertebral fractures, which are the most common osteoporoitic fractures. [14] It is predicted that the number of yearly fractures worldwide will significantly rise within the next 50 years. [11] Gullberg B et al. even stated, that by 2050, the worldwide incidence of hip fracture in men is projected to increase by 310% and 240% in women, compared to rates in 1990. [28] Furthermore, the combined annual costs of all osteoporotic fractures have been estimated to be $20 billion in the United States and €30 billion in the European Union. [16]

Besides this large socio-economic burden osteoporosis leads to death in about 20% to 30% of patients within 1 year after experiencing a hip fracture. [32] For the remaining patients, osteoporotic fractures often mean a severe decrease in quality of life and in the case of compression fractures of vertebrae an elevated risk of back pain. [57] Novel drugs could achieve improvements by preventing up to 50% of these fractures, if patients were diagnosed early enough. [56]

However, diagnosis of osteoporosis in individual patients is a critical issue in itself. Osteoporosis is still mainly defined and diagnosed by measuring aBMD, i.e. bone mass. However, it is widely acknowledged that bone mass alone cannot completely predict fracture risk, and that bone architecture and other factors must also influence the apparent mechanical properties of whole bones. [8] There is growing evidence that changes in bone quality due to alterations of the mineral, organic, and water phases are also involved. Bone is a composite

Die approbierte gedruckte Originalversion dieser Diplomarbeit ist an der TU Wien Bibliothek verfügbar.
The approved original version of this thesis is available in print at TU Wien Bibliothek.
TU Bibliothek Your knowledge hub WIEN

material with a hierarchical structure resulting in a complex interplay between hard and soft phases determining its overall mechanical properties. It has, as other biological materials, dynamic behavior, which means it is remodelled over time. Bone resorption and formation are continuously occurring throughout the structure as a natural repair mechanism. Nevertheless, as mentioned above, aBMD is currently the main parameter used for diagnosing and assessing efficacy of treatment. The most effective route to stop the reduction of aBMD during aging is an anti-resorptive treatment, which reduces the degradation of bone material by inhibiting the activity of osteoclasts, the cells that are responsible for bone resorption. Until now there exist no concrete studies about its influence on bone repair mechanisms. The formation, as well as the mechanical properties at the tissue level of new bone material could be impaired, which potentially leads to an increased amount of microscopic damage and changes in damage behavior, problems which are the focus of this research project. [44][8]

1.3 Thesis Structure

This thesis is structured in 8 chapters. First, an introduction is given, containing the motivation and the definition of the research problem, as well as the aim of this thesis and its structure. Chapter 2 provides the biological and pharmaceutical background required for this topic. This comprises information about bone, osteoporosis and pharmaceutical treatments for osteoporosis. The methodological background is provided in chapter 3, which explains the necessity for mechanical testing of bone and methods for microdamage assessment. In chapter 4, used materials and methods are defined, which includes the sample preparation, mechanical testing as well as the analysis of the test data and damage assessment. Results are given in chapter 5 and discussed in chapter 6, which also gives a discussion of the materials, methods, and a short outlook.

Die approbierte gedruckte Originalversion dieser Diplomarbeit ist an der TU Wien Bibliothek verfügbar.
The approved original version of this thesis is available in print at TU Wien Bibliothek.
TU Bibliothek Your knowledge hub WIEN

The conclusion of this research project can be found in chapter 7. Chapter 8 provides the appendix.

Die approbierte gedruckte Originalversion dieser Diplomarbeit ist an der TU Wien Bibliothek verfügbar.
The approved original version of this thesis is available in print at TU Wien Bibliothek.

2 Biological and Pharmaceutical Background

2.1 Bone Tissue

Bone tissue is the main component in the skeletal system, which is a multifunctional organ that constitutes about 15% of the total body weight. Besides its function as the main load-bearing structure of the body, it also fulfills tasks such as protection of vital organs, production of blood cells as well as storage and supply of minerals. To achieve these requirements at the lowest possible weight, bone is organized as a hierarchical multiscale nano-composite material. [44]

Figure 2.1 shows the hierarchical organization of bone from its macroscopic level down to its molecular structure. At the macroscopic level, its composite structure can be seen in the form of dense cortical bone, which builds an outer shell around the cancellous (spongy, trabecualar) bone inside the marrow cavity. The next level presents the micro- and sub-microstructure of both cancellous and cortical bone, which shows that cortical bone is made up of osteons that consist of concentric layers (lamellae), which are surrounding a central canal containing nerves and blood vessels for the bones' blood supply. Cancellous bone comprises a combination of aligned lamellae and osteonal-like regions. (Details about cancellous and cortical bone are described in chapter 2.2.) Lamellae are aligned with the stress lines. They are composed of water (10% w/w) and organic phases (25% w/w), which are the inner softer matrix in which elongated collagen fibers (cross-linked type I collagen) are arranged in parallel layers, contributing to the elasticity of the bone. The nano- and ultrastructure shows the mineralization (65% w/w) in between the collagen fibers and within the collagen fibrils. These mineral phases are a deposition of

Die approbierte gedruckte Originalversion dieser Diplomarbeit ist an der TU Wien Bibliothek verfügbar.
The approved original version of this thesis is available in print at TU Wien Bibliothek.
TU Bibliothek Your knowledge hub WIEN

calcium and phosphate crystals (nanocrystalline carbonated apatite) between the collagen layers to give bone its strength and rigidity. Coupled deformation between collagen and mineral phases allows collagen to transfer loads to the mineral component. Collagen fibrils are made up of triple helix molecules, which is shown at the molecular level. These molecules are cross-linked within the fibrils by connections that are formed either enzymatically or non-enzymatically, which has a profound effect on the mechanical behavior of the whole bone. [8] Furthermore, non collageneous proteins (NCPs), which comprise about 10 % of the organic matrix in bone, are proposed to act as a glue at the collagen-mineral interface and thus enhance the resistance to separation of the mineralized fibrils. [20][53][6] Bone is not composed in this manner for damage prevention but rather to be more damage tolerant. It allows cracks to occur but limits crack growth due to its microstructural interfaces, thus providing high toughness at a low weight. [8]

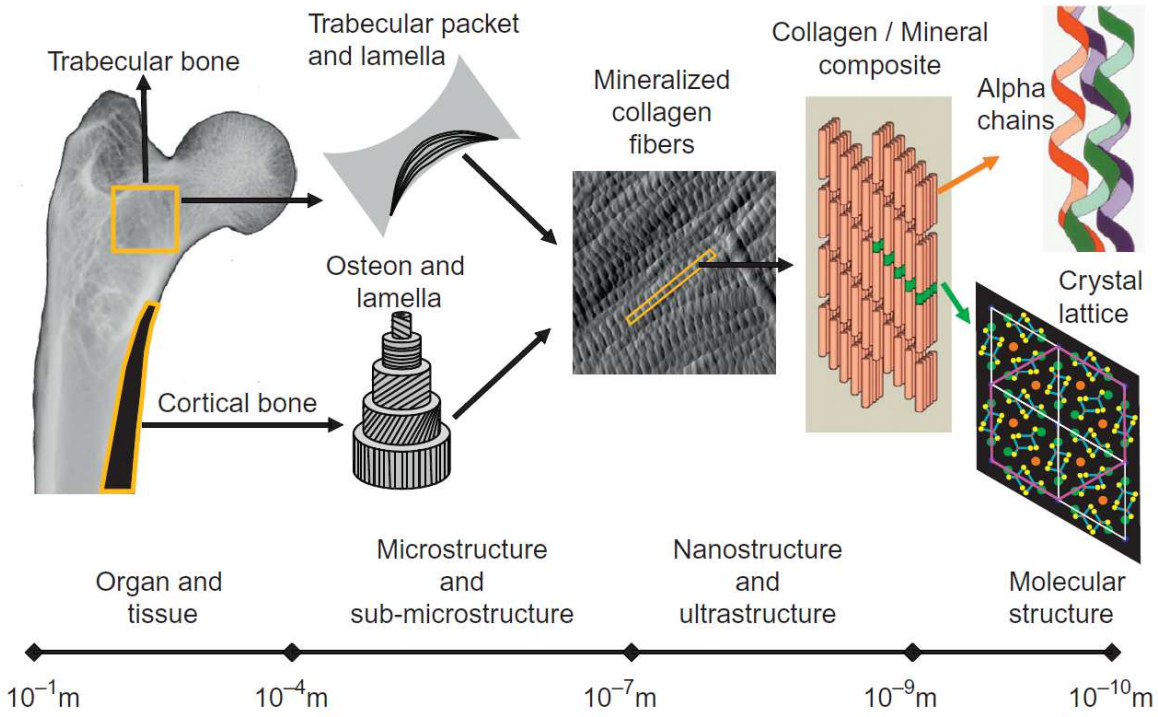

Figure 2.1: The hierarchical organization of bone. [8]

Die approbierte gedruckte Originalversion dieser Diplomarbeit ist an der TU Wien Bibliothek verfügbar.
The approved original version of this thesis is available in print at TU Wien Bibliothek.
TU Bibliothek Your knowledge hub WIEN

Because of this hierarchical structure and its basic components, bone is an anisotropic and heterogeneous material whose overall material properties are determined by a complex interplay between hard and soft phases.

Bone, as a biological material, has dynamic behavior, which means it changes over time and adapts to different conditions such as repetitive loading (to avoid failure and fatigue), nutrition, medication, age or diseases. Therefore, resorption and formation continuously occur throughout the whole structure and work as a natural repair mechanism. Bone consists of three main types of cells. These cells are osteoblasts, osteocytes, and osteoclasts. Osteoblasts form new bone matrix, osteocytes help to maintain bone tissue and osteoclasts resorb bone. [12]

2.2 Cancellous Bone versus Cortical Bone

At the macroscopic level, two different types of bone can be distinguished by their porosity. Cancellous bone, which has high porosity (approx. 85%), can be found in flat bones, vertebral bodies and ends of long bones. It is surrounded by a thin shell of cortical bone, which has lower porosity (approx. 5%, caused mainly by vascular channels) and is the main constituent in shafts of long and short bones. Cancellous bone shows a typical density range of 1.0–1.4 g/cm3, compared to about 1.8–2.0 g/cm3 for compact bone [37]. Dense and solid cortical bone surrounds the marrow space, whereas cancellous bone is made of a network of trabecular plates and rods of about 50 to 400μm thickness, interspersed in the marrow compartment where hematopoiesis occurs. Cortical bone constitutes most of the bone mass (approx. 80%) [13], bearing the majority of loads and providing protection, whereas the primarily function of cancellous bone is the redirection and distribution of loads to the the outer shell of cortical bone. This principle is also used in engineering in form of composite sandwich structures.

Die approbierte gedruckte Originalversion dieser Diplomarbeit ist an der TU Wien Bibliothek verfügbar.
The approved original version of this thesis is available in print at TU Wien Bibliothek.
TU Bibliothek Your knowledge hub WIEN

Struts in cancellous bone are oriented in various angles, thought to be aligned to the stress lines to provide optimal support. Osteons are the chief structural unit of both cortical and trabecular bone. Cortical osteons consist of cylindrical shaped layers (laminae) concentrically surrounding the vascular channels, which contain nerves and small blood vessels for the bones blood supply. These osteons are approximately 400μm to several millimeters long and 200μm wide, tending to be oriented along the long axis of a bone and forming a network throughout the whole cortical region. A ductile interface, called cement line, is separating them from the other bone matrix. In the human skeleton cortical bone is less metabolically active than cancellous bone. [13] Osteons of cancellous bone are called packets, which have a semilunar shape. These are composed of more or less parallel to the trabecular surface arranged lamellae, not containing vascular channels since blood supply is provided directly from the marrow cavity. [8] Osteocytes, the most common cells in bone, which maintain bone tissue, are inside small spaces called lacunae, which are located at the borders of adjacent lamellae in cortical bone. In cancellous bone, these lacunae are located inside the trabeculae. Communication between these cells and their nutrition is provided through canaliculi, which are small channels inside the bone matrix. [12] Figure 2.2 and figure 2.3 show the composition of cortical bone and cancellous bone respectively.

Die approbierte gedruckte Originalversion dieser Diplomarbeit ist an der TU Wien Bibliothek verfügbar.
The approved original version of this thesis is available in print at TU Wien Bibliothek.
TU Bibliothek Your knowledge hub WIEN

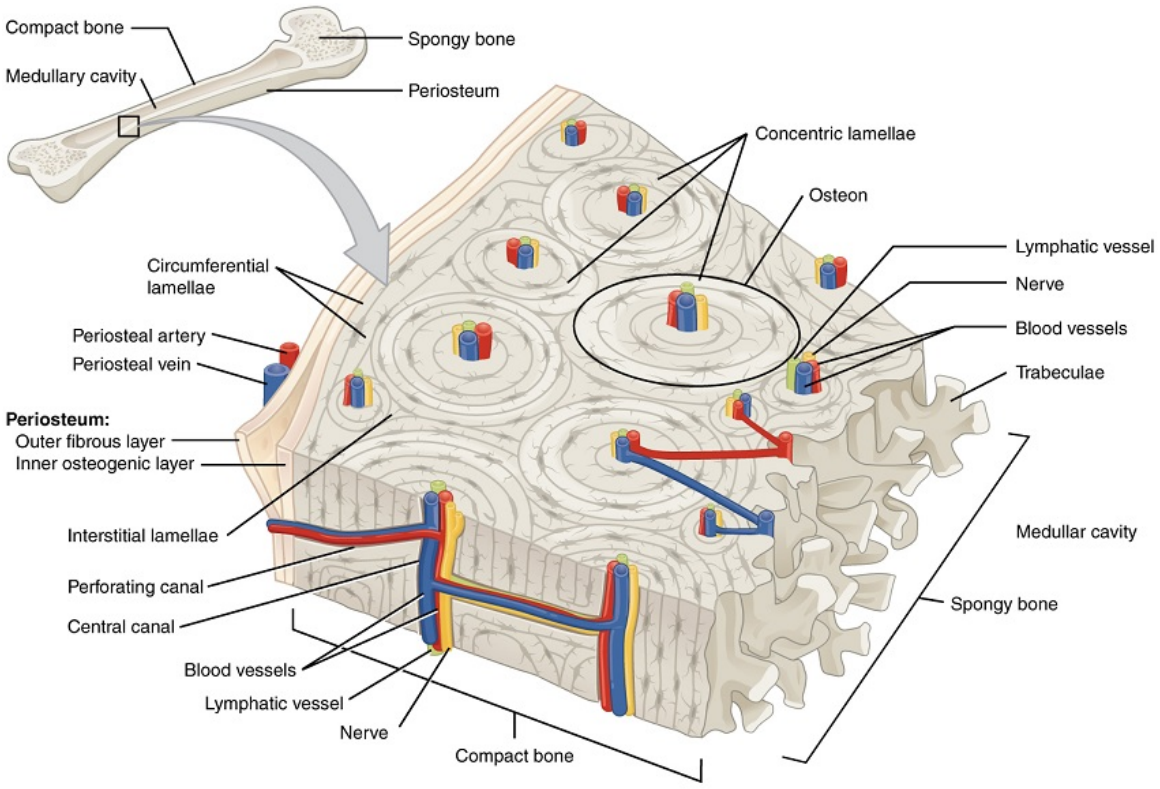

Figure 2.2: Composition of cortical bone. [12]

Die approbierte gedruckte Originalversion dieser Diplomarbeit ist an der TU Wien Bibliothek verfügbar.
The approved original version of this thesis is available in print at TU Wien Bibliothek.

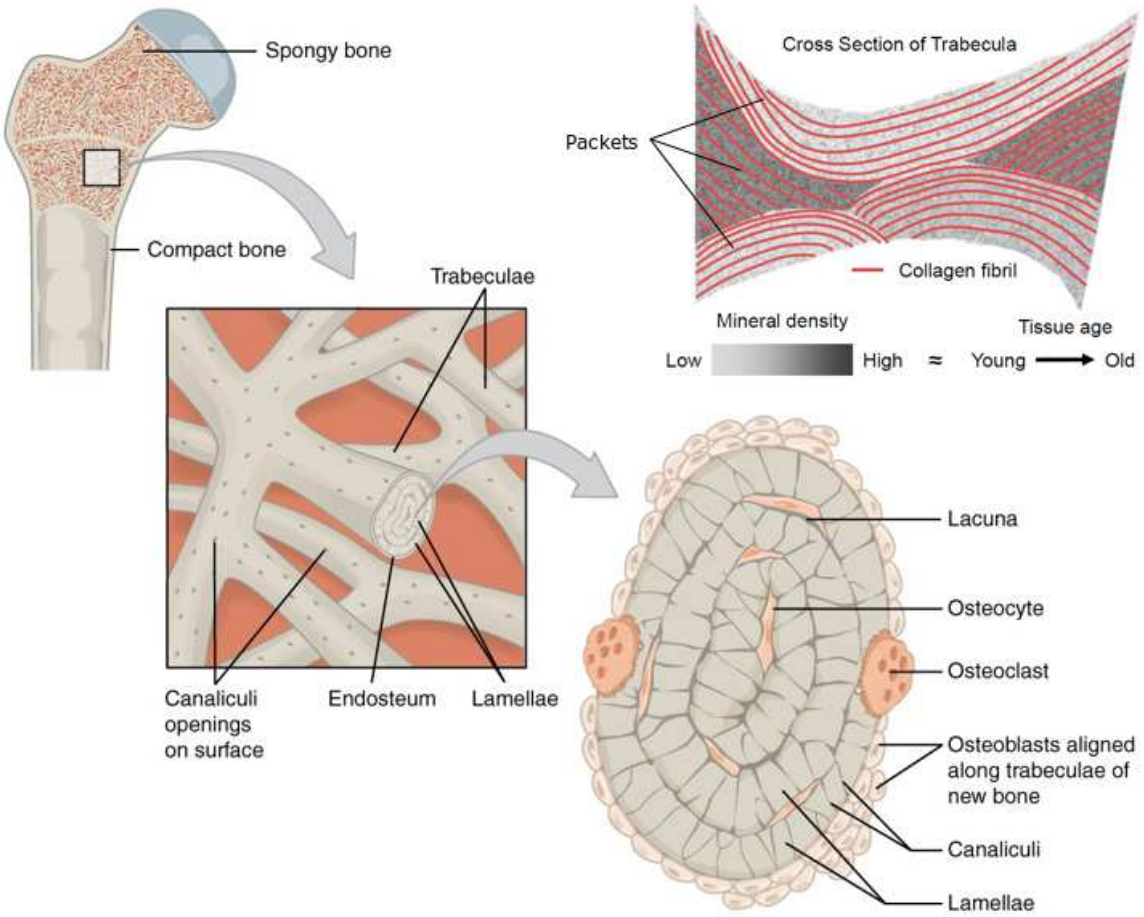

Figure 2.3: Composition of cancellous bone. Edited from [12][29]

2.3 Bone Quality and Bone mineral density

Bone quality is dependent on various characteristics, which also significantly effect bone fracture and failure such as bone (micro)architecture and geometry, material bone mineral density (BMD), collagen content, hydration, cross-linking, microdamage and bone turnover, which in turn affects each other characteristic.

Die approbierte gedruckte Originalversion dieser Diplomarbeit ist an der TU Wien Bibliothek verfügbar.
The approved original version of this thesis is available in print at TU Wien Bibliothek.

However, clinical practices rely primarily on areal bone mineral density (aBMD)[1] as the only indicator of fracture risk, which has therefore poor predictive ability. Resorption and remodeling of bone is constantly occurring, effecting aBMD dependent on the rate of bone turnover. Faster turnover leads to lower aBMD. Partly resorbed trabeculae or resorption cavities can occur, leading to a small decrease in aBMD but can significantly decrease trabecular strength and increase the risk of microdamage accumulation due to stress concentrations at the cavities, which can have even more severe effects on bone strength. This is especially when influencing the trabecular architecture by perforating trabeculae or reducing the connectivity between trabecular plates, which way be independent from aBMD. Figure 2.4 shows the importance of bone architecture. Low bone mineralization decreases its strength and stiffness, leading to reduced bone quality. However, bone becomes brittle when it is too highly mineralized. Both can occur locally, not altering the overall BMD. The amount and quality of type I collagen and how it is cross-linked, as well as microdamage also have a strong effect on bone strength, stiffness and impact behavior. [8]

[1] aBMD is measured as an average density, taking into account not only bone material, but also marrow cavities, haversiancanals, etc. Thus aBMD also takes BMD into account

Die approbierte gedruckte Originalversion dieser Diplomarbeit ist an der TU Wien Bibliothek verfügbar.
The approved original version of this thesis is available in print at TU Wien Bibliothek.
TU Bibliothek Your knowledge hub WIEN

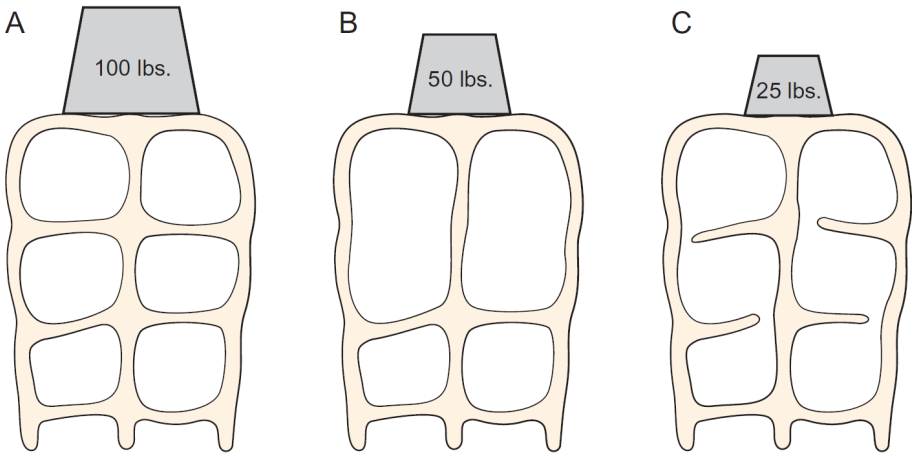

Figure 2.4: The importance of bone architecture, independent of BMD
Although (C) has the same BMD as (A), it is inferior, capable of supporting only a fraction of the loads, due to disconnections of cross struts whereas a lower BMD with proper connectivity as shown in (B) is able to support higher loads than (C). [8]

2.4 Microdamage

Bone undergoes a continuous microdamage accumulation due to daily activities, which cause repetitive loading. This is an important mechanism, since microdamage formation leads to energy dissipation that prevents the tissue from catastrophic failure. However, the presence of such cracks and especially their coalescence into macrocracks are adverse to the mechanical properties of bone. [8]

There are two main types of microdamage, described as linear microcracks and diffuse damage as well as cross-hatching, which can often be observed in cancellous bone as a result of intermediate sized cracks forming specific cross-hacked patterns. Figure 2.5 shows a basic fuchsin stained trabeculae containing

Die approbierte gedruckte Originalversion dieser Diplomarbeit ist an der TU Wien Bibliothek verfügbar.
The approved original version of this thesis is available in print at TU Wien Bibliothek.
TU Bibliothek Your knowledge hub WIEN

all three types of damage. Although diffuse damage is less well understood, it is assumed to have the same importance from a mechanical and a biological perspective than linear microcracks.

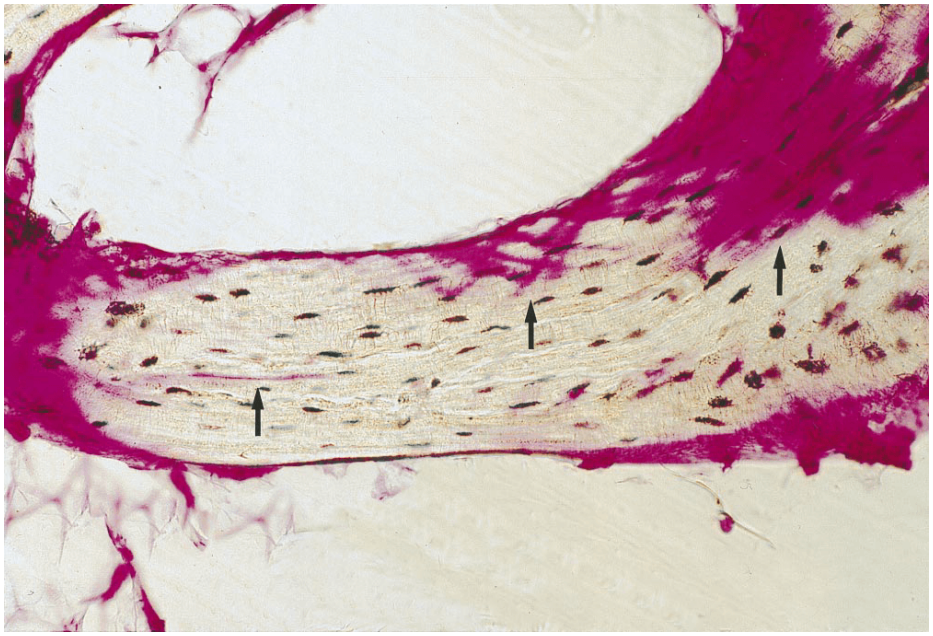

Figure 2.5: Basic fuchsin stained trabeculae shows types of microdamage. [21] From left to right: Linear microcrack, cross-hatching, diffuse damage

Linear microcracks are sharply defined cracks with an approximately length of 50-100 μm. Most of these cracks can be found in older bone, which endured the highest amount of stress cycles and has higher levels of non-enzymatic collagen cross linking and mineralization, which furthermore makes it easier for cracks to occur. It was shown that formation, as well as accumulation of microcracks have deteriorating effects on stiffness, strength and toughness. [48]

Diffuse damage on the other hand is shown as a cluster of sublamellar-sized cracks. They are described as crazing cracks that separate mineral aggregates from each other and from the surrounding organic matrix. This type of damage appears to occur more easily than others types of damage. Even at low cyclic

Die approbierte gedruckte Originalversion dieser Diplomarbeit ist an der TU Wien Bibliothek verfügbar.
The approved original version of this thesis is available in print at TU Wien Bibliothek.
TU Bibliothek Your knowledge hub WIEN

loads and constant loads, which are applied for long time periods, diffuse damage can be observed. Diffuse damage occurs predominantly in tensile regions whereas linear microcracks are formed mainly in shear and compression loaded areas, thus diffuse damage is not a precursor of linear microcracks. However, both types of microdamage seem to have the same probability distribution. [48]

Remodeling processes as well as numerous microstructural interfaces are effective bone characteristics to prevent crack growth. Thus, cracks tend to remain small and follow the preferential microstructural grain of the material, parallel to lamellae and osteons, approximately parallel to the longitudinal axis of the long bones, which is the direction of lowest resistance. [43] Microstructural interfaces, such as lamellae and tissue heterogeneity among osteons as well as mineral and collagen interfaces, represent effective barriers for cracks to grow and therefore have a major impact on the materials toughness. It appears that growth of diffuse damage leads to even higher amounts of energy dissipation than growth of linear microcracks probably due to a larger cracksurface area. Various studies have shown that the amount of microcracks is increasing with age. Schaffler et al. even described an exponential relation between microdamage accumulation and age. [38] However, Zeynep Seref-Ferlenge et al. have shown that in contrast to linear microcracks, diffuse damage accumulation has no dependency on age [48], which is refuted by others [15].

Figure 2.6 shows that cyclic loading causes damage accumulation, which is a nonlinear process that can be divided into three different phases. Phase I represents a fast modulus drop due to damage initiation. In phase II, only little damage is initiated, but toughening mechanisms due to the bones microstructure, such as lamellae or osteons, become more dominant. Crack growth in this phase is slow but absorbs a lot of energy while stiffness and strength stay almost constant. This phase represents most of the materials lifetime. In phase III material properties decrease rapidly since microcracks coalescence

Die approbierte gedruckte Originalversion dieser Diplomarbeit ist an der TU Wien Bibliothek verfügbar.
The approved original version of this thesis is available in print at TU Wien Bibliothek.
TU Bibliothek Your knowledge hub WIEN

into macrocracks, finally leading to total failure. [48]

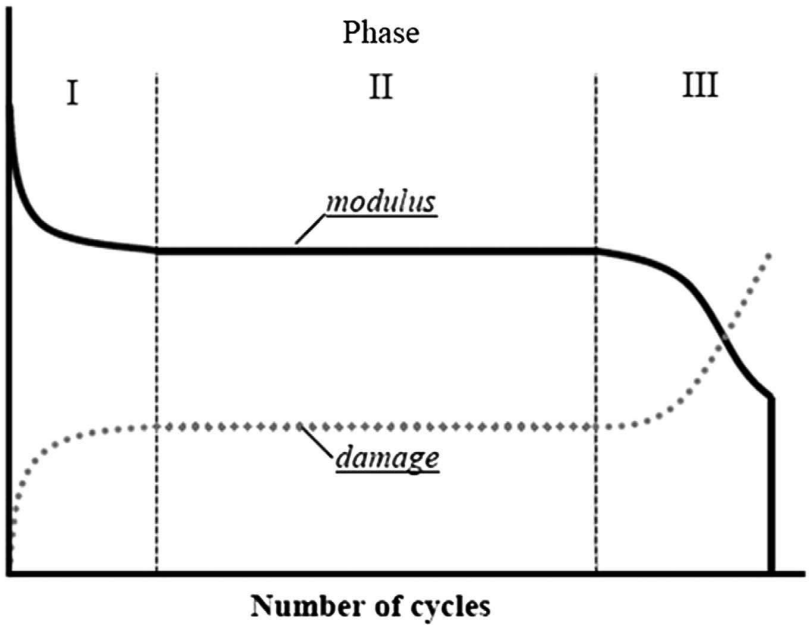

Figure 2.6: Damage accumulation and modulus drop during cyclic loading. [48]

Parameters primarily used to describe cracks are the average crack density, also called number density, the average crack length and the surface crack density, which describes the total crack length per unit area and is simply the product of the other two parameters. [43]

Remodeling decrease with aging, disease, and certain drug treatments. Reduced remodeling leads to faster microdamage accumulation as well as loss of tissue heterogeneity. Both contribute additively to reduced fracture toughness. [48]

2.5 Modeling and Remodeling

Bone modeling is a process in which bone matrix is resorbed by osteoclasts on one surface and deposed/formed by osteoblasts on another surface, which

Die approbierte gedruckte Originalversion dieser Diplomarbeit ist an der TU Wien Bibliothek verfügbar.
The approved original version of this thesis is available in print at TU Wien Bibliothek.
TU Bibliothek Your knowledge hub WIEN

takes place during growth. It is responsible for the development and growth of the skeleton. [12] Furthermore, also the process in which bone is adapting to frequent external loads is considered as modeling. Formation occurs at areas of high strain, while areas of low strain are resorbed. On trabecular surfaces, modeling occurs to normalize loading induced strains as shown in figure 2.7 [8]

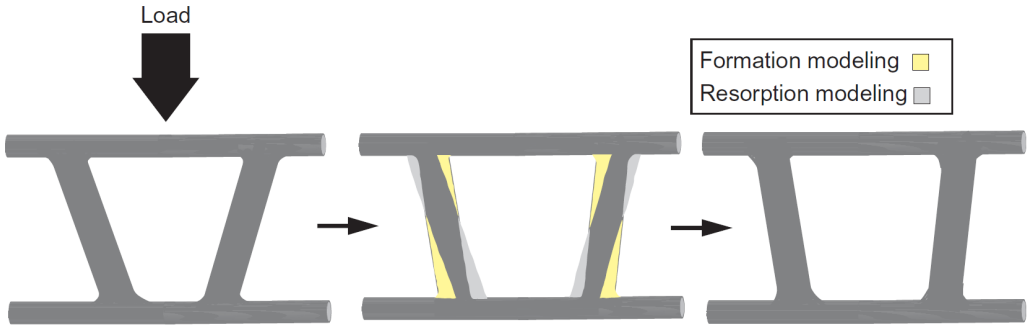

Figure 2.7: Modeling occurs on trabecular surfaces in order to normalize loading-induced strains. [8]

In contrast to modeling, remodeling usually does not change size and shape of bone but rather maintains the tissue, which preserves the skeletons structural and functional integrity. [44] Remodeling is a life-long process where old or damaged bone gets resorbed by osteoclasts and replaced with new bone by osteoblasts to maintain bone quality. [51] Old bone has reduced flexibility and rigidity due to alterations of the matrix and lower mineralization. Furthermore, fractures of whole bones must be repaired as well as microdamage, which is occurring throughout the whole lifetime due to daily activities, which severely increases bone fragility. Therefore, remodeling is a necessary process, especially in trabecular bone, since its strength is primarily determined by its integrity. The whole skeleton is being replaced about 3-4 times in a lifetime due to remodeling. Activities of osteoclasts and osteoblasts are independent for modeling but coupled for remodeling. [44] They combine to form, together with their associated blood vessels, a bone multi-cellular unit (BMU), shown in figure

Die approbierte gedruckte Originalversion dieser Diplomarbeit ist an der TU Wien Bibliothek verfügbar.
The approved original version of this thesis is available in print at TU Wien Bibliothek.
TU Bibliothek Your knowledge hub WIEN

2.8. This unit is a cavity about 200 μm in diameter, which is proposed by Klein-Nulend to move along a bone, parallel to the direction of principal stress at a speed of approximately 40 μm per day.

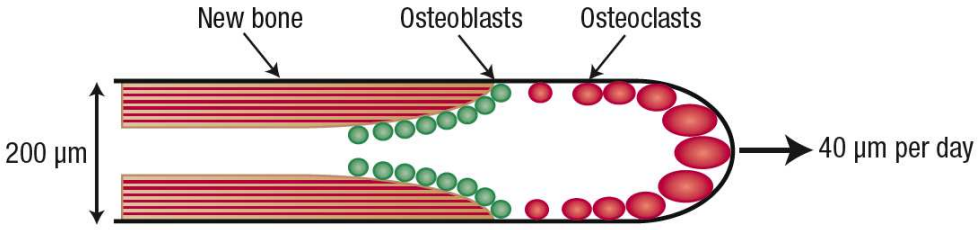

Figure 2.8: BMUs are the primary way by which bone maintains its structural integrity. [51]

These BMU form new bone of circular cross-section called osteons. This process is similar in cancellous and cortical bone. However, in cancellous bone, BMUs work on the surfaces inside the cancellous tissue. Remodeling is not only a random stochastically distributed process but also, at least to some degree, a targeted process, driven by changes in the tissue integrity due to damage. Therefore, there is increased incidence of BMUs at areas of damage to remove this inferior tissue with new bone. In contrast to targeted remodeling, stochastic remodeling is thought to play more of a role for calcium homeostasis. [8]. The answer how damage is detected can still not be answered. Research is focusing on osteocytes, cells that live inside the bone in small cavities called lacunae and being linked to their neighbors over small canaliculi by extensions named cellular processes. These cellular processes form a network between osteocytes and bone lining cells and could be used to detect and control the amount of allowed damage in the surrounding bone. Essential nutrients are transported to osteocytes through a constantly flowing fluid inside these canaliculi. Klein-Nulend and co-workers showed that flow rates are low immediately ahead of BMU cavities. This leads to cell death in this region, probably due to the lack of

Die approbierte gedruckte Originalversion dieser Diplomarbeit ist an der TU Wien Bibliothek verfügbar.
The approved original version of this thesis is available in print at TU Wien Bibliothek.
TU Bibliothek Your knowledge hub WIEN

nutrition. Also cracks and regions of diffuse damage lead to cell death of nearby cells, probably due to disruption or other reasons that change the fluid flow inside canaliculi. They proposed that this cell death is deliberate (apoptosis) and osteocytes are attracted to these apoptotic cells and therefore preferentially reabsorb bone in these regions and thus initiate repair. [51] Remodeling can get inhibited by pharmacological treatments who inhibit cell apoptosis, even when microdamage is produced. [8]

The rate with which bone gets remodeled is very high during growth and slows down until peak bone mass is attained. It is strongly dependent on age, genetics, health, hormonal activity, medication, nutrition, and many other factors. A strong increase in the bone remodeling rate can be seen in women starting at menopause due to the loss of circulating estrogen, which suppresses osteoclast apoptosis. The remodeling rate also increases for men although about a decade later and less severe. The amount of bone formed relative to the amount of bone resorbed by an individual BMU is called bone remodeling balance. In healthy individuals, this balance is slightly negative, which means that more bone gets resorbed than formed. Some diseases, such as post-menopausal osteoporosis lead to even more negative balances. Furthermore, formation takes about 4-5 times longer than resorption, which additionally leads to a temporary reduction of bone mass. However, some pharmacological treatments have shown to change this balance to positive values. [8]

There are certain differences in remodeling between cancellous and cortical bone. Cortical bone is very compact and has a lower surface-to-volume ratio compared to cancellous bone. Therefore, cortical bone has a much slower rate of remodeling, which replaces about 2-5% in contrast to the replacement of about 25% in cancellous bone. Thus, cancellous bone is more liable to undergo unbalanced remodeling and therefore bone loss can be measured first in these areas. [44]

Die approbierte gedruckte Originalversion dieser Diplomarbeit ist an der TU Wien Bibliothek verfügbar.
The approved original version of this thesis is available in print at TU Wien Bibliothek.
TU Bibliothek Your knowledge hub WIEN

2.6 Osteoporosis

Osteoporosis is the most common human metabolic bone disorder. It is related to an imbalance in the usually coordinated activity of osteoclasts and osteoblasts that leads to a strong negative bone balance within the individual BMUs. Increased osteoclastic activity results in a higher number of active remodeling sites and therefore higher bone resorption, which consequently leads to decrease in bone mass. This effects both cancellous and cortical bone, whereby the former is effected to a greater extend, especially in early stages of the disease. [23] Osteoporosis can occur in all ages. However, women after their menopause and men over 60 years of age are most prone due to a decrease in steroid hormones, i.e. estrogen in women. [8] Too little peak bone mass is another contributing factor in the development of osteoporosis. [23] Figure 2.9 shows the total mass of skeletal calcium in grams over men's and women's lifetime. A critical drop in bone mas can be seen after the menopause in women at the age between 50 and 60 years.

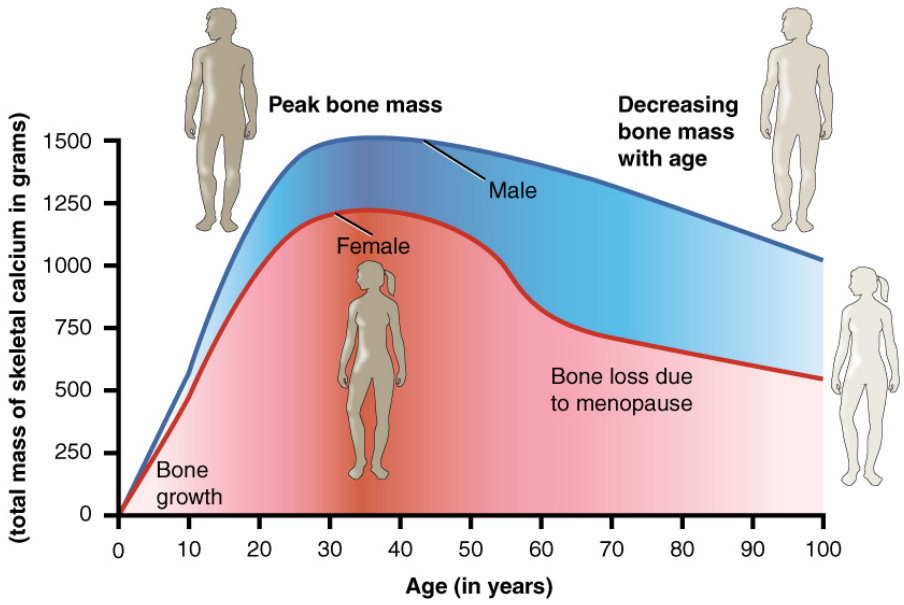

Figure 2.9: Bone mass over the years for men and women.[12]

Die approbierte gedruckte Originalversion dieser Diplomarbeit ist an der TU Wien Bibliothek verfügbar.
The approved original version of this thesis is available in print at TU Wien Bibliothek.
TU Bibliothek Your knowledge hub WIEN

One of many definitions for osteoporosis is:
"A systemic skeletal disorder characterized by a decrease in bone mass and deterioration of the microarchitecture of the bones with a corresponding reduction in strength and an increase in fracture risk." [44]

It is important to notice that this definition includes the term bone strength, which is dependent not only on bone density but also on every other characteristic of bone quality as explained in chapter 2.3. Bone strength cannot be measured noninvasively at the present time, but several studies have shown that bone density and fracture risk are closely related. Thus, the World Health Organization (WHO) proposed a relatively simple bone areal mineral density measurement (aBMD) to diagnose osteoporosis for which Dual-energy X-ray absorptiometry (DXA) is used. Consequently, an alternative, but more quantitative definition of osteoporosis is proposed by the WHO:
"Osteoporosis is present when the bone mass is more than 2.5 standard deviations (SD) below that of healthy premenopausal adult females, the T score" [44]

Although this definition does quantitatively help to diagnose osteoporosis, it is not ideal to diagnose osteoporosis on individuals since it does not provide information about other bone quality aspects besides bone mass. As mentioned before, high remodeling rates reduce bone strength but may have no effect on bone mass. Therefore, the highest third of the population for aBMD who have high bone turnover are at greater risk than those at the lowest third of aBMD with lower bone turnover. [8]

Die approbierte gedruckte Originalversion dieser Diplomarbeit ist an der TU Wien Bibliothek verfügbar.
The approved original version of this thesis is available in print at TU Wien Bibliothek.

2.7 Pharmaceutical Treatments for Osteoporosis

Pharmaceutical treatments for osteoporosis can improve the mechanical strength of bone by mechanisms that lead to alterations in bone mass, composition, architecture and thus the overall quality of the bone. [23] Today's most promising treatments effect the bone remodeling cycle by inhibiting the activity of osteoclasts and therefore bone resorption to restore the balance of osteoclast and osteoblast activity. Thus, these treatments are known as anti-resorptive treatments. However, since bone remodeling is a coupled process, not only bone resorption, but also bone formation is suppressed. [8]

Bisphosphonates such as alendronate are the most commonly used anti-resorptive treatments. These agents reduce bone remodeling by about 70%, leading to a stable or even increasing aBMD, increase bone volume (thickness), and furthermore have shown to reduce all kind of osteoporotic fractures. [8] It also appears that alendronate changes the collagen cross-linking state, reduces size of failure process zone[2] relative to trabecular thickness, leads to more brittle fractures without altering the average length of the cracks, and increases ultimate load and stiffness. It is suggested to be most effective for patients with very low bone mass. [49]

Although these treatments have shown positive results for many years, some side effects, like osteonecrosis of the jaw or unusual fractures of the femoral shaft, have been observed. This could be due to unknown effects of anti-resorptive treatments on bone tissue beyond the intended effect of impeding osteoclast activity and therefore warrant deeper investigation. A possible reason for such unusual fractures could be the accumulation of microdamage due to reduced

[2] The failure process zone is the zone where nonlinear deformations occur that lead to failure of the tissue. [58]

Die approbierte gedruckte Originalversion dieser Diplomarbeit ist an der TU Wien Bibliothek verfügbar.
The approved original version of this thesis is available in print at TU Wien Bibliothek.
TU Bibliothek Your knowledge hub WIEN

remodeling, which usually acts as a natural repair mechanism. Therefore, unpaired microcracks could coalesce to macrocracks and furthermore lead to catastrophic fractures.

Selective Estrogen Receptor Modulators (SERMs) are another type of anti-resorptive agents used to treat osteoporosis. These are based on the skeletal benefits of estrogen but with a better balance between benefits and risks. Raloxifene, which is the only SERM used in the United States to treat osteoporosis, does not primarily appear to reduce fracture risk by increasing bone mass. It was shown that bisphosphonates increase aBMD by about 7% while raloxifene increases it by only 1-2% in the first 3 years of treatment. [8] However, it appears to increase trabecular thickness, changes the collagen cross-linking state less than alendronate, increase ultimate load and stiffness and the size of the failure process zone relative to the trabecular thickness, leads to more ductile fractures and increased crack lengths but to a smaller increase in microcrack density than alendronate. Raloxifene is suggested to be most effective for patients with milder osteoporotic symptoms. [49] The mechanism by which raloxifene reduces fracture risk is thus far unknown. It is assumed that raloxifene is altering the bone matrix itself, by mechanisms that increase the fraction of bound water[3] at the interface between the collagen and the mineral phase, which could have a positive effect on bone strength. [8]

[3]Suggested articles about bound water are [35] and [19].

Die approbierte gedruckte Originalversion dieser Diplomarbeit ist an der TU Wien Bibliothek verfügbar.
The approved original version of this thesis is available in print at TU Wien Bibliothek.
TU Bibliothek Your knowledge hub WIEN

3 Methodological Background

3.1 Mechanical testing of Bone

Bone forms the main load bearing structure (skeleton) of the body. Impacts, as occurr in accidents, can cause fractures, leading to questions about maximum forces that can be withstand by the bone structure. This is important for safety measures, as example in means of transportation. Additionally, bone undergoes a continuous microdamage accumulation due to daily activities, which cause repetitive loading. This can result in a great risk, especially for elderly people or people with bone diseases like osteoporosis. Furthermore, bone-implant interfaces rely on detailed information about the local properties of bone, which also increased the interest for mechanical tests to determine material properties and damage behavior of bone. [4]

Mechanical tests can simulate different loading conditions such as tension, compression or shear, making them of great importance. Tests can be conducted for the tissue level or the entire bone organ. It is obvious that the latter is not only dependent on the material properties itself, but also on its architecture. However, when thinking of the macroscopic structure of bone, where it can be distinguished into cancellous and cortical bone, one can see that material properties at the tissue level of cancellous bone are hard to assess without taking bone architecture into consideration. Thus, numerous studies of cortical bone have been conducted whereas studies about cancellous bone are rare. Most researchers have tested cubic or cylindrical cores of cancellous bone with dimensions of the order of 5 to 10 mm in compression tests to obtain bulk material properties of the trabecular structure. [4] However, due to strong variations in bone architecture, e.g. trabecular alignment, density, etc., it is impossible to obtain exact and significant material properties at the tissue

Die approbierte gedruckte Originalversion dieser Diplomarbeit ist an der TU Wien Bibliothek verfügbar.
The approved original version of this thesis is available in print at TU Wien Bibliothek.
TU Bibliothek Your knowledge hub WIEN

level when using this approach. Early studies and models of cancellous bone assumed that the tissue modulus of cancellous and cortical bone is identical. Thus, bulk tissue stiffness of cancellous bone was often modeled by assuming that cancellous bone was simply a more porous cortical bone tissue. Refined models have shown that this assumption was just a rough estimation. [45] More detailed information about the tissue level of cancellous bone has become more important, leading to novel testing methods for individual trabeculae.

First tensile tests on individual trabeculae were performed by Ryan and Williams [46] and Rho et al. [45] The small size of single trabeculae makes it a very challenging undertaking. Besides the enormous effort and necessary precision to harvest, handle and prepare the samples, also the test execution and data acquisition itself brings many hurdles, which must be taken account for. Measurements must be taken at a sufficient distance from the fixed ends to ensure that edge effects and stress concentrations due to the clamps do not falsify the results by influencing the general homogeneous stress state. [4] Recently, M. Frank et. al. developed a mechanical testing setup where individual trabeculae are tested under tension in a close to physical environment.[26] This setup provides the basis for the tests used in this research project.

Outcome parameters for mechanical tests usually include elastic modulus, yield stress and strain as well as ultimate stress and strain, and normalized work to failure (modulus of toughness). A typical load-displacement curve, obtained from a mechanical test is shown in figure 3.1

Die approbierte gedruckte Originalversion dieser Diplomarbeit ist an der TU Wien Bibliothek verfügbar.
The approved original version of this thesis is available in print at TU Wien Bibliothek.
TU Bibliothek Your knowledge hub WIEN

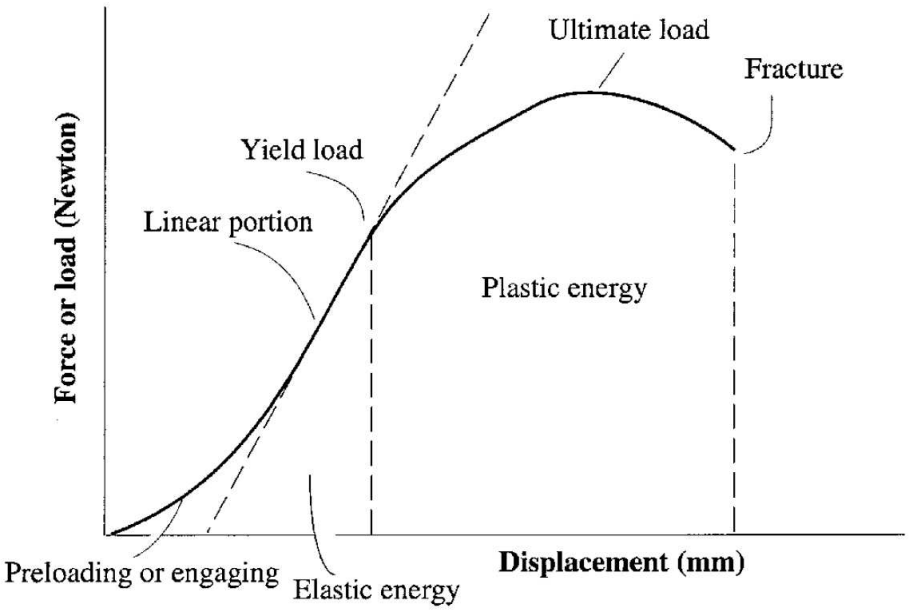

Figure 3.1: A typical load-displacement curve.[4]

Destructive tests provide data on damage behavior as well as material properties at the tissue level, whereas tests, which are stopped prior to failure, mainly provide information about the damage behavior of the bone.

There are several factors affecting the test results such as specimen preparation and storage, machine compliance, specimen-fixture interface, specimen size and geometry and testing conditions (temperature, hydration), which have to be taken into consideration. [4]

3.2 Assessment of Microdamage

Microdamage formation is a key determinant of bone strength. Due to daily activities, continuous accumulation of microdamage occurs, which contributes to an increased fracture risk. Therefore, a profound assessment of microdamage is crucial to better understand bone quality and bone fracture. It is important to differentiate between pre-existing damage, which was sustained in vivo, damage

Die approbierte gedruckte Originalversion dieser Diplomarbeit ist an der TU Wien Bibliothek verfügbar.
The approved original version of this thesis is available in print at TU Wien Bibliothek.
TU Bibliothek Your knowledge hub WIEN

sustained during mechanical tests, and artefactual damage incurred during specimen preparation. [42]

3.2.1 Microcrack Staining

Several methods have been developed to assess microdamage in vivo as well as in vitro. In this research project, only staining with **basic fuchsin** as well as the contrast agent **barium sulfate** are considered.

En bloc staining with **basic fuchsin** has become one of the most trusted methods to assess microdamage and microdamage accumulation. As basic fuchsin is soluble in alcohol but insoluble in water, stained specimens can be processed in an aqueous environment without the risk of leaching out and penetrating new defects, which would label misleading artefactual damage. However, artefactual cracks can be partially stained, which have to be distinguished by careful observation using transmitted light or epifluorescence microscopy. Both microscopy methods are applicable since basic fuchsin is a fluorochrome as well as a diachrome, as it appears colored under transmitted light. Its major constituents are three triarylmethane dyes, which are pararosanalin, rosanilin and magenta II. The heterocyclic molecular structures are responsible for their fluorescence properties. [10] Linear microcracks, as well as diffuse damage can be identified using basic fuchsin. The former appear as sharp bordered cracks within the bone matrix with an intermediate size, larger than canaliculi but smaller than vascular channels. Diffuse damage can be identified as a contained volume of multiple submicron cracks. [42]. An example of the basic fuchsin stained types of damages inside a single trabeculae was shown in figure 2.5.

A new protocol was developed by Burr et al. in which samples get stained through a graded series of alcohols under vacuum, which drastically reduced the incubation time. [9] However, several difficulties have been encountered

Die approbierte gedruckte Originalversion dieser Diplomarbeit ist an der TU Wien Bibliothek verfügbar.
The approved original version of this thesis is available in print at TU Wien Bibliothek.
TU Bibliothek Your knowledge hub WIEN

using this technique. Uneven stain can be the result of inadequate dehydration during the staining procedure. Therefore, the recommended graded series of alcohols should be followed. Further, basic fuchsin penetrates by diffusion, wherefore not all cracks may be stained. Thus, quantification of microdamage may underestimate the true amount of microdamage present. This makes it important to use vacuum during the whole staining procedure. However, staining with basic fuchsin is not suitable to visualize submicroscopic damage. Staining times have to be reduced for poorly mineralized or very small bones. Density variations inside one bone make it difficult to find the right staining protocol since areas of higher density can be understained. The best result is when canaliculae, lacunae and canals are darkly stained whereas the bone matrix is unstained or just lightly stained. Most adequate results were achieved with basic fuchsin from the J.T. Baker Co. [9]

Barium sulfate (BaSO4) is used as a contrast agent in radiological evaluation of microdamage with micro-computed tomography (μCT). Through 3D rendering, three dimensional images of damage can be obtained. Independent solutions of barium and sulfate ions diffuse into voids within the tissue including microdamage. These spaces provide nucleation sites for precipitation of barium sulfate on tissue surfaces. The staining is a result of the following precipitation reaction: [42]

$$BaCl2(aq) + Na2SO4(aq) \rightarrow BaSO4(s) + 2NaCl(aq). \quad (1)$$

3.2.2 Confocal Laser Scanning Microscopy (CLSM)

Confocal Laser Scanning Microscopy (CLSM) has become an important tool for a great range of histology applications, especially for imaging of fluorescently labeled biological specimens. Images of high contrast and resolution of single sections, as well as a collection of serial optical sections from thick specimens

Die approbierte gedruckte Originalversion dieser Diplomarbeit ist an der TU Wien Bibliothek verfügbar.
The approved original version of this thesis is available in print at TU Wien Bibliothek.
TU Bibliothek Your knowledge hub WIEN

up to 100 μm at multiple wavelengths are possible. [41] Optical sections are produced by scanning the specimen point-by-point with a laser beam focused in the specimen. This beam is confocal with the point of light focused at pinholes in front of the photodetector and the light-source, which is a spatial-filtering technique that only allows information from the focal plane if interest to reach the photodetector. This design reduces, in combination with background noise reduction, unwanted fluorescence from above and below the focal plane of interest. Thus, a look inside the specimens without the need of physical sectioning is possible. Typical CLSM's have a theoretical lateral resolution of 0.14μm and a vertical resolution of 0.23μm with a lens of 1.4 numerical aperture. [40]

Figure 3.2 shows the principle design and light path of a CLSM.

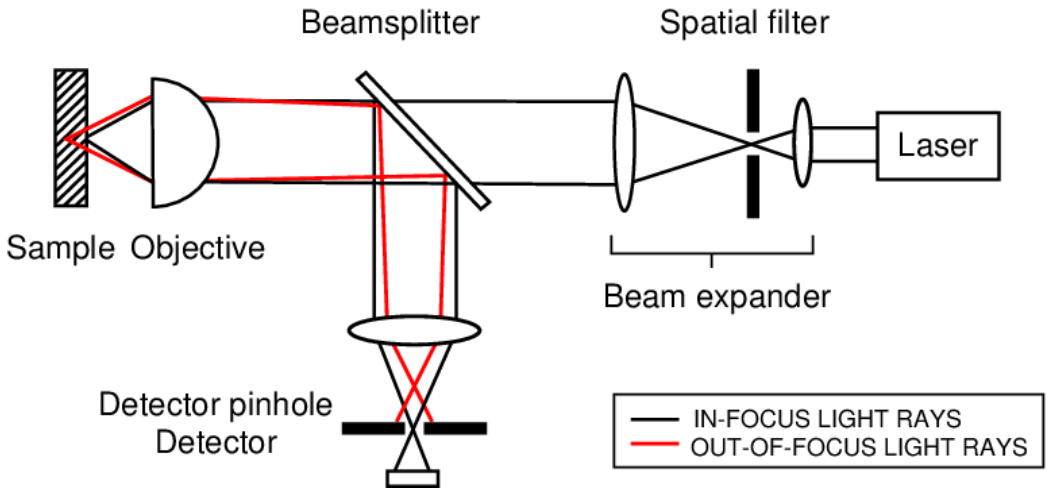

Figure 3.2: Simplified set-up of a confocal microscope, adapted from Corle and Kino (1996). [33]

Adjustment of the depth of field is another important feature of CLSMs. In combination with advanced image-procession software packages, three-dimensional reconstructions as well as surface and volume computations can be realized combining the information from multiple two-dimensional optical sections. [41]

Die approbierte gedruckte Originalversion dieser Diplomarbeit ist an der TU Wien Bibliothek verfügbar.
The approved original version of this thesis is available in print at TU Wien Bibliothek.
TU Bibliothek Your knowledge hub WIEN

3.2.3 Micro-computed Tomography (micro-CT)

In contrast to conventional destructive methods, such as imaging of basic fuchsin stained histological sections under a microscope, micro-computed tomography allows to visualize and assess microdamage in bone without the need for mechanical sectioning of the samples. Samples get therefor illuminated by a micro-focus x-ray emitter and a planar x-ray detector collects magnified projection images. These are gray-scale images, where higher gray values indicate higher bone density. [7] Three-dimensional images are reconstructed by a digital process from a series of two-dimensional trans-axial projections of a sample, which are generated by rotation of the sample or the emitter and detector. Therefore, whole samples keep preserved and a three-dimensional assessment of microdamage density and spatial distribution within the bone can be done throughout the whole structure. [42]

Die approbierte gedruckte Originalversion dieser Diplomarbeit ist an der TU Wien Bibliothek verfügbar.
The approved original version of this thesis is available in print at TU Wien Bibliothek.

4 Materials and Methods

4.1 Materials

Materials from two completed animal studies were used. [1][2] Non-ovariectomized skeletally mature female beagle dogs (average age at beginning of treatment was 1.3 ± 0.2 years) were treated orally for 12 months with clinically relevant doses of alendronate (ALN, 0.2 mg/kg/day) or raloxifene (RAL, 0.5 mg/kg/day). [2] Additional material from an untreated group of these dogs was used as a control-group (CON). Altogether, single trabeculae from 15 thoracic (T8-T12) vertebrae (5 from each group, ALN, RAL, CON) from different animals were tested for this research project. 24 trabeculae were successfully harvested from vertebrae of CON-treated animals, 28 trabeculae from vertebrae of RAL-treated animals and 30 trabeculae from ALN-treated animals.

These samples were utilized as a wealth of complementary data exists from other tissues in these animals that is suggestive of changes in material properties and damage behavior due to these drug treatments. Additional data also suggest that raloxifene may produce fundamentally different effects at the tissue level compared to bisphosphonates. [3]

It should be mentioned that trabeculae excised from femoral heads of humans as well as bovine bones were used for practice purposes, showing that dimensions of these trabeculae are larger than trabeculae found in vertebrae of the mentioned beagle dogs (canine). Trabeculae found in dog vertebrae used for this project were rather plate-like (rectangular cross-section) than ro-likes (circular cross-section), with almost the same average length as height (aspect ratio of ~1). Table 4.1 lists a comparison of the sizes of human, bovine and canine trabeculae, which are measured from micro-CT datasets and the open source software ImageJ.

Die approbierte gedruckte Originalversion dieser Diplomarbeit ist an der TU Wien Bibliothek verfügbar.
The approved original version of this thesis is available in print at TU Wien Bibliothek.
TU Bibliothek Your knowledge hub WIEN

Table 4.1: Comparison of trabecualae dimensions

	Human	**Bovine**	**Canine (beagle)**
Minimal Width (average) [μm]	160	176	124
Minimal Height (average) [μm]	100	193	194
Length (average) [μm]	800	648	204

To keep all bone samples hydrated during storage, vertebrae were wrapped in cloth, which was soaked in Hank's Buffered Salt Solution (HBSS) with a pH of 7.4 and singe trabeculae were put into vials filled with the same HBSS. Vertebrae were frozen at -18°and excised single trabeculae were refrigerated at 3°C to prevent damage from additional freeze thaw cycles.

4.2 Sample Preparation

4.2.1 Sectioning of Vertebrae

Frozen dog vertebrae from a previous animal study were defrosted at room temperature. Excessive fat and other soft tissue were removed using scalpels and tweezers. Vertebrae are shown before and after removing soft tissue in figure 4.1 and 4.2 respectively. This was a necessary step since bone cutting blades that are not ideal for cutting soft tissue were used.

Die approbierte gedruckte Originalversion dieser Diplomarbeit ist an der TU Wien Bibliothek verfügbar.
The approved original version of this thesis is available in print at TU Wien Bibliothek.

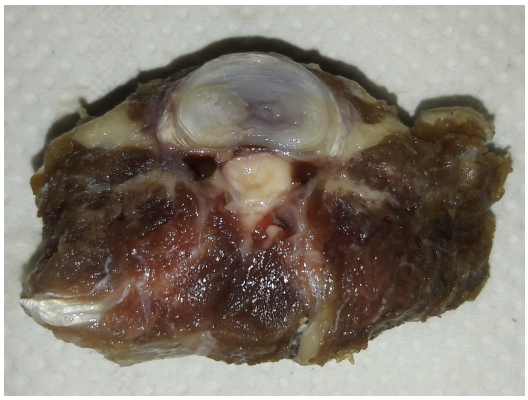

Figure 4.1: Vertebrae (with soft tissue)

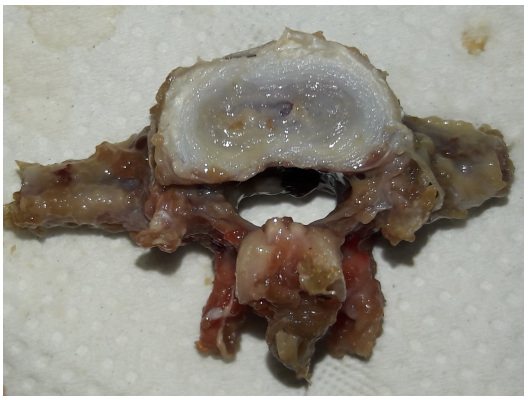

Figure 4.2: Vertebrae (removed soft tissue)

The vertebrae were cut into 300 μm cross-sectional slices using a Buehler IsoMet low speed saw shown in figure 4.3. To avoid fraying of the samples' cut surface, low speed, distilled water as a coolant and lubricant and no additional weights for feeding were used.

Figure 4.3: IsoMet

Die approbierte gedruckte Originalversion dieser Diplomarbeit ist an der TU Wien Bibliothek verfügbar.
The approved original version of this thesis is available in print at TU Wien Bibliothek.
TU Bibliothek Your knowledge hub WIEN

4.2.2 Excising of Single Trabeculae

Marrow was removed using a dental water jet (OralB, Germany) to unveil the trabecular structure. This was done under water, inside a big measurement cup, to avoid splashing and damaging of trabeculae. Figure 4.4 shows vertebrae slices before and after marrow removal.

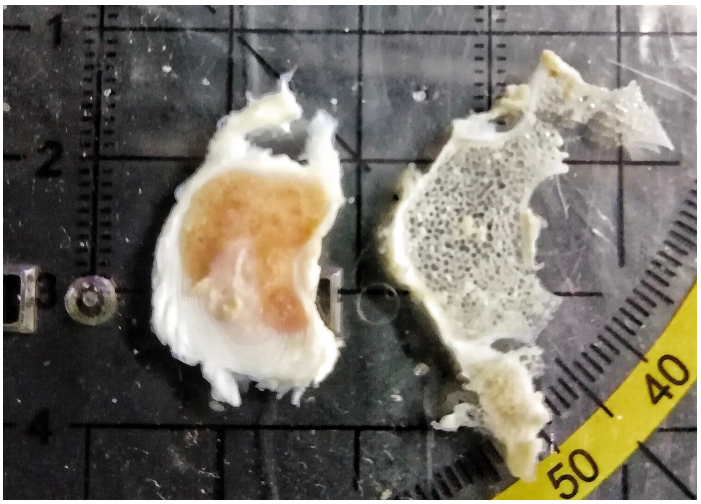

Figure 4.4: Vertebrae slices before and after marrow removal

Slices were then put into a Petri dish filled with HBSS to prevent them from drying out.

The previously cut slices were inspected using a stereo microscope (SZX10, Olympus Corporation, Japan), to identify suitable trabeculae, which ideally have circular cross-sections with an aspect ratio of 3 and a length of 500 μm. Surprisingly, trabeculae from vertebrae of beagle dogs have primarily plate like cross-sections and a length of 200 μm. Furthermore, it had to be ensured that enough bone material was present at each end of the trabeculae to embed the ends into epoxy. This was necessary to mount the samples to the sample holder of the load frame. Tweezers were used to hold the samples in position while trabeculae were excised using a triangular shaped scalpel with a sharp

Die approbierte gedruckte Originalversion dieser Diplomarbeit ist an der TU Wien Bibliothek verfügbar.
The approved original version of this thesis is available in print at TU Wien Bibliothek.
TU Bibliothek Your knowledge hub WIEN

point and flat cutting edge. This was an extremely delicate procedure. No pressure but rather a sawing movement had to be applied to avoid damaging of the trabeculae. (For other studies, where larger trabeculae were excised, a Dremel 400 DIGITAL hand milling tool with a diamond dental drill was used.) To ensure a strong embedding, each end of the trabeculae had to have a larger cross-section than the trabecula shaft to avoid embedment failure or failure outside the shaft. The black dotted lines in figure 4.5 show examples of where to cut to excise single trabeculae from a vertebral slice.

Figure 4.5: Excample on where to cut to excise a specimen

Trabeculae were often mistaken with plates since the microscopic 2D view from the top makes it hard to perceive detailed depth information. The best method to guess the thickness of trabeculae was to look for transparency, which is a good indication for small diameters. Nevertheless, vertebrae were cut into very thin slices (300μm) to limit the depth-dimension of the plates, which then got almost square cross-sections and therefore could also be used for this research project.

Die approbierte gedruckte Originalversion dieser Diplomarbeit ist an der TU Wien Bibliothek verfügbar.
The approved original version of this thesis is available in print at TU Wien Bibliothek.
TU Bibliothek Your knowledge hub WIEN

4.2.3 Micro-CT-Imaging and Measurement of Trabeculae

After excision, trabeculae were imaged with micro-CT to obtain information about their geometry, size and mineral density, which was needed to analyse stress-strain-curves and for complementary FE-simulations. To keep samples immobilized in an upright position, trabeculae were stuck to a slice of plastic by using a thin layer of play doh as an adhesive agent. This plastic slice was then inserted into a sample tube, which was filled with HBSS, to prevent the samples from drying. Samples were scanned using a micro computed tomography system (μCT100, Scanco Medical AG, Switzerland) at a nominal resolution of 3.3 μm, an integration time of 200 ms and 1500 projections. Furthermore, an aluminium filter of 0.5 mm, a voltage of 55 kV and a current intensity of 145 μA were used. The open source software ImageJ was then used to measure the length, width, height and cross-sectional area of the trabeculae from the gray-scale micro-CT datasets. Width and height were measured using straight freehand lines, which were drawn perpendicular from one border to the other border of the trabeculae's cross-section. The area was measured using the freehand selection tool by tracing the contours of the trabeculae's cross-sectional border, which automatically calculated the internal area. All measurements were taken at the trabeculae's thinnest location. A previous study, by Frank et al., has shown that there are little differences in cross-sectional surface area when using a volume divided by length approach instead of measurements at the thinnest location, but that the most representative value lies in between of them. [24] Original grey-scale images were opened as image sequences, where the beginning and the end of each trabeculae were found at areas where significant changes of the bones' cross-section area were observed. The number of images showing the trabeculae region multiplied with the resolutions in longitudinal direction of the scanner (3.3 μm) gives the length of the trabeculae. Table 4.2 shows the arithmetic mean values of the trabeculae dimensions.

Die approbierte gedruckte Originalversion dieser Diplomarbeit ist an der TU Wien Bibliothek verfügbar.
The approved original version of this thesis is available in print at TU Wien Bibliothek.
TU Bibliothek Your knowledge hub WIEN

Table 4.2: Arithmetic mean values of trabeculae dimensions

Minimal Width (average)	124 [μm]
Minimal Height (average)	194 [μm]
Length (average)	204 [μm]
Minimal cross-sectional Area (average)	192 [μm^2]

Furthermore, **bone mineral density (BMD)** measurements were done using the acquired CT-datasets. It is crucial to distinguish between areal bone mineral density (aBMD) and the material bone mineral density measured in this project (for reasons of simplification in the following referred to as BMD). aBMD is the bone mineral density used to determine fracture risk in patients by measurement of, e.g. femoral heads, where an average density is calculated, taking into account not only bone tissue, but also marrow cavities, haversian canals, etc. In contrast, BMD determined in this project was measured from individual trabeculae at the tissue level, which results in higher density values. Measurements were executed with a calibrated micro-CT, by using a phantom with a defined hydroxyapatite (HA) desity of 800 mg/cm^3. Thus extrapolations of the micro-CTs gray-values (Houndsfield Units) into densities were necessary, since bone has a higher density of approximately 1000 $mgHA/cm^3$.

4.2.4 Embedding of Trabeculae

Excised specimens include surrounding tissue that was embedded using custom-made silicone-molds to produce circular epoxy end-pieces. These were made to fit custom sample holders for a small-scale mechanical testing system (SEL-mini, Thelkin AG, Switzerland). To obtain the right dimensions for the silicon molds, a negative of the sample holder was made from epoxy and polished to perfectly fit into the sample holder of the testing system with a small clearance. This

Die approbierte gedruckte Originalversion dieser Diplomarbeit ist an der TU Wien Bibliothek verfügbar.
The approved original version of this thesis is available in print at TU Wien Bibliothek.
TU Bibliothek Your knowledge hub WIEN

approach enabled easy movement of the samples, which should prevent them from additional damage. The silicone used to manufacture the molds was a two compounds picodent twinsil addition-curing duplicating silicone with a shore hardness of 22. Its elasticity was necessary to enable embedding and removal of the sample from the mold. A small groove was cut into the mold, which was used to inspect the samples from the side with a mirror to ensure exact positioning during embedding. Furthermore, a light microscope (Zeiss Axio Imager, Carl Zeiss AG, Germany) was used for the last fine alignment by using changes in focus. The finished mold is shown in 4.6.

Figure 4.6: Silicone mold for trabeculae embedment

The whole embedding procedure had to be carried out extremely carefully under a stereomicroscope and the usage of tweezers. Samples were prone to damage and even minimal deviations in position could have a huge impact on the test results. Play doh was rolled into many thin strings and staged into the center of the mold. These strings had to be aligned with the groove and carefully pressed together to build a tiny wall, up to about two third of the mold's depth, to separate the two circular end piece cutouts. This was to prevent the later inserted epoxy from flowing around the samples' trabecular, which was placed inside the central area of the mold, right on top of the play doh. It was very important to ensure a horizontal positioning of the trabecula. Only the

Die approbierte gedruckte Originalversion dieser Diplomarbeit ist an der TU Wien Bibliothek verfügbar.
The approved original version of this thesis is available in print at TU Wien Bibliothek.
TU Bibliothek Your knowledge hub WIEN

trabeculae had to be in contact with the play doh wall. Both ends of the samples had to be free from play doh and pointing towards the circular end piece cutouts of the mold to allow epoxy flowing around them. More play doh strings were then placed on top of the trabeculae and carefully pressed together to finish the wall up to the top of the mold. The whole trabecula had to be covered with play doh, which protected it from the epoxy and kept it in position. The ends of the sample were still free. Finally, the two-component epoxy (UHU Plus Endfest 300, Germany) was mixed together and put into a vacuum to remove trapped air, dyed with black ink to get a better contrast between bone and epoxy, and added into the circular end piece out cuts of the mold.

After the epoxy has cured for sixteen hours in air at room temperature, the samples were removed from the mold. This was done by first using a very thin needle to remove the play doh from the trabeculae and the epoxy. Then a small pen was placed underneath the mold, aligned with the samples' longitudinal-axis to apply a slight and well distributed pressure from the bottom of the mold. The flexible mold was then carefully bent around the pen while stretching the mold around the circular end piece cutout to widen and loosen this area without introducing any bending moment to the sample. The samples should fall out by themselves at this point. Paper towels were used to prevent samples from breaking when falling. Finally, a scalpel was used to cut off excessive parts of the epoxy. Figure 4.7 shows an embedded sample next to a quarter dollar coin to illustrate its size.

Die approbierte gedruckte Originalversion dieser Diplomarbeit ist an der TU Wien Bibliothek verfügbar.
The approved original version of this thesis is available in print at TU Wien Bibliothek.
TU Bibliothek Your knowledge hub WIEN

Figure 4.7: Embedded trabecula, next to a quarter dollar coin.

4.2.5 Application of the Speckle Pattern

A speckle pattern was administered to samples for optical strain tracking during the tensile tests. Due to the tiny size of the samples, a very fine pattern was needed. The pattern had to consist of very small dots, equally distributed over the whole trabecular surface. Therefore, the samples could not be sprayed directly, which would have covered the whole sample-surface with color. Thus, samples were put into a corner of a box and an indirect mist of a black spray paint can (RAL9005, Dupli-Color, Motip dupli, Germany) was used by spraying to the opposite corner for about three seconds. Right after, the box was closed for about five minutes to allow the scattered color particles to settle down on the trabeculae's surface. A stereo microscope was used to check the speckle pattern and the whole procedure was repeated until the desired pattern was reached. Usually three to four rounds were enough to obtain good results.

Die approbierte gedruckte Originalversion dieser Diplomarbeit ist an der TU Wien Bibliothek verfügbar.
The approved original version of this thesis is available in print at TU Wien Bibliothek.
TU Bibliothek Your knowledge hub WIEN

4.3 Mechanical Testing of Individual Trabeculae

Samples were tested at the "Interfacultary Laboratory for Micro- and Nanomechanics of Biological and Biomimetical Materials" at the TU Wien. Before testing, samples were hydrated for at least 2 hours by putting them into HBSS to mimic a physiological environment. Frank et al. have shown that trabeculae's material properties are strongly dependent on their level of hydration. [27]

4.3.1 Setup

Tests were performed with a small-scale mechanical testing system (SELmini - 001, Thelkin AG, Switzerland), which is a servo-electric load frame. To measure loads, a 10N load cell (HBM-S2M,Germany) with a relative error of 0.02% was used. A horizontal bar was fixed above the load cell and two magnetic security stops were attached to the sides of the load frame acting as a latch to avoid damage of the samples and the load cell due to erroneous behavior of the testing system. This was important since an unintended load or displacement limit overshoot would have caused a drop of the load cell. To ensure hydration during test execution, samples were placed in a custom-made sample holder inside a HBSS-filled water bath. The bottom part of the sample holder was mounted inside the water bath that sat on the load frame's base plate, which could be positioned by screws guided inside t-slots. This was important since both parts of the sample holder had to get exactly aligned to avoid sheer stress and ensure uni-axial loading while tests were performed. The top part of the sample holder was mounted to the load cell. The circular notches of the custom-made sample holder corresponded to the epoxy end-pieces of the samples and had a small clearance to allow self-alignment when a pre-load was applied. Furthermore,

Die approbierte gedruckte Originalversion dieser Diplomarbeit ist an der TU Wien Bibliothek verfügbar.
The approved original version of this thesis is available in print at TU Wien Bibliothek.
TU Bibliothek Your knowledge hub WIEN

flaps were installed over the notches to prevent samples from tilting forward. It turned out that using only the top flap leads to the best results and minimizes the risk of damaging the samples. These were further important measures to ensure uni-axial loading. A video camera (UI-3250CP-M-GL, IDS GmbH, Germany) with a KITO-D zoom objective (mounted on a KITO-ADP-0.5 adapter, Kitotec GmbH, Germany) was used to assess sample strain and movement during test execution as well as the alignment of the top and bottom sample holder and the samples. Videos were recorded with a frequency of 10Hz. A 2-branch cold LED light source system for microscopy applications (SCHOTT) was used to illuminate the samples. The test setup is shown in figure 4.8

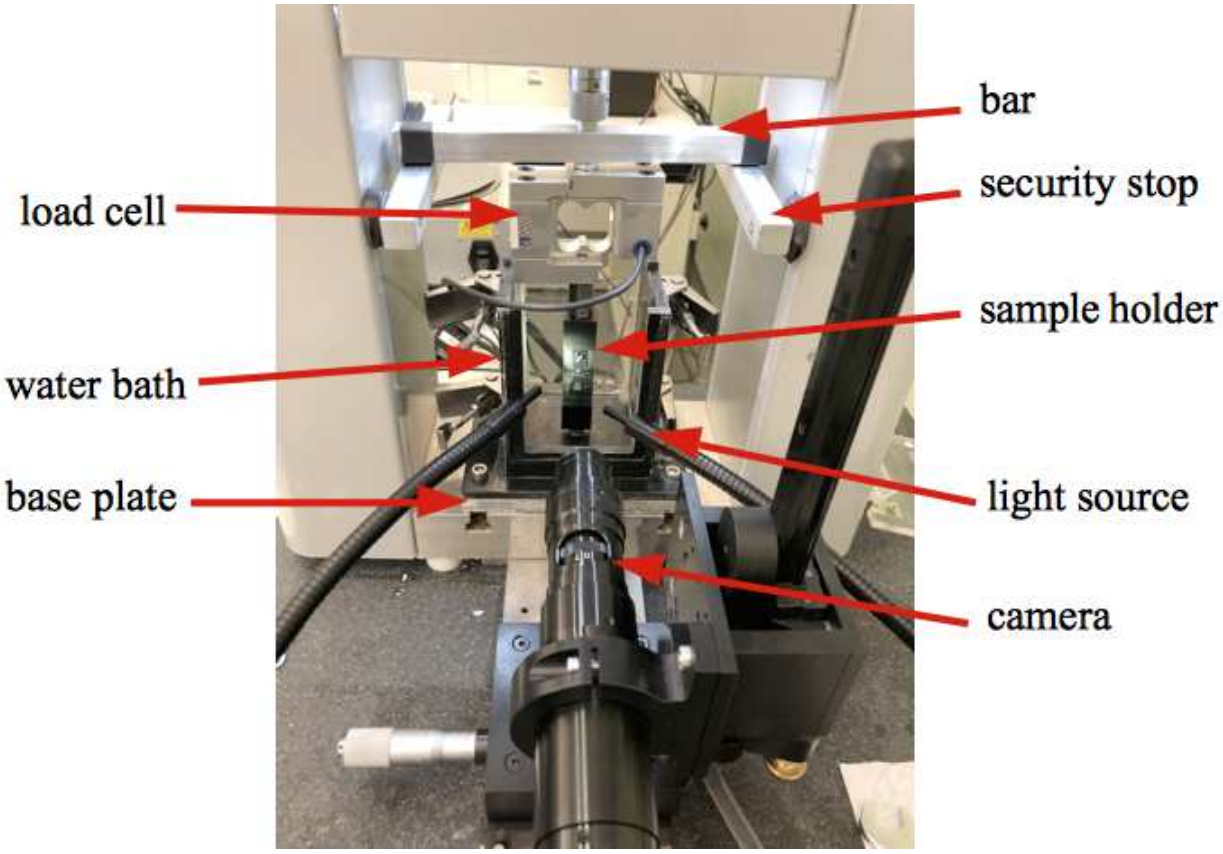

Figure 4.8: Test setup, borrowed from [22]

Die approbierte gedruckte Originalversion dieser Diplomarbeit ist an der TU Wien Bibliothek verfügbar.
The approved original version of this thesis is available in print at TU Wien Bibliothek.
TU Bibliothek Your knowledge hub WIEN

All tests were performed with displacement control (force-controlled tests have shown inferior stability). Cyclic loading was performed with an increasing step function as the testing profile, which specified the position over time as shown in figure 4.9. Thus samples experienced alternating tension and relaxation, leading to slower crack-initiation and propagation. As a consequence, damage was detected earlier, which made it easier to stop tests prior to failure.

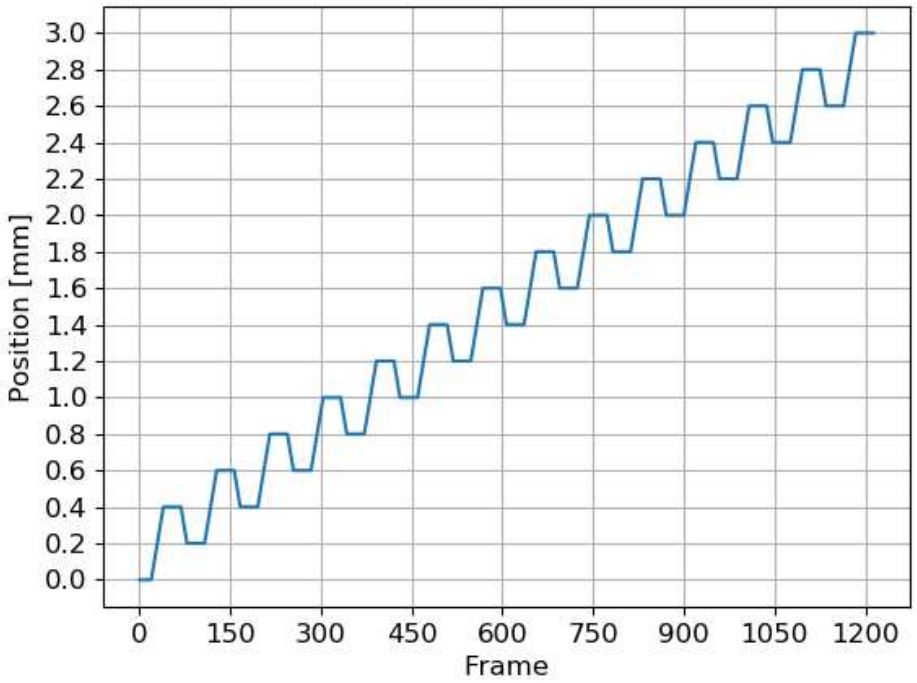

Figure 4.9: Testing Profile

Limits for positions were set reasonable, but higher than needed, since each test was stopped manually before reaching them and limits for loads were set according to the load frame boundaries. Tuning settings, which were specific control engineering settings, had to be arranged to achieve a satisfying signal for a smooth displacement control. Table 4.3 shows the final profile and logging settings, as well as the chosen limits and tuning settings for the Telkin software.

Die approbierte gedruckte Originalversion dieser Diplomarbeit ist an der TU Wien Bibliothek verfügbar.
The approved original version of this thesis is available in print at TU Wien Bibliothek.
TU Bibliothek Your knowledge hub WIEN

Table 4.3: Telkin Settings

Profile Settings:		**Logging Settings:**	
Control Mode:	Position	**Log. Offset:**	0
Prof. Frequ.:	0.002 [Hz]	**Nr. of Log. Cycles:**	6000
Nr. of Cycles:	1	**Nr. of Log. Blocks:**	1
Profile Source:	Custom	**Log. Frequ.:**	10 [Hz]
Limits:		**Tuning:**	
Max Position:	25 [mm]	**Kp:**	1.5
Min Position:	-3 [mm]	**KV:**	1.5
Max Load:	10 [N]	**Ti:**	12
Min Load:	-10 [N]	**Kp Load:**	30
		Ti Load:	0.2

4.3.2 Stop Criterion

Destructive as well as nondestructive tests were performed to determine material properties and microscopic damage behavior of individual trabeculae. Therefore, a stop criterion had to be used, which made it possible to stop the tests before total failure of the samples but ensured existing damage inside the trabeculae. Thurner et al. have shown that trabeculae whiten at damaged regions. [54]. Thus the **whitening effect**, as a visual stop criterion, turned out to be the easiest and most reliable way to determine emerging microdamage inside the bones during tests. Figure 4.10 shows the whitening effect at a trabecular shaft under tension at different strains.

Another stop criterion is based on a change of the elastic modulus, which also indicated damage initiation. Therefore, the Load-Displacement curve was observed to detect nonlinearities. However, it was not possible to stop tests

Die approbierte gedruckte Originalversion dieser Diplomarbeit ist an der TU Wien Bibliothek verfügbar.
The approved original version of this thesis is available in print at TU Wien Bibliothek.
TU Bibliothek Your knowledge hub WIEN

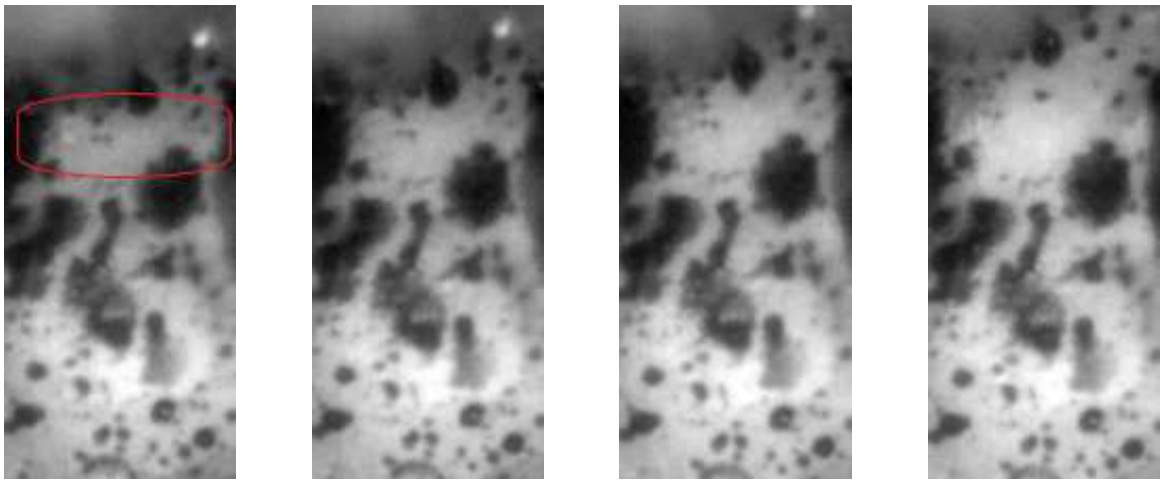

(a) $\varepsilon = 0$ (b) $\varepsilon = 0.04$ (c) $\varepsilon = 0.08$ (d) $\varepsilon = 0.11$

Figure 4.10: Whitening during tensile test at different strains ε. Region of whitening onset labeled with a red circle

prior to failure using this criterion.

4.3.3 Test Procedure

After setting up the mechanical testing system according to section 4.3.1, two trial runs without a sample and without the load cell had to be performed. This was due to erroneous behavior of the system during the first two measurements of each session, which could have led to uncontrollable movement and damage of both parts. Further trial runs had to be performed by using an epoxy sample and the load cell to ensure exact alignment of the sample holders and the samples. This was done by observing video data provided by the camera setup at maximum magnification. Any unwanted movements of the sample indicated bad alignment of the holder. The software packet (μEye Cockpit) was used in monochrome mode. JPEG quality was set to 100% and "Calc Frame" to 10. Furthermore, the Telkin settings were verified by observing the load displacement curve of the Telkin software. These runs were stopped prior to

Die approbierte gedruckte Originalversion dieser Diplomarbeit ist an der TU Wien Bibliothek verfügbar.
The approved original version of this thesis is available in print at TU Wien Bibliothek.
TU Bibliothek Your knowledge hub WIEN

5N to not risk a limit overshoot, which could have damaged the load cell. Trial runs had to be performed until all requirements were fulfilled.

Then, single trabeculae samples, which were hydrated for at least 2 hours by putting them into HBSS, were tested. They were put into the sample holder where only the top flap was used to fix the epoxy top end piece of the sample to avoid tilting. Due to hydration of the samples, adhesion effects were pulling the samples inside the sample holder without the need for external forces. (This effect also had to be taken care of when removing samples from the sample holder after testing.) The next step was to fill up the water bath, in which the samples were mounted, with HBSS (pH = 7.4), to mimic a physiologic environment during tests. Following, a reasonable pre-load was applied, which was dependent on the samples that were tested. This was done by checking the samples for further alignments due to clearance at the sample-fixture interface. Usually, a pre-load of 0.05N to 0.2N was sufficient. These differences in pre-loads were later being taken under consideration by linear extrapolations in Python as illustrated in figure 4.11.

Die approbierte gedruckte Originalversion dieser Diplomarbeit ist an der TU Wien Bibliothek verfügbar.
The approved original version of this thesis is available in print at TU Wien Bibliothek.
TU Bibliothek Your knowledge hub WIEN

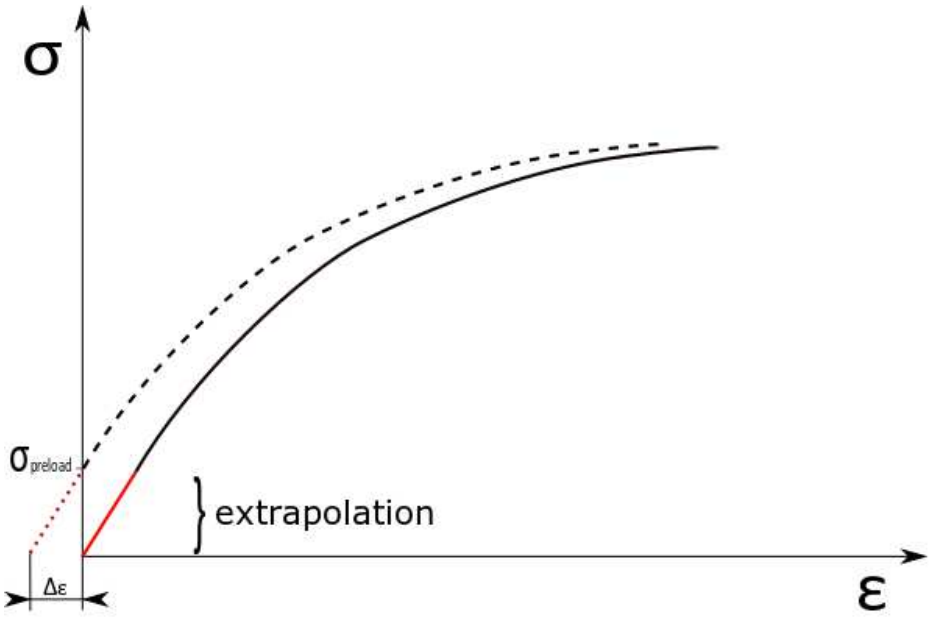

Figure 4.11: Illustration of how pre-loads were taken under consideration. Linear extrapolation of the stress-strain diagram from the pre-loads and shifting the whole curve for $\Delta\varepsilon$ into the zero point.

Finally, after setting the displacement to zero, the testing system and the camera recording were started and stopped when whitening or failure occurred. Due to a limited video buffer of the camera, test-runs that exceeded 4 GB of video-data had to be paused and a new video had to be started.

After testing, the water bath was evacuated, and the samples were removed carefully to avoid further damage. They were then stored in 30% EtOH inside small vials and packed for shipment to the laboratory at the IUPUI in Indianapolis USA for microdamage analyses.

Die approbierte gedruckte Originalversion dieser Diplomarbeit ist an der TU Wien Bibliothek verfügbar.
The approved original version of this thesis is available in print at TU Wien Bibliothek.
TU Bibliothek Your knowledge hub WIEN

4.4 Analysis of Mechanical Test-Data

Mechanical data were determined with Python scrips, using information from video data (image sequences), which were processed with ImageJ.

4.4.1 Strain Determination

A video camera (UI-3250CP-M-GL, IDS GmbH, Germany) with a KITO-D zoom objective (mounted on a KITO-ADP-0.5 adapter, Kitotec GmbH, Germany) was used to assess strain during mechanical tests. Video data was imported into the open source software ImageJ. After converting to grayscale, images were cropped at the top and bottom onset of the curvature and at the sides to only show the trabeculae shafts. The plugin StackReg was used to remove translational rigid body movement of the whole trabeculae through a subpixel registration algorithm. [52] Brightness and contrast were adjusted using the automated build in tool of ImageJ. Resulting data was saved as a tiff-image sequences. The Python scrip trackpy (v.0.3.2, 2016, [18]), which is a particle tracking algorithm, was used to determine the trajectories of individual points from the spackle pattern throughout the whole image sequences. It tracks the centroids of these points using subpixel resolution. According to Savon and Doyle ([47]) an estimation of the median uncertainty in particle location was calculated as 0.4 μm. Approximately 6, over the width distributed pairs of points, close to the top and bottom region at the onset of the curvature of the trabeculae, were selected by the algorithm. To determine the trabecula's change in length ΔL, the average changes in distance between corresponding points were calculated as shown in figure 4.12.

Die approbierte gedruckte Originalversion dieser Diplomarbeit ist an der TU Wien Bibliothek verfügbar.
The approved original version of this thesis is available in print at TU Wien Bibliothek.
TU Bibliothek Your knowledge hub WIEN

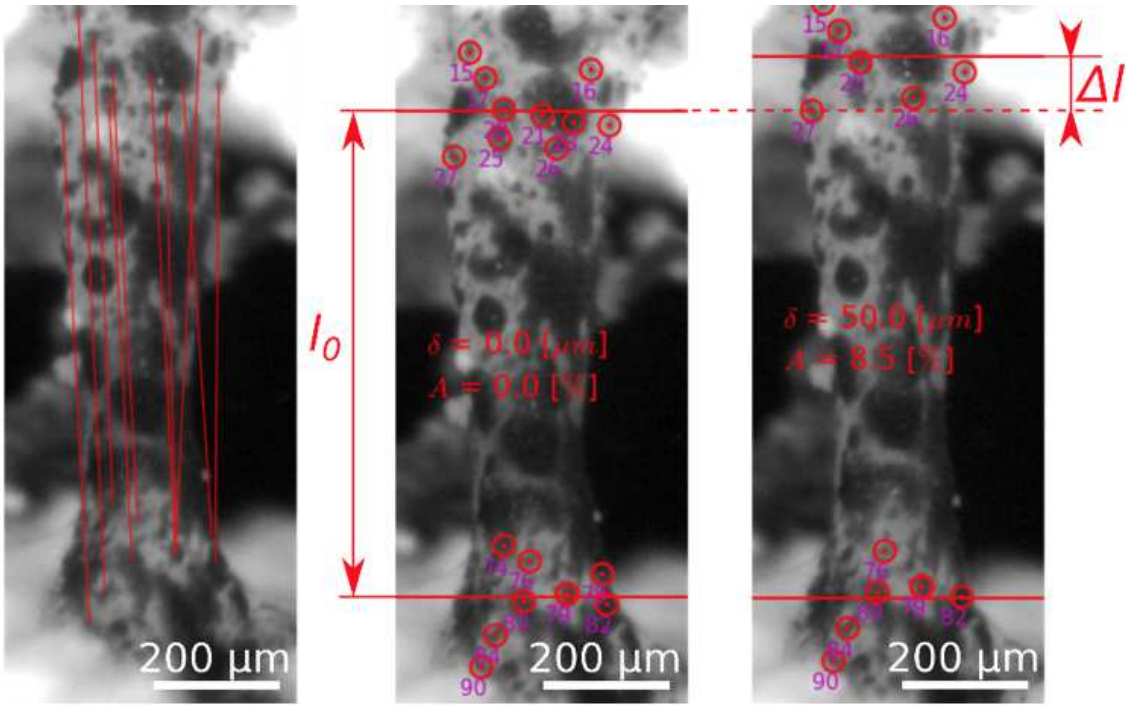

Figure 4.12: Example for point tracking with trackpy at a bovine trabeculae from a previous study [22]. Left: Length between corresponding points in the first frame. Middle: Average distance between corresponding points at preload l_0. Right: Average length right before fracture and change in length Δl

Hydrated trabeculae reach relatively large ultimate strains. Strains sometimes exceed 10%, as already shown by M. Frank et al.[26] Therefore true strain ε_T, rather than engineering strain ε_E[4] had to be used. True strain was calculated according to [36] as

[4] If $\Delta L \ll L$ then $L \approx L_0$

$$\varepsilon_E \equiv \frac{1}{L_0}\int_{L_0}^{L_F} dL = \frac{L_F - L_0}{L_0} = \frac{\Delta L}{L_0} \tag{2}$$

Die approbierte gedruckte Originalversion dieser Diplomarbeit ist an der TU Wien Bibliothek verfügbar.
The approved original version of this thesis is available in print at TU Wien Bibliothek.

$$\varepsilon_T \equiv \int_{L_0}^{L_F} \frac{dL}{L} = ln(\frac{L_F}{L_0}) = ln(1 + \frac{\Delta L}{L_0}) = ln(1 + \varepsilon_E) \tag{3}$$

where L_0 is the initial and L_F the final mean length of the trabecula. [25]

Load and displacement data from the load cell and the Telkin-software were manually synchronized. This was done by searching for a drop in the load signal and a corresponding drop in the displacement signal, which indicated the point of failure of the samples. In cases where tests were stopped prior to failure, data was synchronized through comparison of noticeable changes of both signals.

4.4.2 Stress Determination

Stress was determined using the trabeculae's minimal cross-sectional area A_{min}, which was measured from μCT-scans with the open source software ImageJ as described in section 4.2.3. Due to large deformations, as already mentioned earlier, true stress σ_T was calculated using engineering stress σ_E according to [5]:

$$\sigma_T = \sigma_E(1 + \varepsilon_E) \tag{4}$$

with engineering stress calculated as

$$\sigma_E = \frac{F}{A_{min}} \tag{5}$$

where F is the load measured from the load cell. [25]

4.4.3 Material Properties Determination

Material properties of the bone were described by two different constitutive behaviors, one for the elastic and one for the post yield region. For the linear

Die approbierte gedruckte Originalversion dieser Diplomarbeit ist an der TU Wien Bibliothek verfügbar.
The approved original version of this thesis is available in print at TU Wien Bibliothek.
TU Bibliothek Your knowledge hub WIEN

elastic region, the behavior is given by Hooke's law

$$\sigma_T = E * \varepsilon_T \tag{6}$$

where E represents the Young's modulus, which was calculated using the slope of a linear regression according to [50]. Herein, the R^2 value was calculated as a function of the used data window. The size of the data window, which was defined by the number of used frames, changed the residuals and the R^2 value. A larger data window in the linear region results in smaller residuals and a larger R^2 value. On the contrary, a larger data window at the non-linear region results in larger residuals and a smaller R^2 value. Thus, the yield point was defined by the frame that corresponds to the maximum R^2 value and yield stress σ_y as well as yield strain ε_y were determined at this point.

For the non-linear region, where current strain exceeds yield strain, the constitutive behavior is given by

$$\sigma_T = \sigma_y + \sigma_h * (1 - e^{(-B*\varepsilon_{pl})}) \tag{7}$$

where σ_h represents hardening stress, ε_{pl} the plastic strain, and B the hardening coefficient.

Hardening stress σ_h was calculated as

$$\sigma_h = \sigma_u - \sigma_y \tag{8}$$

where σ_u represents the ultimate stress and the plastic strain ε_{pl} was calculated as

$$\varepsilon_{pl} = \varepsilon_T - \varepsilon_y. \tag{9}$$

The hardening coefficient B was determined with an exponential fit of data using SciPy (V0.18.0). Ultimate stress σ_u and ultimate strain ε_u were determined at

Die approbierte gedruckte Originalversion dieser Diplomarbeit ist an der TU Wien Bibliothek verfügbar.
The approved original version of this thesis is available in print at TU Wien Bibliothek.
TU Bibliothek Your knowledge hub WIEN

the last recorded point and therefore should not be confused with maximum stress σ_{max} and strain at maximum stress $\varepsilon_{[\sigma_{max}]}$. These values provide even less (ultimate)information for samples where tests were stopped prior to failure, and therefore have to be handled very carefully. Numerical integration of the stress-strain curve from zero to the yield point ε_y was used to calculate elastic work W_{el}

$$W_{el} \equiv \int_0^{\varepsilon_y} d\sigma_T \tag{10}$$

whereas integration from the yield point ε_y to failure ε_u was used to calculate post yield work W_{py}

$$W_{py} \equiv \int_{\varepsilon_y}^{\varepsilon_u} d\sigma_T, \tag{11}$$

which was also neglected for samples where tests were stopped prior to failure. These integrations were done using the *trapz* function of numpy (V 0.18.0). [25]

4.5 Labeling of microscopic damage

4.5.1 Basic Fuchsin

Microscopic damage of trabecular bone specimens tested in Austria was assessed in the USA at D. Burr's laboratory using an adjusted, from Burr and coworkers developed, en-bloc staining approach with basic fuchsin. [10] For this, specimens were first preserved for 48 hours or longer in 70% ethanol (EtOH). Thereafter they were stained in 1% basic fuchsin in a graded series of alcohols under vacuum. Basic fuchsin from J.T. Baker (Phillipsburg, NJ, Cat. No. B660-03) was made up in a series of 1% stock solutions in 80%, 95%, and 100% EtOH. It does not easily go into solution and therefore was stirred for several hours or overnight. Times for each solution depend on the size and density of the bone. Multiple

Die approbierte gedruckte Originalversion dieser Diplomarbeit ist an der TU Wien Bibliothek verfügbar.
The approved original version of this thesis is available in print at TU Wien Bibliothek.
TU Bibliothek Your knowledge hub WIEN

additionally harvested test-samples were stained for different times to find a suitable protocol for single trabeculae. It turned out that staining-times of one hour per step yields the most satisfying results. Following preservation in 70% EtOH, specimens were placed in the following solutions under a 20-psi vacuum:

1. 1% basic fuchsin in 80% EtOH for one hour under a 20-psi vacuum.
2. Change solution.
3. 1% basic fuchsin in 80% EtOH for one hour under a 20-psi vacuum.
4. Change solution.
5. 1% basic fuchsin in 90% EtOH for one hour under a 20-psi vacuum.
6. Change solution.
7. 1% basic fuchsin in 90% EtOH for one hour under a 20-psi vacuum.
8. Change solution.
9. 1% basic fuchsin in 100% EtOH for one hour under a 20-psi vacuum.
10. Change solution.
11. 1% basic fuchsin in 100% EtOH for one hour under a 20-psi vacuum.
12. Change solution.
13. Rinse in 100% EtOH for 30 minutes under a 20-psi vacuum to remove excess stain.
14. Change solution
15. Rinse in 100% EtOH for 30 minutes under a 20-psi vacuum to remove excess stain.

Finally, specimens were stored in 70% EtOH.

Die approbierte gedruckte Originalversion dieser Diplomarbeit ist an der TU Wien Bibliothek verfügbar.
The approved original version of this thesis is available in print at TU Wien Bibliothek.
TU Bibliothek Your knowledge hub WIEN

4.5.2 Barium Sulfate

Another approach to detect bone microdamage was by using micro-CT. With this technique a three-dimensional assessment of microdamage density and spatial distribution within the bone can be done without the need for histological sectioning. Bones were therefore labeled with the contrast agent barium sulfate ($BaSO_4$). Each sample was scanned before and after staining. Different staining protocols were used and modified multiple times to get satisfying results for single trabeculae, which was not possible during the time frame of this research project.

First, two separate solutions were made up by mixing 6.1065 g barium chloride ($BaCl_2$) or 3.551 g sodium sulfate (Na_2SO_4) into double-deionized water with a magnetic stirrer. Due to precipitation after a couple of minutes after stirring, new solutions were prepared on top of a hot plate (~50°C). No precipitation was observed after this measure.

Calculations for barium chloride solution of 50mL using double-deionized water:[5]

$$\frac{50\,mL\ solution * 0.5\,mol\ BaCl_2 * H_2O}{1000\,mL\ solution} * \frac{244.26\,g\ BaCl_2 * H_2O}{1\,mol\ BaCl_2 * H_2O} = 6.1065\,g$$

Calculations for sodium sulfate solution of 50mL using double-deionized water:[6]

$$\frac{50\,mL\ solution * 0.5\,mol\ Na_2SO_4}{1000\,mL\ solution} * \frac{142.04\,g\ Na_2SO_4}{1\,mol\ Na_2SO_4} = 3.551\,g$$

To spare previously and arduously prepared and tested samples, newly and carelessly (to ensure incurrence of damage) harvested single trabeculae samples were used to study different protocols.
Since no expertise on individual trabeculae was available, the unmodified protocol according to Wang et al.[55], developed for 8.21 mm cores of trabecular

[5]Molar Mass of $BaCl_2 * H_2O$ = 244.26 grams/mol (Sigma-Aldrich Product # 217565-500G)
[6]Molar Mass of Na_2SO_4 = 142.04 grams/mol (Sigma-Aldrich Product # 239313-1KG)

Die approbierte gedruckte Originalversion dieser Diplomarbeit ist an der TU Wien Bibliothek verfügbar.
The approved original version of this thesis is available in print at TU Wien Bibliothek.
TU Bibliothek Your knowledge hub WIEN

bone, was used as a first try, with both, the previously heated and unheated (during preparation) solutions as follows:

1. Specimens were soaked in an aqueous solution of 0.5 mol $BaCl_2$ for 48 hours under a 20-psi vacuum.
2. Specimens were then soaked in an aqueous solution of 0.5 mol Na_2SO_4 for 48 hours under a 20-psi vacuum.
3. Specimens were agitated in buffer saline (PBS) solution for one hour to remove excessive $BaSO_4$.
4. Specimens were stored in buffered saline (PBS) solution.

Buffered saline (PBS) was mixed by dissolving 9.88 g of a concentrate containing 8 g of $NaCl$, 0.2 g of KCl, 1.44 g of Na_2HPO_4 and 0.24 g of KH_2PO_4. into 800 mL double-deionized water. The pH-value was adjusted to 7.3-7.5 using HCL or NaOH. Then the volume was raised to 1L with additional double-deionized water.

Results did not highlight cracks and thus made an assessment of microdamage impossible. Therefore, soaking times got changed to 24 and 32 hours without improvements.

Another protocol according to Landrigan et al., 2011, [17] originally developed for 2.5 mm cores of cortical bone was tested. Therefore, two new solutions were mixed, containing either 0.5 mol ($BaCl_2$) or 0.5 mol Na_2SO_4 in equal parts of buffered saline (PBS) and double-deionized water. Also these solutions got mixed with a magnetic stirrer. Due to precipitation after a couple of minutes after stirring, new solutions were prepared on top of a hot plate (~50°C). Again, no precipitation was observed after this measure. Landrigan's protocol was then used with both, the previously heated and unheated (during preparation) solutions as follows:

Die approbierte gedruckte Originalversion dieser Diplomarbeit ist an der TU Wien Bibliothek verfügbar.
The approved original version of this thesis is available in print at TU Wien Bibliothek.
TU Bibliothek Your knowledge hub WIEN

1. Specimens were soaked in a solution of equal parts buffered saline (PBS), 0.5 mol ($BaCl_2$) in deionized water, and acetone for 3 days under a 20-psi vacuum.
2. Specimens were rinsed with deionized water to minimize ions or particles on specimen surfaces.
3. Specimens were then soaked in a solution of equal parts buffered saline (PBS), 0.5 mol Na_2SO_4 in deionized water acetone, and 0.5 mol Na_2SO_4 in deionized water for 3 days under a 20-psi vacuum.
4. Specimens were rinsed with deionized water to minimize ions or particles on specimen surfaces.
5. Specimens were stored in buffered saline (PBS) solution.

Also this protocol, even after changing soaking times to 24 and 48 hours, did not lead to micro-CT images with highlighted cracks.

To make sure this was not due to missing damage inside the singe trabeculae samples, a rat femur from a previous fatigue test, which was loaded for 2 million load cycles in 3-point bending without breaking was used to test these staining methods. First the femur was cut in half using a hand held dremel at the mid shaft since greatest damage was assumed at this region. One half was stained using the protocol by Wang et al. and the other half by using the protocol according to Landrigan et al. with soaking times of each 48 hours. Due to cutting in half of the sample, stain could easily flow into the central bone cavity. However, again no valuable results were obtained.

Staining results were visualized using micro-computed tomography and discussed in section 6.3.

Die approbierte gedruckte Originalversion dieser Diplomarbeit ist an der TU Wien Bibliothek verfügbar.
The approved original version of this thesis is available in print at TU Wien Bibliothek.
TU Bibliothek Your knowledge hub WIEN

4.6 Micro-CT-Imaging

Non-destructive 3D images, based on micro-CT, were taken using a Bruker Skyscan 1172 micro-CT scanner. Samples were scanned prior and after labeling with the contrast agent barium sulfate ($BaSO_4$). Resolutions of 3 μm as well as 1.5 μm (image pixel size), an 0.5 mm aluminum filter, frame averaging of 2 and flat field corrections were used. A detailed list of the used settings, which led to the best image quality within an reasonable scanning time, is shown in the appendix 8.3. Each scan with a resolution of 1.5 μm took on average 3 hours in case no other programs such as NRecon, DataViewer or CTAn were running in the background, which prolonged the scanning time to up to 10 hours per scan. However, these scans did not yield expected results and will be discussed in section 5. Bunker's NRecon program was used to reconstruct the micro-CT scan projection images into cross-section images. [34] A detailed list of settings leading to best results is shown in the appendix 8.4. Numerous different settings for both scans and reconstructions were tested to obtain better results and to reduce scanning times without success.

Bruker's DataViewer software was used for 3D registration of scans from samples before and after labeling to make it easier to detect changes in gray values caused by $BaSO_4$. Followed steps can be found in the appendix 8.1.

Bruker's CTAn software was used to create threshold values to highlight stronger stained areas, which should coincide with damaged areas. Followed steps can be found in the appendix 8.2

4.7 CLSM Imaging

Previously tested (section 4.3.3) and basic fuchsin stained (section 4.5.1) samples were examined for microdamage using the CLSM (Zeiss Axiolab) at the TU

Die approbierte gedruckte Originalversion dieser Diplomarbeit ist an der TU Wien Bibliothek verfügbar.
The approved original version of this thesis is available in print at TU Wien Bibliothek.
TU Bibliothek Your knowledge hub WIEN

Wien.

4.7.1 Sample Preparation and Setup

Prior to microscopy, whole samples were embedded into the same empoxy as used for the circular end pieces (UHU Plus Endfest 300, Germany). Thus, a thin layer of epoxy was applied on glass microscopy sample slides. Each sample was then placed on a different slide on top of the still wet epoxy layer and additional epoxy was poured over the samples until they were completely covered. After curing for 16 hours samples were packed for shipment from the the IUPUI (Indianapolis, USA) to the TU Wien, where further preparations were executed.

In Vienna, excessive epoxy was milled off using a Dremel 400 DIGITAL hand milling tool. Progress was checked every couple of seconds under a stereo microscope (SZX10, Olympus Corporation, Japan). Wetted cotton swabs were used to remove milling dust from the samples to get a better view. Hand milling was stopped as soon as the trabeculae were visible, shortly before setting free of the trabeculae. Further milling was done by an ultramiller (Leica SP2600 [39]). First a pre-miller cutter was used until the surface of the trabeculae was reached. This was again checked under the stereo microscope at 6x magnification. From there a finishing miller was used for a couple of samples to mill down for additional 1 or 2 μm to get a smoother surface. Table 4.4 shows the settings used for the pre-miller and the finishing miller.

Die approbierte gedruckte Originalversion dieser Diplomarbeit ist an der TU Wien Bibliothek verfügbar.
The approved original version of this thesis is available in print at TU Wien Bibliothek.
TU Bibliothek Your knowledge hub WIEN

Table 4.4: Leica SP2600 Ultramiller settings

Setting Type	Value
Rotational Speed [rpm]	1200
Horizontal Feed [mm/s]	1.5
Vertical Feed (Pre-Miller) [μm/s]	2
Vertical Feed (Finishing Miller) [μm/s]	1

As already shown in a previous study [22], the surface quality was still not satisfying after using the finishing miller. This was probably due to light scattering on the samples surface. Therefore, samples were further polished by hand to reach a better surface quality. First, samples were ground with sandpaper with a grit number of 2400 for 3 minutes. Then they were cleaned with distilled water to remove residues of the grit. Finally, some samples were polished in two steps for each 3 minutes with Buehler MetaDi monocrystalline diamond suspensions of 3 μm, and 0.25μm with textile polishing cloths. CLSM images obtained after polishing didn't show any improvements compared to the images obtained after grinding with sandpaper with a grit number of 2400. Therefore, and because of technical problems with the miller cutter, all other samples were ground in 5 steps using sandpapers with grit numbers of 80 and 240 until the trabeculae were reached and 800, 1500, and 2400 for each 2 minutes after using the Dremel hand milling tool.

4.7.2 CLSM Procedure

A confocal laser scanning microscope (CLSM, Zeiss Axiolab) with the Zeiss ZEN Black software for fluorescent materials was used to access previously basic fuchsin stained microdamage (3.2.1). First, an objective with 20x magnification was used to get an overview of the sample. This was done under epi-fluorescent

Die approbierte gedruckte Originalversion dieser Diplomarbeit ist an der TU Wien Bibliothek verfügbar.
The approved original version of this thesis is available in print at TU Wien Bibliothek.
TU Bibliothek Your knowledge hub WIEN

light in the green range (555 nm) and a rhod-reflector. Next, an oil immersed objective with 65x magnification was used to analyze damage in more detail. Due to the thick layers and high amount of trapped air inside the epoxy in which the samples were embedded, transient light got scattered, making detailed assessments of stained microstructures like canaliculi and z-stacks for 3-dimensional assessments impossible. Thus, only one section of each sample was investigated under the CLSM and images were taken at 20x magnification. Used CLSM and Zeiss ZEN Black software settings and objectives are listed in table 4.5.

Table 4.5: CLSM and Zeiss ZEN Black software settings

Setting Type	**Value**
10x Objective	EC Plan-Neouar 10x/0.30 M27, pixel size: 2.5 μm
20x Objective	EC Plan-Neouar 20x/0.50 M27, pixel size: 1.25 μm
65x Objective	Plan-Apo 63x/1.4, pixel size: 0.65 μm
Laser Intensity	20-30 %
Pinhole	100.4
Gain (Master)	401
Digital Offset	0
Digital Gain	9.2

4.8 Analysis of CLSM Image-Data

Obtained CLSM images were imported into the open source software package ImageJ. Since 3-channels were imported, but only one channel contained information, the other two had to be closed.[7] Then the regions of interest (ROI) were selected with the polygon selection tool. These selections were based on the

[7] Image - Color - Split Channels

Die approbierte gedruckte Originalversion dieser Diplomarbeit ist an der TU Wien Bibliothek verfügbar.
The approved original version of this thesis is available in print at TU Wien Bibliothek.

previously cropped images from the tensile tests for which image tracking was executed, thus only containing the trabecular shaft between the top and bottom onsets of the curvatures of the trabeculae. Images were then transformed into grayscale 8-bit images with 256 gray values.[8] A threshold value was used so that damage (red colored due to basic fuchsin stain) was shown as white pixels. Damage area and density was then assessed by counting the amount of white and black pixels inside the trabeculae. To ensure that after the thresholding operation, pixels with value 0 are shown as black and those with value 255 as white, the "Black background" had to be activated in the binary options.[9] This step is not strictly required, but it enforces the convention: $255 = white$, $0 = black$. A default black and white (B&W) threshold was used with a top value of 75 and the bottom value of 255. After checking the "Dark Background" box, brighter pixels were highlighted in red. These red pixels were mapped to white and the rest to black after clicking the "Apply" button leading to binary images.[10] Then the RIO was restored[11] and the amount of white and black pixels were counted with the Histogram function.[12] Since the resolutions of the images are known as listed in table 4.8, pixels were easily converted into μm^2.

For destroyed trabeculae, which were split apart, each side was first analyzed individually and later added together to obtain damage area and density for the whole trabeculae.

[8] Image - Type - 8-bit
[9] Process - Binary - Options
[10] Image - Adjust - Threshold
[11] Edit - Selection - Restore Selection
[12] Analyze - Histogram

Die approbierte gedruckte Originalversion dieser Diplomarbeit ist an der TU Wien Bibliothek verfügbar.
The approved original version of this thesis is available in print at TU Wien Bibliothek.
TU Bibliothek Your knowledge hub WIEN

4.9 Statistical Analysis

For statistical analyses the software package SPSS, provided by the Institute of Lightweight Design and Structural Biomechanics, was used. First, results were tested for normality with both, a Kolmogorov-Smirnov test combined with a Lilliefors Significance Correction and a Shapiro-Wilk test. Since most data was not normally distributed, a nonparametric Independent-Samples Kruskal-Wallis Test was used to check for significant differences between the different groups and a pairwise comparison was made calculating asymptotic significances (2-sided tests) with a significance level of 0.05. Significance values were adjusted by the Bonferroni correction for multiple tests.

Die approbierte gedruckte Originalversion dieser Diplomarbeit ist an der TU Wien Bibliothek verfügbar.
The approved original version of this thesis is available in print at TU Wien Bibliothek.

5 Results

In total, 82 individual trabeculae were tested successfully with the aforementioned mechanical protocol. These were comprised of 30 samples from alendronate (ALN) treated, 28 samples from raloxifene (RAL) treated and 24 samples from untreated (CON) animals, which were used as a control group. Additionally, two samples of each group were prepared with the same steps as the other samples but have not been mechanically tested. This was to assess possible damage incurrence during preparation steps. None of these six untested samples have shown any signs of damage. However, many of the tested samples failed outside of the trabecular shaft, either due to insufficient embedment or due to too little or damaged material at the ends of the shaft. A list of cases that occurred during tensile tests is shown in table 5.1.

Micro-CT scans did not lead to satisfying results and will be discussed in section 6.3.

Table 5.1: Tensile test outcome

Group:	**CON**	**RAL**	**ALN**	**Total**
Vertebrae:	5	5	5	**15**
Failure inside trab:	7	13	9	**29**
Failure outside trab:	8	9	11	**28**
Cracks inside trab:	1	5	4	**10**
Cracks outside trab:	4	1	0	**5**
Embedding failure:	4	0	6	**10**
Total:	**24**	**28**	**30**	**82**

Microdamage was assessed for all of these samples under the CLSM at the TU Wien. Further, additional samples prepared at IUPUI, were assessed using

Die approbierte gedruckte Originalversion dieser Diplomarbeit ist an der TU Wien Bibliothek verfügbar.
The approved original version of this thesis is available in print at TU Wien Bibliothek.
TU Bibliothek Your knowledge hub WIEN

micro-CT images, which did not lead to satisfying results.

5.1 Material Properties

Material property determination as described in section 4.4.3 provided valid results for 30 alendronate (ALN) samples, 21 raloxifene (RAL) samples and 22 samples from the control group (CON). It was shown that both treatments, ALN and RAL significantly increased stiffness and maximum load of single trabeculae. Samples from ALN-treated animals showed a more brittle behavior than the untreated control group, while samples from RAL-treated animals showed a more ductile behavior than the control group. The RAL-group showed a high increase in ultimate strain whereas the ALN-group showed just a little increase. Again, ultimate stresses and strains have to be treated carefully in this context since they only represent the end of measurement and should not be confused with maximum stress σ_{max} and strain at maximum stress $\varepsilon(\sigma_{max})$. Figures 5.1 to 5.3 show examples of stress-strain-curves for each group.

Die approbierte gedruckte Originalversion dieser Diplomarbeit ist an der TU Wien Bibliothek verfügbar.
The approved original version of this thesis is available in print at TU Wien Bibliothek.
TU Bibliothek Your knowledge hub WIEN

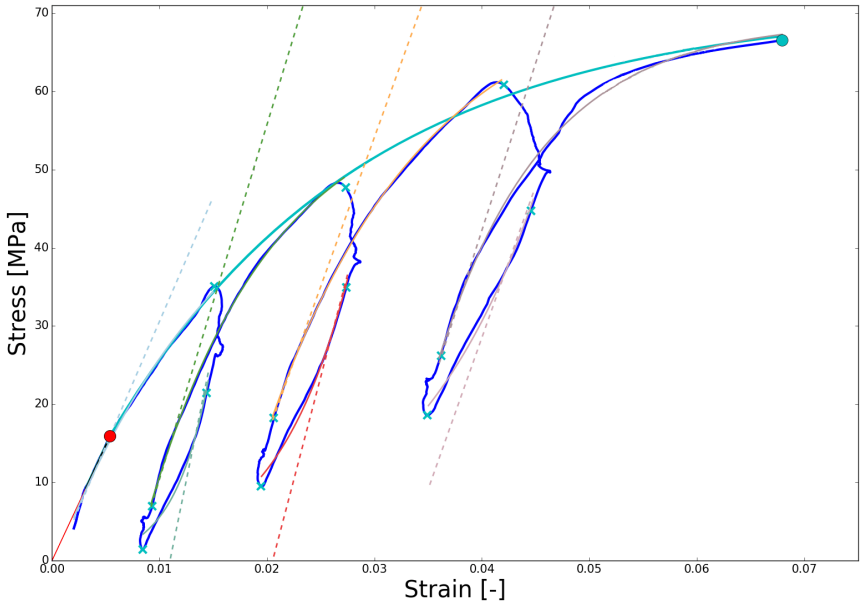

Figure 5.1: Stress-strain-curve of a sample from the ALN-group

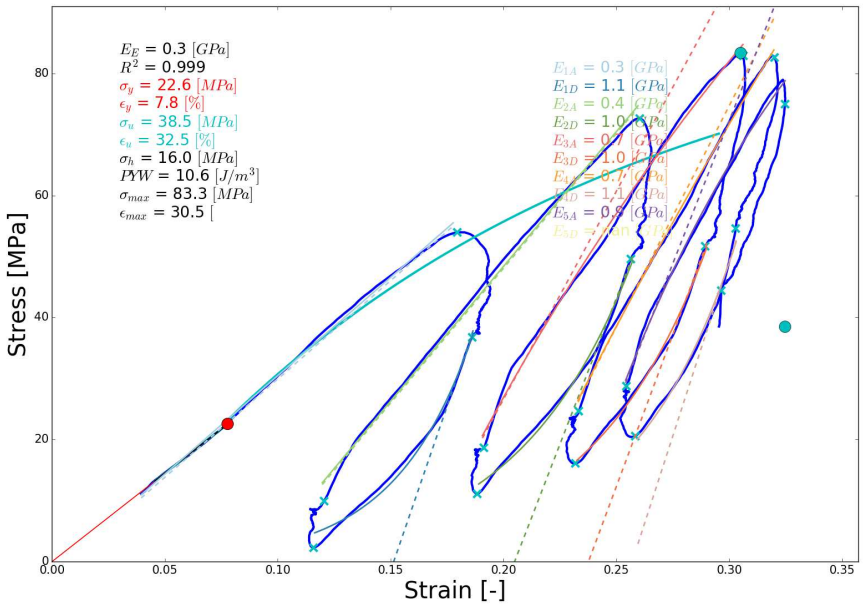

Figure 5.2: Stress-strain-curve of a sample from the CON-group

Die approbierte gedruckte Originalversion dieser Diplomarbeit ist an der TU Wien Bibliothek verfügbar.
The approved original version of this thesis is available in print at TU Wien Bibliothek.
TU Bibliothek Your knowledge hub WIEN

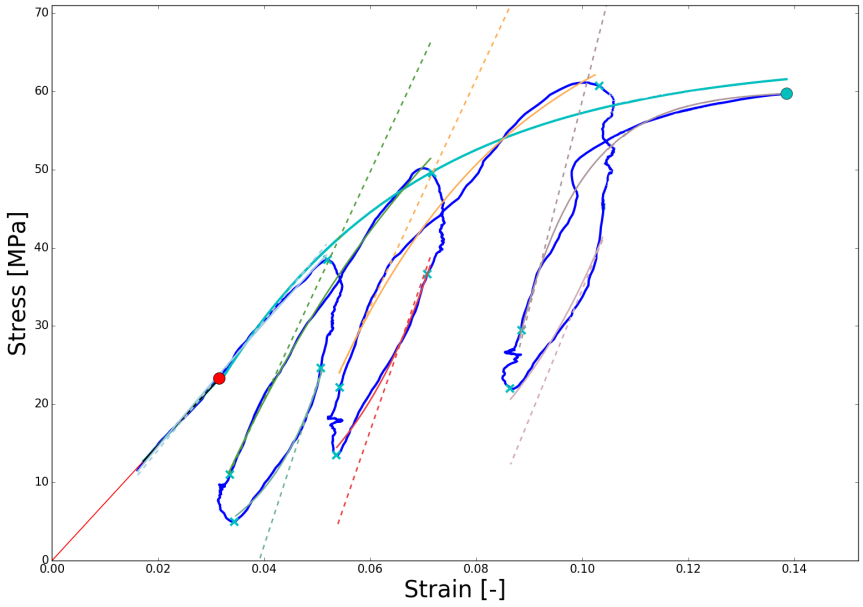

Figure 5.3: Stress-strain-curve of a sample from the RAL-group

A comparison of the results of the arithmetic mean values, including standard deviations and statistical significances, is shown in table 5.2 for all groups. Only results from nonparametric tests are displayed since most of results did not show normal distributions, neither with a Kolmogorov-Smirnov, nor with a Shapiro-Wilk test, which was expected due to the strong variability of the biological specimens. The ending "fit" indicates samples that were tested until failure inside the trabeculae shaft. Thus, results about ultimate and maximum stress, ultimate and maximum strain and PYW have high significance for those samples. However due to a smaller population thereof (7 CON, 13 RAL, 9ALN) statistical relevance is a big issue for which data, such as yield stress and strain and elastic work, from the total population should be given more account to.

Die approbierte gedruckte Originalversion dieser Diplomarbeit ist an der TU Wien Bibliothek verfügbar.
The approved original version of this thesis is available in print at TU Wien Bibliothek.
TU Bibliothek Your knowledge hub WIEN

Table 5.2: Comparison of material properties (arithmetic mean values ± standard deviation), pairwise comparison between CON-RAL, CON-ALN, RAL-ALN with asymptotic significances (2-sided tests) for statistically significant properties (p<0.05(K.W.)), adjusted by the Bonferroni correction for multiple tests and the asymptotic significances from an independent Kruskal-Wallis test (K.W.). The ending "fit" indicates samples that were tested until failure inside the trabeculae shaft

	ALN	**CON**	**RAL**	**C-R**	**C-A**	**R-A**	**K.W.**
E [MPa]	2.7 ± 1.9	1.5 ± 1.8	1.7 ± 1.6	1.000	0.006	0.039	0.004
E_{fit} [MPa]	2.8 ± 2.3	2.3 ± 2.5	1.9 ± 1.5	–	–	–	–
σ_y [MPa]	23.9 ± 13.2	21.4 ± 13.1	19.4 ± 12.0	–	–	–	0.582
ε_y [%]	1.3 ± 1.3	2.8 ± 2.5	2.1 ± 2.2	–	–	–	0.094
σ_{max} [MPa]	71.2 ± 27.4	38.7 ± 33.3	55.5 ± 35.1	0.174	0.001	0.190	0.001
σ_{maxfit} [MPa]	65.3 ± 25.5	56.9 ± 33.5	68.2 ± 32.6	–	–	–	–
$\varepsilon(\sigma_{max})_{fit}$ [%]	6.7 ± 3.7	7.8 ± 5.3	9.3 ± 4.6	–	–	–	–
σ_u [MPa]	66.9 ± 30.8	35.1 ± 27.5	55.2 ± 31.9	0.056	0.001	0.556	0.002
σ_{ufit} [MPa]	64.6 ± 26.3	53.1 ± 32.6	66.3 ± 30.9	–	–	–	–
ε_u [%]	7.6 ± 3.9	9.7 ± 7.7	11 ± 5.9	–	–	–	0.128
ε_{ufit} [%]	7.5 ± 4.2	9.6 ± 5.9	11 ± 4.4	–	–	–	–
PYW_{fit} [J/m^3]	3 ± 2.5	2.2 ± 2.8	4 ± 3.2	0.267	0.043	1.000	0.045
PYW [J/m^3]	2.5 ± 1.3	2.9 ± 2.1	4.3 ± 2.7	–	–	–	–
W_e [MPa]	0.2 ± 0.3	0.4 ± 0.5	0.2 ± 0.3	–	–	–	0.448
σ_h [MPa]	41.2	14.7	37.2	–	–	–	–
e_h [1]	50.2	65.5	25.1	–	–	–	–

Furthermore, mean stress-strain curves are compared in figure 5.4, which are calculated using equations 6 to 9. This is followed by diagrams, illustrating some key-values using Box and Whisker charts. In these diagrams, data points are shown as dots, medians as horizontal lines inside these boxes and the arithmetic

Die approbierte gedruckte Originalversion dieser Diplomarbeit ist an der TU Wien Bibliothek verfügbar.
The approved original version of this thesis is available in print at TU Wien Bibliothek.
TU Bibliothek Your knowledge hub WIEN

mean values are indicated by a "x". The top border of a box represents the median of the top half of the values of the data set and the bottom border the median of the bottom half of the data set. A data point is considered an outlier if it exceeds a distance of 1.5 times the total box height in either direction outside of the box's borders. When outliers are existing, horizontal lines at the ends of the whiskers represent the maximum or minimum data points inside these 1.5 times box height in both directions. If no outliers are present, these lines represent the maximum and minimum value of the whole data set. Figures 5.5 to 5.12 show Box and Whisker charts for yield stress σ_y, yield strain ε_y, maximal stress σ_{max}, strain at maximal stress $\varepsilon(\sigma_y)$, ultimate stress σ_u, ultimate strain ε_y, elastic work W_e, and post yield work PYW of the different groups in comparison.

Die approbierte gedruckte Originalversion dieser Diplomarbeit ist an der TU Wien Bibliothek verfügbar.
The approved original version of this thesis is available in print at TU Wien Bibliothek.
TU Bibliothek Your knowledge hub WIEN

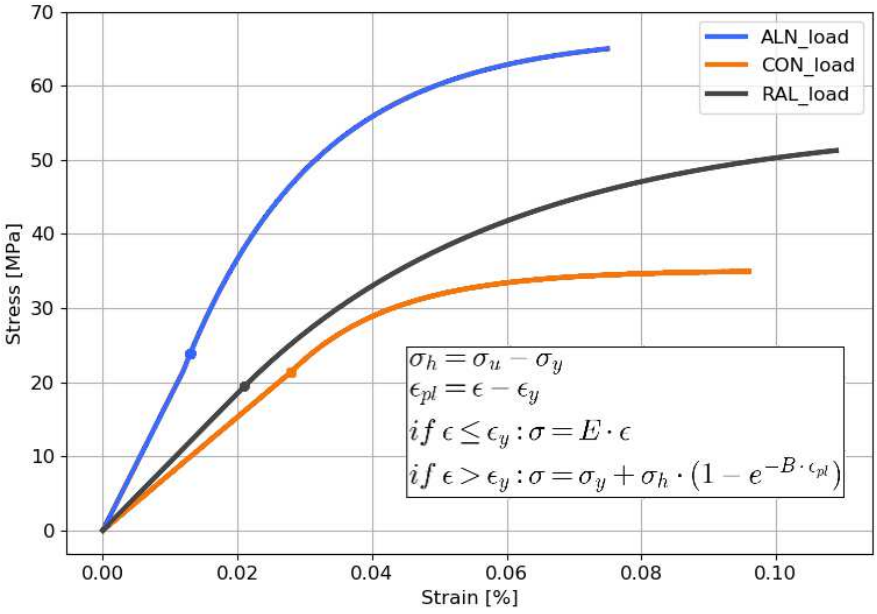

Figure 5.4: Comparison of mean stress-strain curves calculated using equations 6 to 9. Mean Young's moduli for this curves were calculated using mean yield-stress and mean yield-strain $E = \frac{\sigma_y}{\varepsilon_y}$ in contrast to calculating the arithmetic mean value for each group, as done for the results table 5.2 and the curves in figures 5.13 to 5.17. Yield points are marked with dots.

Die approbierte gedruckte Originalversion dieser Diplomarbeit ist an der TU Wien Bibliothek verfügbar.
The approved original version of this thesis is available in print at TU Wien Bibliothek.

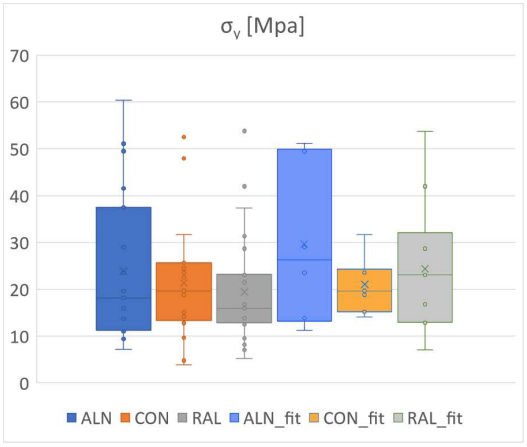

Figure 5.5: Yield Stress

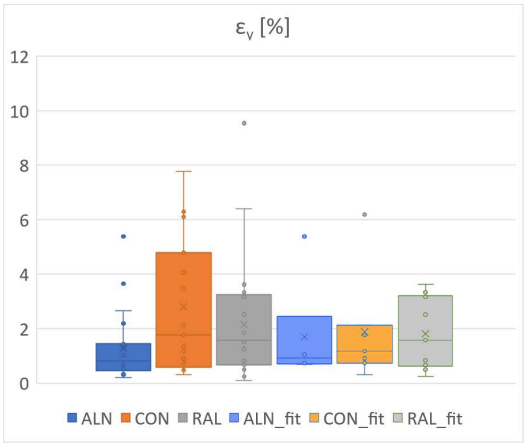

Figure 5.6: Yield Strain

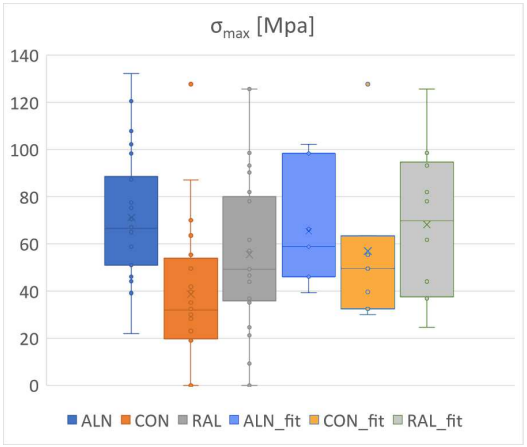

Figure 5.7: Maximal stress

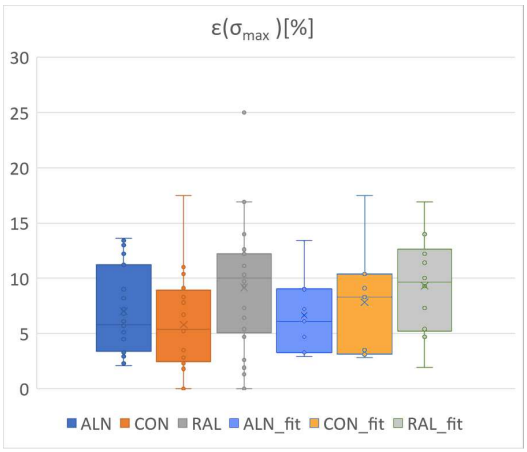

Figure 5.8: Strain at maximal stress

Die approbierte gedruckte Originalversion dieser Diplomarbeit ist an der TU Wien Bibliothek verfügbar.
The approved original version of this thesis is available in print at TU Wien Bibliothek.

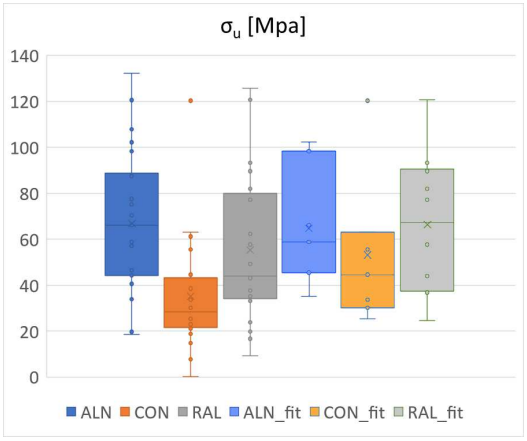

Figure 5.9: Ultimate Stress

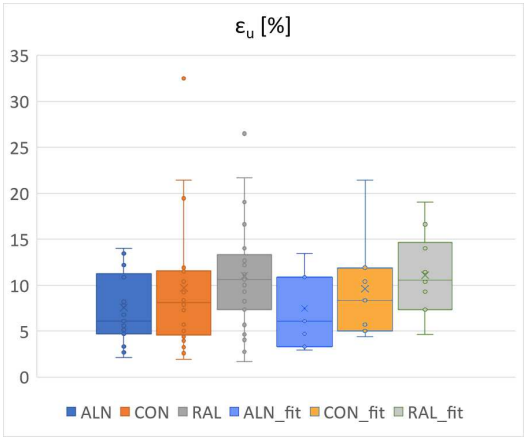

Figure 5.10: Ultimate Strain

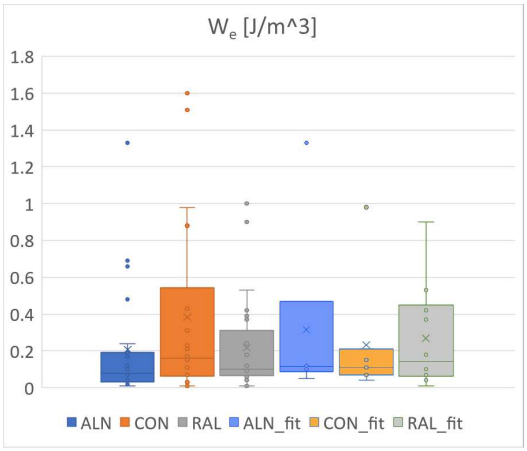

Figure 5.11: Elastic Work

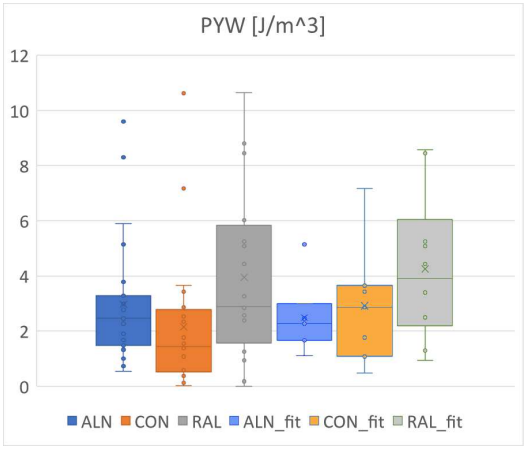

Figure 5.12: Post Yield Work

Figures 5.13 to 5.17 show the Young's moduli of each loading and unloading cycle with 95% confidence intervals ($E_{mean} \pm z^* * SEM, z^* = 1.96$) from the different groups in comparison where E_{mean} is calculated as the arithmetic mean

$$E_{mean} = \frac{1}{n} \sum_{i=1}^{n} E_i \tag{12}$$

and the standard error of the mean SEM as

Die approbierte gedruckte Originalversion dieser Diplomarbeit ist an der TU Wien Bibliothek verfügbar.
The approved original version of this thesis is available in print at TU Wien Bibliothek.
TU Bibliothek Your knowledge hub WIEN

$$SEM = \sqrt{\frac{\sum_i^n (E_i - E_{mean})^2}{(n-1) * n}}. \tag{13}$$

The moduli of the first cycle are significantly higher for alendronate and not significantly higher for raloxifene compared to the control group, for both, loading and unloading. Furthermore, the first moduli are always significantly higher for unloading than for loading cycles in all groups, which was expected since unloading usually shows a more representing modulus that should be higher than the modulus measured for unloading cycles. Determination at higher cycle numbers became inaccurate due to scattered measurements, which caused fitting problems of the Python-algorithm, and thus, should be taken with a grain of salt.

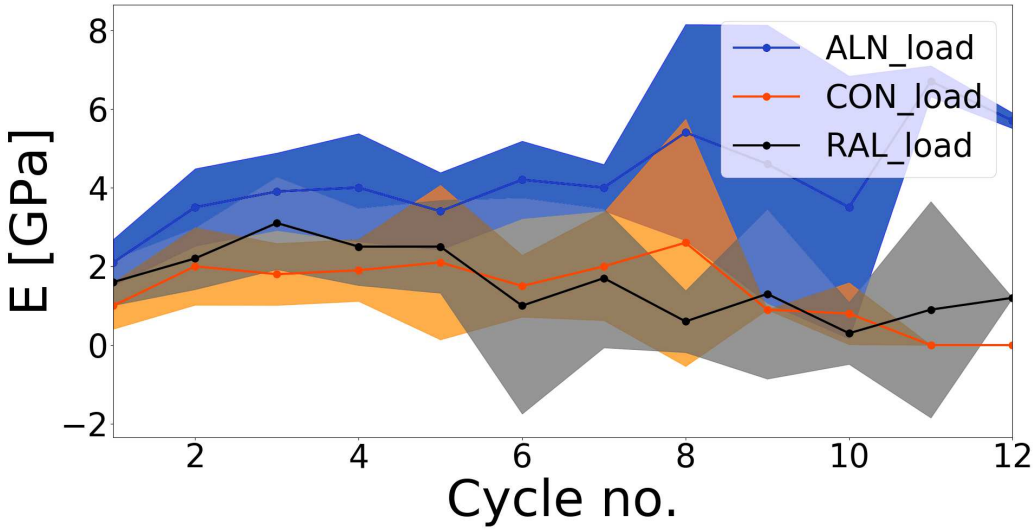

Figure 5.13: Young's modulus at loading cycles for all groups

Die approbierte gedruckte Originalversion dieser Diplomarbeit ist an der TU Wien Bibliothek verfügbar.
The approved original version of this thesis is available in print at TU Wien Bibliothek.
TU Bibliothek Your knowledge hub WIEN

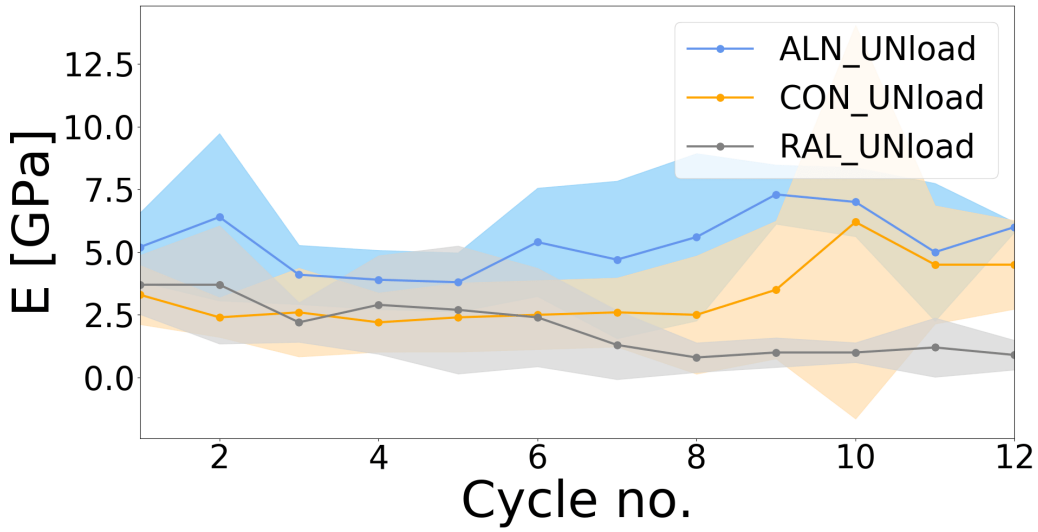

Figure 5.14: Young's modulus at unloading cycles for all groups

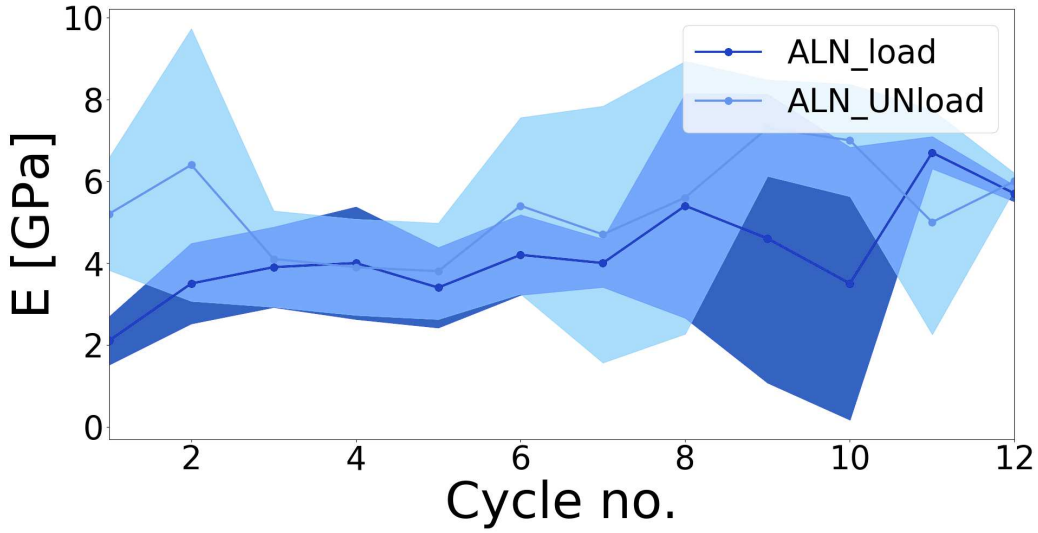

Figure 5.15: Young's modulus at loading and unloading cycles for ALN

Die approbierte gedruckte Originalversion dieser Diplomarbeit ist an der TU Wien Bibliothek verfügbar.
The approved original version of this thesis is available in print at TU Wien Bibliothek.

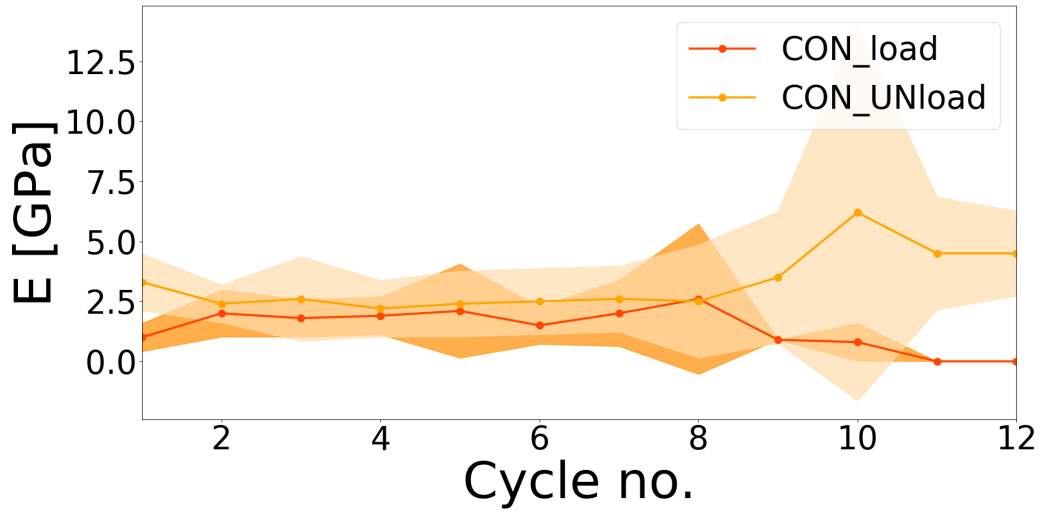

Figure 5.16: Young's modulus at loading and unloading cycles for CON

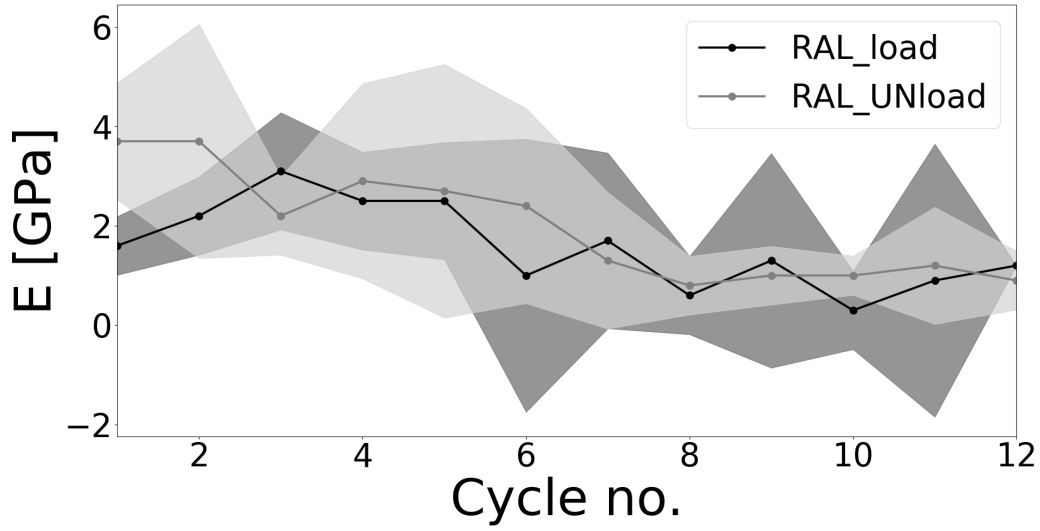

Figure 5.17: Young's modulus at loading and unloading cycles for RAL

For each sample, the mean BMD, its standard deviation and the median of the BMD were determined. From this, the mean BMD of the whole groups, the mean standard deviations, the mean medians and furthermore also the standard deviations thereof were calculated, which are shown in table 5.3.

Die approbierte gedruckte Originalversion dieser Diplomarbeit ist an der TU Wien Bibliothek verfügbar.
The approved original version of this thesis is available in print at TU Wien Bibliothek.
TU Bibliothek Your knowledge hub WIEN

Table 5.3: Mean values for mean BMD, the standard deviations and medians of each group ± standard deviations

Group:	**CON**	**RAL**	**ALN**
BMD_{mean} [mg HAcm^{-3}]	931 ± 28	930 ± 27	956 ± 28
BMD_{std} [mg HAcm^{-3}]	177 ± 9	181 ± 10	175 ± 9
BMD_{median} [mg HAcm^{-3}]	994 ± 39	1018 ± 164	1010 ± 28

Table 5.4 shows statistical significances and pairwise comparison of statistical differences of BMD between all groups. P-values smaller than 0.05 represent statistically significant differences between the groups.

Table 5.4: Pairwise comparison of BMD between CON-RAL, CON-ALN, RAL-ALN with asymptotic significances (2-sided tests) for statistically significant properties (p<0.05), adjusted by the Bonferroni correction for multiple tests and the asymptotic significances from an independent Kruskal-Wallis test (K.W.)

	C-R	**C-A**	**R-A**	**K.W.**
BMD_{mean} [mg HAcm^{-3}]	1.000	0.068	0.010	0.008
BMD_{std} [mg HAcm^{-3}]	–	–	–	0.235
BMD_{median} [mg HAcm^{-3}]	–	–	–	0.054

Figure 5.18 shows a Box and Whisker chart that illustrates the difference of the BMD_{mean} of the different groups.

Die approbierte gedruckte Originalversion dieser Diplomarbeit ist an der TU Wien Bibliothek verfügbar.
The approved original version of this thesis is available in print at TU Wien Bibliothek.
TU Bibliothek Your knowledge hub WIEN

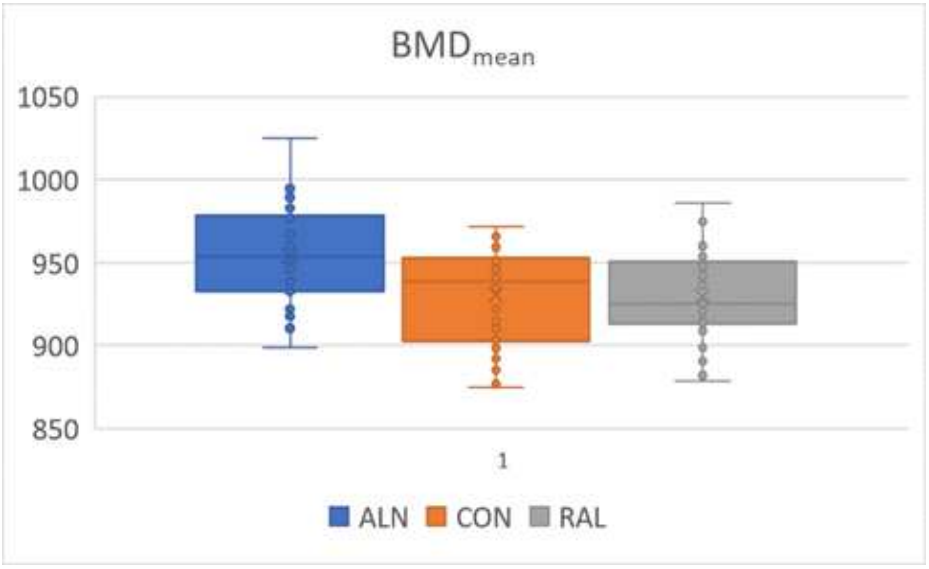

Figure 5.18: Comparison of the BMD_{mean} of the different groups

Pearson, the Kendall's tau b and the Spearman's rho correlations of all material properties as well as damage density with the mean BMD were determined. Only ultimate strain shows a statistically significant but negative correlation (R_P = -0.253, P_P = 0.046), although only for the Pearson correlation. However, the Pearson correlation assumes that both variables are normally distributed, which is not the case for ultimate strains. All other mechanical and material properties, including damage density, do not show a significant correlation with BMD across all groups. However, testing for correlations of the material properties with BMD within each group individually showed, that the raloxifene treated group has significant correlations between some properties and BMD, which are listed in table 5.5. Except for ultimate strain, all significant correlations have a positive correlation coefficient. However, correlation coefficients are relatively small, which indicates a weak relationship.

Die approbierte gedruckte Originalversion dieser Diplomarbeit ist an der TU Wien Bibliothek verfügbar.
The approved original version of this thesis is available in print at TU Wien Bibliothek.
TU Bibliothek Your knowledge hub WIEN

Table 5.5: Person, Kendalls's tau-b, and Spearman correlations between material properties and BMD for raloxifene (RAL). Only properties for which at least one of the three correlations is statistically significant are listed in this table. R_i stands for correlation coefficient and P_i for significance whereby the subscript i defines the correlation type: P ... Pearson, K ... Kendalls's tau-b, S ... Spearman

W_e	$R_P = 0.405$	$P_P = 0.049$
	$R_K = 0.225$	$P_K = 0.129$
	$R_S = 0.322$	$P_S = 0.125$
σ_y	$R_P = 0.639$	$P_P = 0.001$
	$R_K = 0.584$	$P_K = 0.000$
	$R_S = 0.768$	$P_S = 0.000$
σ_u	$R_P = 0.374$	$P_P = 0.072$
	$R_K = 0.330$	$P_K = 0.024$
	$R_S = 0.495$	$P_S = 0.014$
σ_{max}	$R_P = 0.375$	$P_P = 0.071$
	$R_K = 0.298$	$P_K = 0.042$
	$R_S = 0.441$	$P_S = 0.031$
ε_u	$R_P = -.0465$	$P_P = 0.022$
	$R_K = -0.134$	$P_K = 0.359$
	$R_S = -0.235$	$P_S = 0.269$

Material properties for both, the alendronate as well as the control group, did not show any statistically significant correlations with BMD. Figures 5.19 and 5.20 show the correlations between the Young's Modulus (E) and maximum stress σ_{max} with BMD for the RAL-group respectively.

Die approbierte gedruckte Originalversion dieser Diplomarbeit ist an der TU Wien Bibliothek verfügbar.
The approved original version of this thesis is available in print at TU Wien Bibliothek.
TU Bibliothek Your knowledge hub WIEN

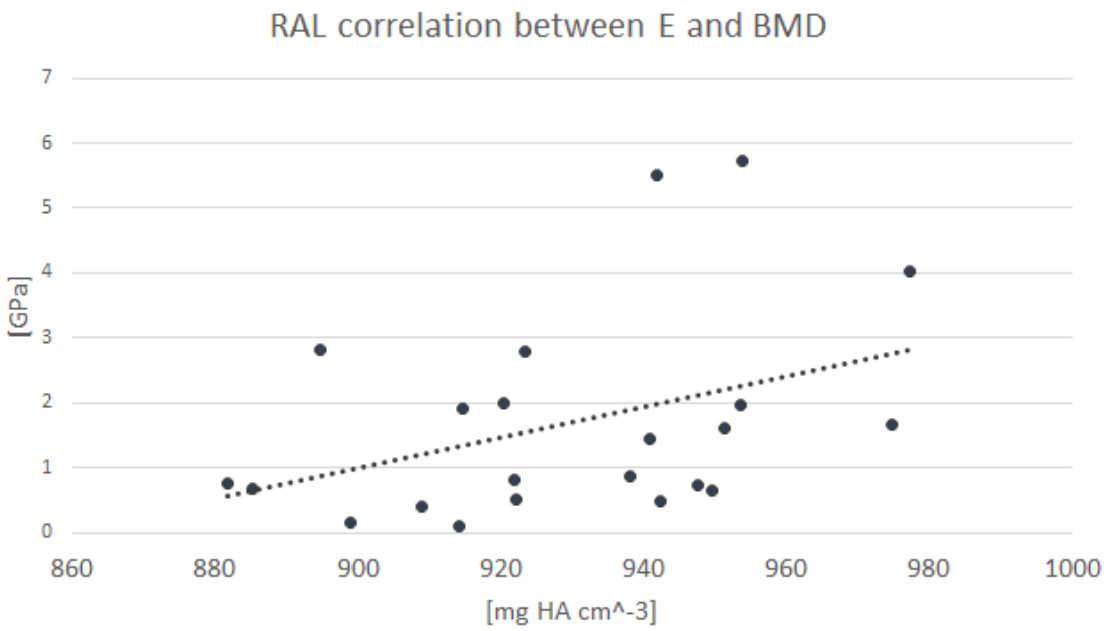

Figure 5.19: Correlation between Young's Modulus (E) and BMD for RAL with $R_P = 0.405$ and $P_P = 0.0049$

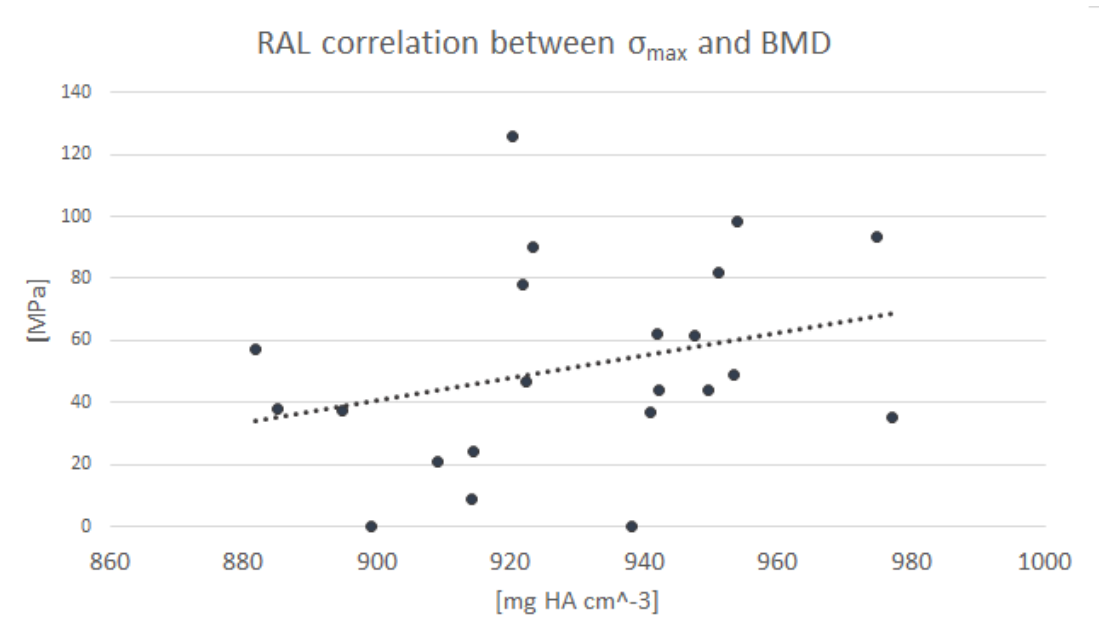

Figure 5.20: Correlation between maximum stress σ_{max} and BMD for RAL with $R_S = 0.441$ and $P_P = 0.031$

Die approbierte gedruckte Originalversion dieser Diplomarbeit ist an der TU Wien Bibliothek verfügbar.
The approved original version of this thesis is available in print at TU Wien Bibliothek.
TU Bibliothek Your knowledge hub WIEN

5.2 Microdamage

5.2.1 CLSM

Tables 5.6 and 5.7 show a comparison of the longitudinal section area, damage area, and damage density between the different groups in form of mean values ± standard deviation and a pairwise comparison and statistical significances respectively. Figures 5.21 and 5.22 show a comparison of damage area and damage density between the different groups in form of Box and Whisker charts respectively. It can be seen that alendronate (ALN) shows a larger damage area. However, the mean damage density is smaller than for raloxifene (RAL) and just slightly higher than for the control group CON. This is due to different sizes (Area_Longitudinal) of the trabeculae, which is illustrated in figures 5.23 and 5.24, which show the mean cross-sectional and the mean longitudinal section area of each group in form of Box and Whisker charts respectively.

Table 5.6: Comparison of the longitudinal section areas, damage areas and damage densities (arithmetic mean values ± standard deviation)

	ALN	**CON**	**RAL**
Area_Long. [μm^2]	58000 ± 50000	31000 ± 10600	27000 ± 11800
Damage Area [μm^2]	16720 ± 15528	9830 ± 4770	9200 ± 4450
Damage Density [%]	0.31 ± 0.13	0.33 ± 0.12	0.35 ± 0.08

Die approbierte gedruckte Originalversion dieser Diplomarbeit ist an der TU Wien Bibliothek verfügbar.
The approved original version of this thesis is available in print at TU Wien Bibliothek.
TU Bibliothek Your knowledge hub WIEN

Table 5.7: Pairwise comparison between CON-RAL, CON-ALN, RAL-ALN with asymptotic significances (2-sided tests) for statistically significant properties ($p<0.05$), adjusted by the Bonferroni correction for multiple tests and the asymptotic significances from an independent Kruskal-Wallis test (K.W.)

	C-R	**C-A**	**R-A**	**K.W.**
Area_Long. $[\mu m^2]$	0.901	0.057	0.000	0.000
Damage Area $[\mu m^2]$	–	–	–	0.083
Damage Density [%]	–	–	–	0.437

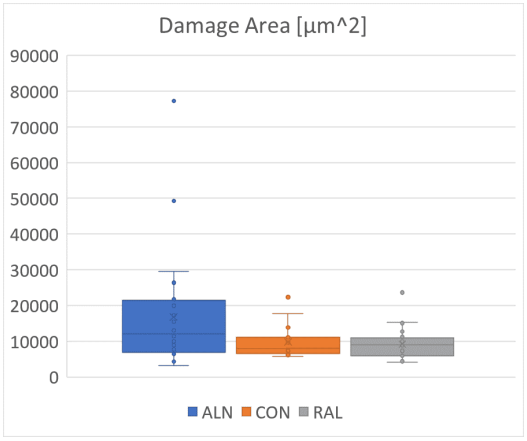

Figure 5.21: Damage Area

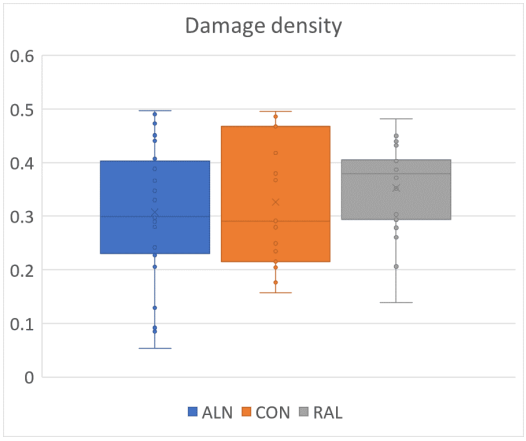

Figure 5.22: Damage Density

Die approbierte gedruckte Originalversion dieser Diplomarbeit ist an der TU Wien Bibliothek verfügbar.
The approved original version of this thesis is available in print at TU Wien Bibliothek.

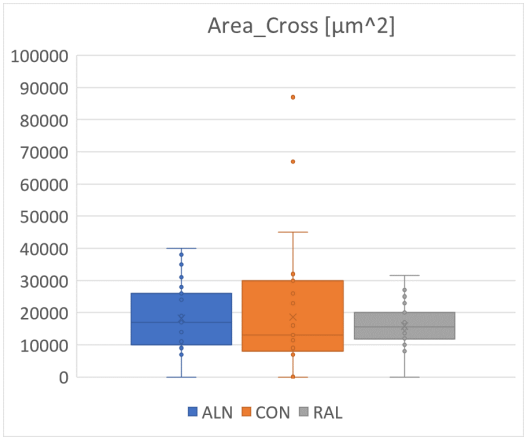

Figure 5.23: Mean cross-sectional area

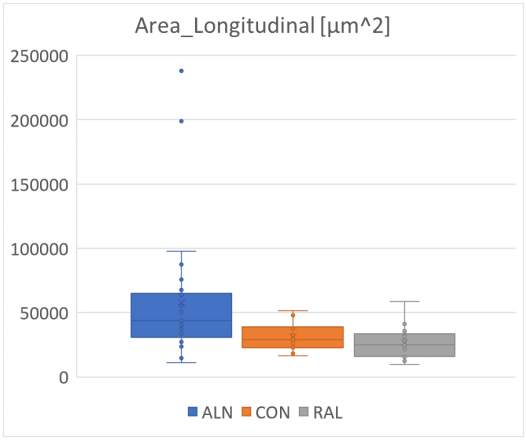

Figure 5.24: Mean longitudinal area

Images of basic fuchsin stained samples (figures 5.25 to 5.34), obtained from the CLSM at the TU Wien, show that mainly diffuse damage occurred at the trabecular shafts, which was expected as Seref-Ferlengez et al. stated that diffuse damage predominantly occurs in tensile regions of bone [48], and Julia Fischer described a stronger increase of diffuse damage compared to linear cracks at higher cycle numbers [22]. Furthermore, strongly damaged regions extend over rather large areas since all tests were stopped only after obvious damage incurrence shortly before or right after failure. Only one sample (which was from the raloxifene treated group) showed crosshatching as depicted in figures 5.25 and 5.26.

Die approbierte gedruckte Originalversion dieser Diplomarbeit ist an der TU Wien Bibliothek verfügbar.
The approved original version of this thesis is available in print at TU Wien Bibliothek.
TU Bibliothek Your knowledge hub WIEN

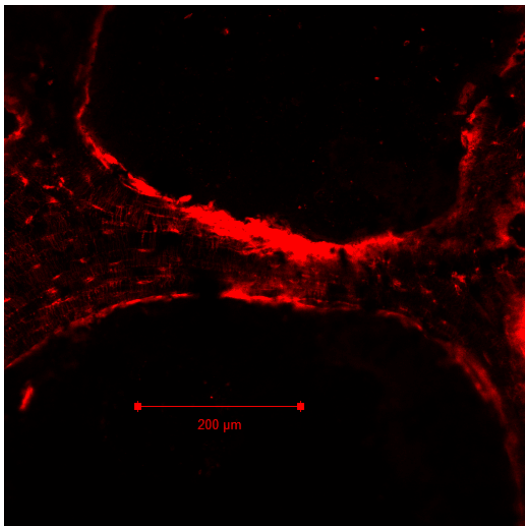

Figure 5.25: Crosshatching RAL, 10x magnification

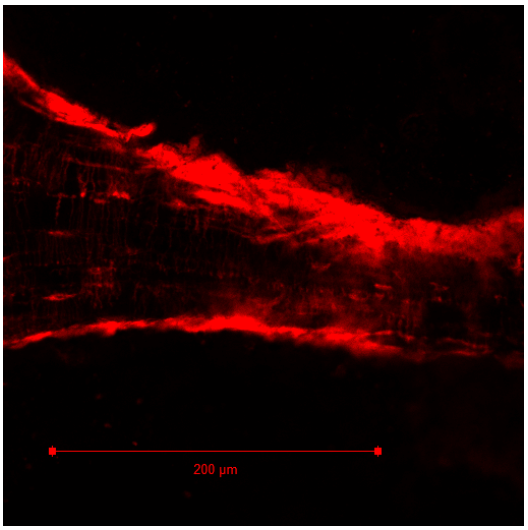

Figure 5.26: Crosshatching RAL, 20x magnification

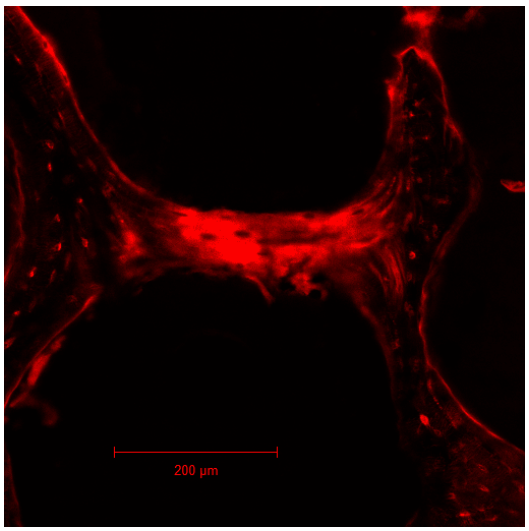

Figure 5.27: CON, 10x magnification

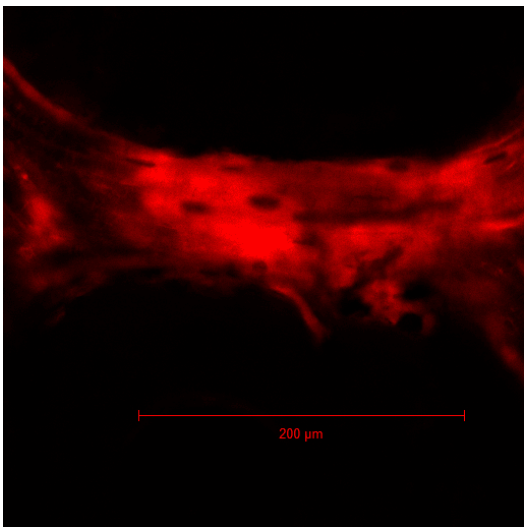

Figure 5.28: CON, 20x magnification

Die approbierte gedruckte Originalversion dieser Diplomarbeit ist an der TU Wien Bibliothek verfügbar.
The approved original version of this thesis is available in print at TU Wien Bibliothek.

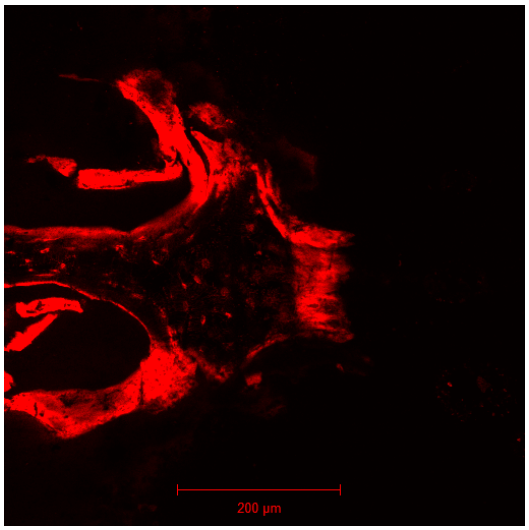

Figure 5.29: ALN, left side 10x magn.

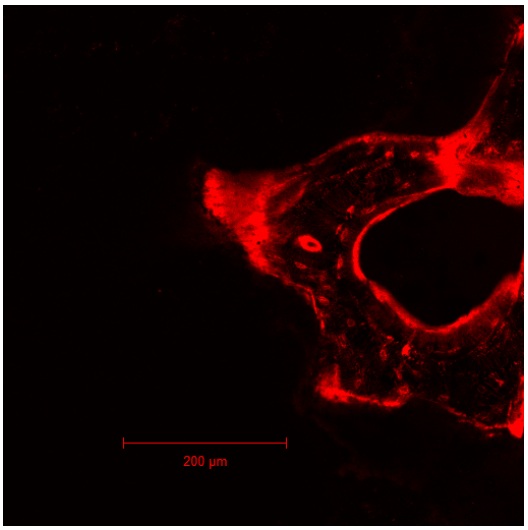

Figure 5.30: ALN, right side 10x magn.

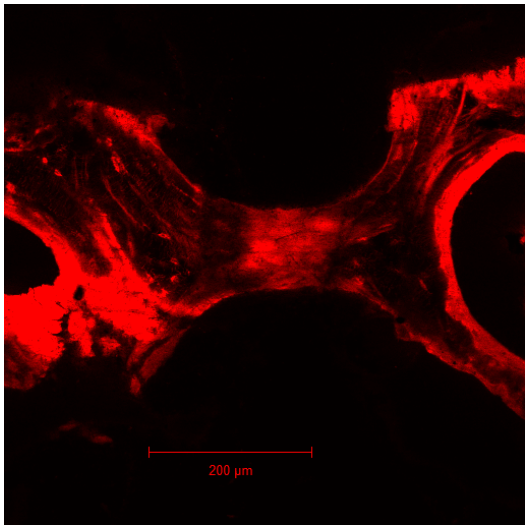

Figure 5.31: ALN, 10x magnification

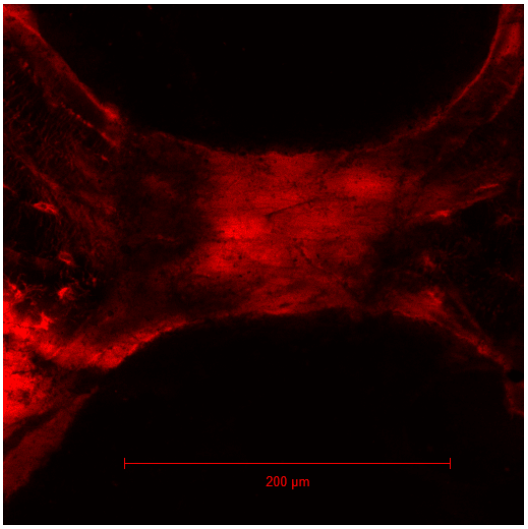

Figure 5.32: ALN, 20x magnification

Die approbierte gedruckte Originalversion dieser Diplomarbeit ist an der TU Wien Bibliothek verfügbar.
The approved original version of this thesis is available in print at TU Wien Bibliothek.

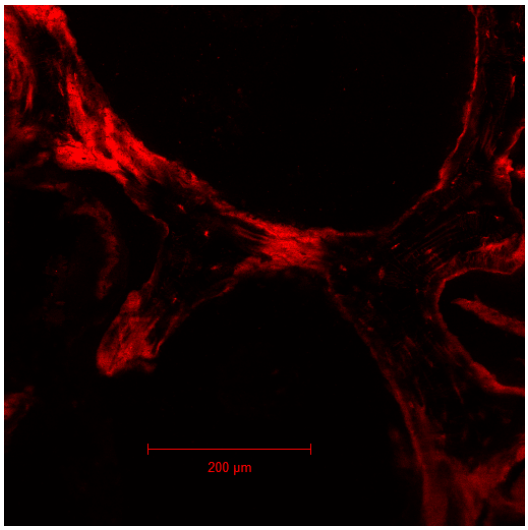

Figure 5.33: ALN, 10x magnification

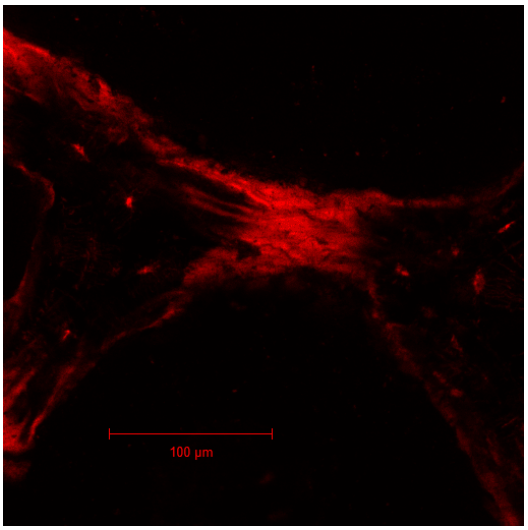

Figure 5.34: ALN, 20x magnification

5.2.2 Micro-CT

Micro-CT scans did not lead to satisfying results, which are therefore discussed in section 6.3.

Die approbierte gedruckte Originalversion dieser Diplomarbeit ist an der TU Wien Bibliothek verfügbar.
The approved original version of this thesis is available in print at TU Wien Bibliothek.
TU Bibliothek Your knowledge hub WIEN

6 Discussion

During this thesis, a novel mechanical testing method, developed at TU Wien, as well as a staining procedure from David Burr's laboratory at IUPUI was successfully used to determine the effect of anti-resorptive treatments on material properties and damage behavior of individual trabeculae of bone. However, major problems and obstacles have arisen during this research project. These will be addressed in this chapters. Results are discussed in section 6.3.

6.1 Materials

Trabeculae used for this research project (harvested from vertebrae of non-ovariectomized skeletally mature female beagle dogs) have shown small dimensions. In contrast to earlier studies [25], conducted with bovine trabeculae or studies with human trabeculae, these canine trabeculae have shown a significantly different geometry; rather short and plate-like rods formed the cancellous bone tissue, which made the already very sensible process of harvesting trabeculae even more effortful, time consuming and prone to failure. Furthermore, due to strongly varying size of the trabeculae, it was almost impossible to gather specimens with as little fluctuations as previously achieved with materials from earlier studies. Thus, structural size effects could have led to errors in the results, obtained from comparison of the different groups that were tested during this research project. Additionally, these geometrical variability also caused larger fluctuations of the mechanical test data, which may have led to some statistically non-significant results. However, there were no statistically significant correlations ($p < 0.05$) of the material properties with sample dimensions, such as length and diameter.

Die approbierte gedruckte Originalversion dieser Diplomarbeit ist an der TU Wien Bibliothek verfügbar.
The approved original version of this thesis is available in print at TU Wien Bibliothek.
TU Bibliothek Your knowledge hub WIEN

6.2 Methods

Sample Preparation for the mechanical tensile tests had to be conducted with high precision, patience, and endurance, which required a lot of experience for each step. It took a long time of practice to acquire the necessary skills, to learn the used methods and to get a feeling for the handling of these tiny samples before first samples were successfully tested. However, due to the extreme fragility of single trabeculae, about 60 % of all samples broke before testing during preparation steps because of unintentionally imposed loads. From the rest of the samples, about 20 % additional samples broke after testing, either already when removing from the sample holder of the testing device or during storing, shipping, staining or other handling steps. The average time needed exclusively for preparation and mechanical testing of a single sample, excluding time used for micro-CT measurements, while also taking time used for unsuccessfully prepared or tested samples under consideration, exceeded 10 hours. This leads to the question if automated, machine-supported, methods could be used for future projects to prepare samples for testing. However, similar trabeculae must be used to obtain reasonable results, but since cancellous bone is strongly inhomogeneous and trabeculae strongly vary in size, shape, and alignment, an automated method is almost impossible to realize. It is important to find better methods to handle samples with a lower risk of introducing damage and to achieve reduced times for each step. Another problem, which did arise was that more than 50% of all samples failed outside of the trabecular shaft. This was probably due to weakening of the bone tissue outside the shaft during excising or due to too little bone tissue in this region. Furthermore, insufficient embedding led to failure in about 12% of all samples. These issues could be avoided when allowing epoxy from the circular end pieces to flow closer to the trabecular shaft, which is a very risky undertaking that requires very high precision to not destroy the trabeculae. Trabeculae from bovine or human femur

Die approbierte gedruckte Originalversion dieser Diplomarbeit ist an der TU Wien Bibliothek verfügbar.
The approved original version of this thesis is available in print at TU Wien Bibliothek.
TU Bibliothek Your knowledge hub WIEN

heads used in previous studies, as well as for training purposes, are on average 4.5 times larger (volume) than trabeculae used in this study. Therefore, the preparation methods had to be adjusted but still need further improvement.

Additional samples of each group, which were prepared and fuchsin stained with the same steps as the other samples, but not mechanically tested, were inspected for possible damage that could have got imposed during preparation. This has shown that no in vivo damage or damage during handling occurred, which leads to the assumption, that unintentionally imposed loads are so large that samples rather break apart than just getting damaged.

The **mechanical test** set-up showed some flaws, which, from time to time, led to erroneous measurements due to noisy signals or even destruction of whole samples due to an unintended load or displacement limit overshoot, which caused a drop of the load cell. Different tuning settings were tested to minimize the noise of the signals, which could not be avoided completely. To minimize the risk of destruction, two magnetic security stops were attached to the sides of the load frame. However, this approach was only capable of saving the load cell. Further issues occurred with the software packet μEye Cockpit, which was used for camera recording. Sometimes recording stopped during tests, which let to periods of time where no strain tracking measurements were made. Thus, great attention had to be paid not only to the samples itself to observe if whitening occurs, but also to any movements of air bubbles. In case there was no movement visible, the camera had to be restarted. More advanced testing set-ups could make future measurements faster, easier, more precise and less prone to errors. The detection of whitening was a critical task to stop tests prior to failure. However, although a slow displacement-controlled testing profile with periods of relaxation was used, it was hard to stop the tests early enough and thus, most samples were tested until failure. Even slower displacement and better camera systems could make it easier to detect whitening prior to failure.

Die approbierte gedruckte Originalversion dieser Diplomarbeit ist an der TU Wien Bibliothek verfügbar.
The approved original version of this thesis is available in print at TU Wien Bibliothek.
TU Bibliothek Your knowledge hub WIEN

Material property **measurements** during mechanical tests had to be taken at a sufficient distance from the fixed ends to ensure that edge effects and stress concentrations due to the clamps do not falsify the results by influencing the general homogeneous stress state. However, due to the extremely short trabeculae, most samples did not even show a trabecular shaft with constant cross-sectional area, but rather one curvature merging into the other, which most probably interfered the homogeneous stress state. Therefore, absolute values should be taken with a grain of salt. However, each sample experienced the same preparation steps and testing procedures and was chosen with as similar dimensions as possible. Thus, there were no statistically significant correlations ($p < 0.05$) between the material properties and sample dimensions, which is a good indicator that comparisons between the 3 different groups are legitimate.

Since no studies were found that describe earlier experience with **basic fuchin** staining of individual trabeculae, David Burr's protocol for cores of bone [9] had to be adjusted until reliable results were obtained. This newly acquired protocol led to promising results but, for sure, could still be improved in terms of sample handling and soaking times. Especially embedding and sectioning of samples after staining turned out be a big problem. Conventional embedding into PMMA and subsequently cutting into 100 um thick sections using a diamond wire saw, as described by M.R. Allen et al. [2], was not possible due to the small size of the single trabeculae. First of all, it would be impossible to align samples inside the PMMA block, which would make it hard to find a feasible cutting plane, and secondly, the wire of the saw has a diameter similar to the trabeculae's diameter, which most likely would lead to total destruction of the whole sample when cutting. Samples were therefore embedded into the same epoxy as the circular end pieces, which is not only an easier, but also faster procedure then embedding into PMMA (16 hours curing of epoxy versus 1 to 2 weeks of multiple steps when using PMMA [2]).

Die approbierte gedruckte Originalversion dieser Diplomarbeit ist an der TU Wien Bibliothek verfügbar.
The approved original version of this thesis is available in print at TU Wien Bibliothek.
TU Bibliothek Your knowledge hub WIEN

Some problems have arisen during **microdamage assessment** using the CLSM at the TU Wien. Firstly, specimens were embedded into thick layers of epoxy, which contained high amount of air. Thus, transient light got scattered, making detailed assessments of stained microstructures like canaliculae and z-stacks for 3-dimensional assessments impossible. In future projects, this problem could be avoided when using vacuum during the curing process, which should lead to less air being trapped inside the epoxy. Furthermore, a more suitable barrier filter could possible lead to better images.

Microdamage assessment using **barium sulfate** staining in combination with **micro-CT** did not show the expected result. Images obtained could not be used to detect stained microdamage but rather an overall higher contrast of the whole sample. This could have various reasons. Firstly, it is suspected that barium sulfate crystals were too big to infiltrate microcracks. However, no individual crystals could be found in micro-CT scans. Furthermore, as already described in section 4.5.2, staining solutions started to precipitate after time, which leads to the assumption that even after various alterations of the staining protocol, for example heating up the solvent during the preparation, certain components still precipitated inside the staining solutions, which was not visible with bare eyes. Some microdamage was visible even before staining but did not change differently in gray value after staining compared to other areas of the bone. Thus, the assessment of microdamage was not possible with this method and no solution could be found due to time restrictions at David Burr's laboratory.

6.3 Results

Obtained data for **material properties** have shown that anti-resorptive treatments increase maximum stress and stiffness of individual trabeculae. Alendronate led to a 2-fold statistically significant ($p = 0.001$) increase of maximum

Die approbierte gedruckte Originalversion dieser Diplomarbeit ist an der TU Wien Bibliothek verfügbar.
The approved original version of this thesis is available in print at TU Wien Bibliothek.
TU Bibliothek Your knowledge hub WIEN

load whereas raloxifene showed no statistical significant change of maximum load ($p = 0.174$) compared to the untreated control group. Young's moduli tend to be higher for treated groups as well, showing that alendronate increased the modulus by a factor of 1.8 with statistical significance ($p = 0.006$) compared to the control group and an almost 1.6-fold increase compared to raloxifene ($p = 0.039$). There was no significant difference between the Young's moduli of raloxifene and the control group. In contrast to expectations, where Young's moduli should stay constant for loading-cycles and decline for unloading-cycles, alendronate-treated samples showed a small increase in modulus for most loading cycles and surprisingly also for the second unloading cycle, which is assumed to be caused by scattered measurements due to the small sample size, thus resulting in fitting problems of the algorithm. No further trends were observed in terms of the modulus change. This is probably due to the big scatter of results caused by strong variability of this biological tissue. Another significant difference was shown for ultimate stresses, which in this research, provides information about when obvious whitening, damage, or even failure occurred and thus test execution was stopped, and therefore should not be confused with maximum stress. The main reason for this differentiation is, that most samples did not completely rip apart spontaneously, but rather one packet failed after another until total failure occurred, which is shown in figure 6.1.

Die approbierte gedruckte Originalversion dieser Diplomarbeit ist an der TU Wien Bibliothek verfügbar.
The approved original version of this thesis is available in print at TU Wien Bibliothek.
TU Bibliothek Your knowledge hub WIEN

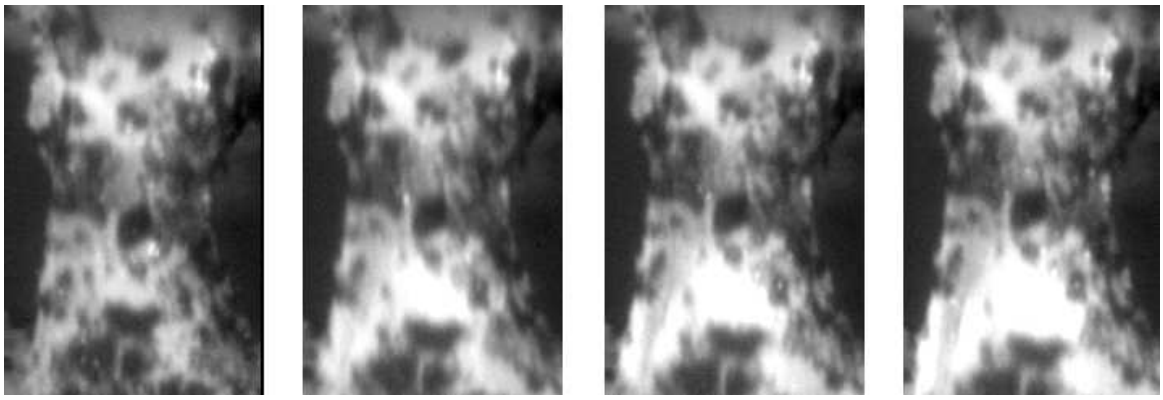

Figure 6.1: Failure onset by continuous rupture of a single trabeculae packet, beginning from the bottom center of the left image.

Thus, no total drop in stress was measured but rather small drops with new peaks and drops followed due to other packets rupturing. Therefore, ultimate loads often represent stresses in the region after the first stress drop where measurements were stopped. This failure mechanism was observed throughout all groups. An example of such a load-frame and stress-strain curve is shown in figures 6.2 and 6.3 respectively.

Die approbierte gedruckte Originalversion dieser Diplomarbeit ist an der TU Wien Bibliothek verfügbar.
The approved original version of this thesis is available in print at TU Wien Bibliothek.
TU Bibliothek Your knowledge hub WIEN

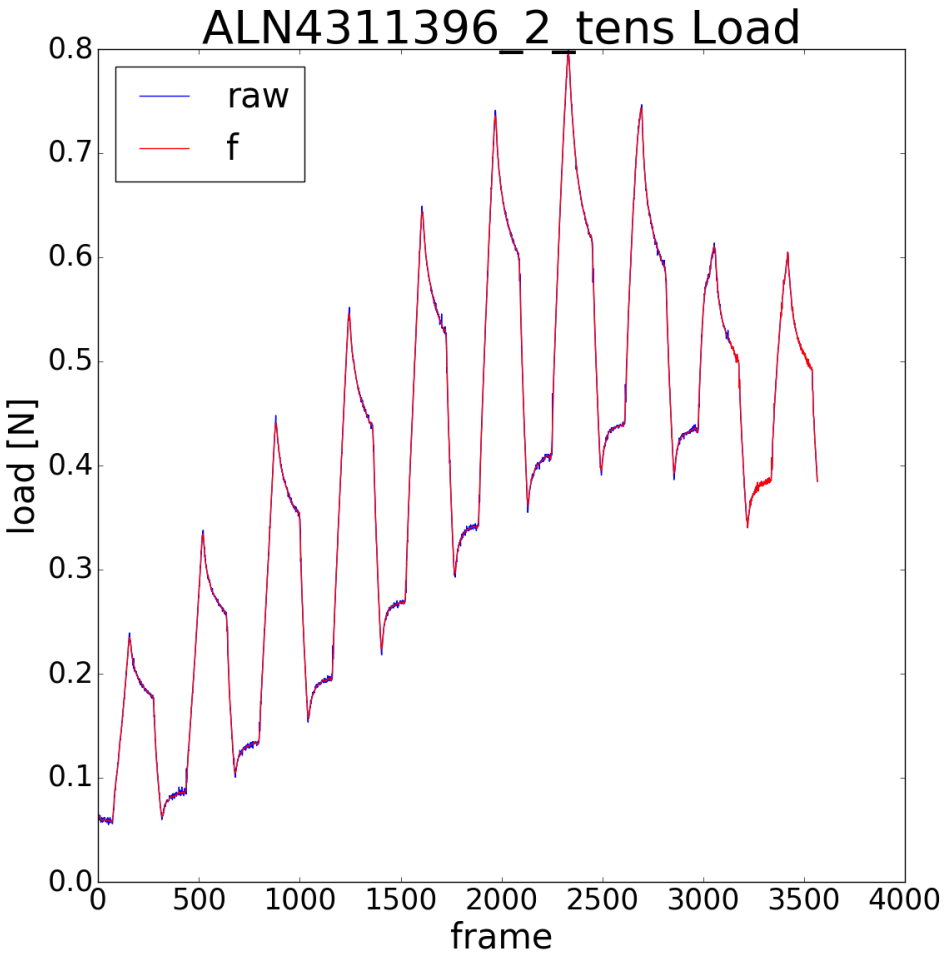

Figure 6.2: Load-frame curve example for small continuous load drops after the maximum load due to rupture of further packets. The blue curve represents the raw data and the red curve the Savitzky-Golay filter smoothed data.

Die approbierte gedruckte Originalversion dieser Diplomarbeit ist an der TU Wien Bibliothek verfügbar.
The approved original version of this thesis is available in print at TU Wien Bibliothek.

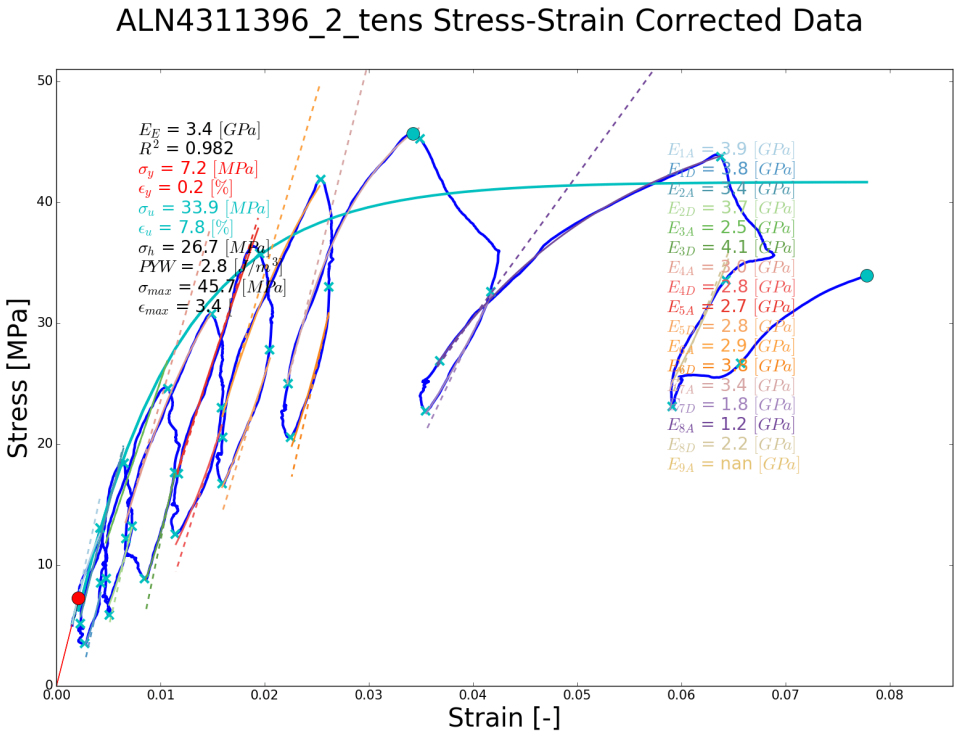

Figure 6.3: Stress-strain curve example for small continuous load drops after the maximum load due to rupture of further packets.

Alendronate showed a 2-fold statistically significant (p = 0.001) increase, whereas raloxifene increased the ultimate stress by a factor of almost 1.6, without statistical significance but showing a trend (p = 0.056). The average ultimate strain of canine trabeculae under tension used in this research project were 7.6% for alendronate, 11% for raloxifene and 9.7% for the control group. In contrast, a previous studies by Hernandez et al. [30], where human trabeculae were tested under tension, an average ultimate strain of 8.8% was shown, and a recent study by M. Frank et al. [25], testing bovine trabeculae under tension, has shown an average ultimate strain of 11% for wet samples. These differences may be due to various reasons, for example that bones were harvested from

Die approbierte gedruckte Originalversion dieser Diplomarbeit ist an der TU Wien Bibliothek verfügbar.
The approved original version of this thesis is available in print at TU Wien Bibliothek.
TU Bibliothek Your knowledge hub WIEN

different species and different anatomical regions, or due to different levels in hydration of the samples. No statistical difference was found for elastic work W_e but for post yield work (PYW): An almost 2.2-fold statistically significant difference was obtained by alendornate ($p = 0.043$) ompared to the control group, whereas no difference was detected for raloxifene. Results, especially from the raloxifene-group, have to be put into the right perspective, since osteoporotic patients usually show an absence of estrogen but only intact non-ovariectomized young beagle dogs were used for this study. Thus, results essentially show, how anti-resorptive treatments would influence the material properties of trabeculae of young healthy patients. The effect on osteoporotic bone models remains to be shown. No statistically significant difference was found for damage area and damage density between the groups. Although samples differed in size and shape, there was no statistically significant correlation between geometrical sample size and any of the material properties.

Neither alendronate nor raloxifene showed a statistically significant increase in **material bone mineral density (BMD)**. However, alendronate showed a trend with a significance of $P = 0.068$ whereas no trend was observed for raloxifene ($P = 1$). This finding resemble earlier findings from M.R. Allen et al. [2] and suggests that raloxifene alters the mechanical properties of bone in a different way than alendronate, that is independent of BMD.

Micro-CT: Figure 6.4 shows an example of a cross-sectional scan of a sample before and after staining with barium sulfate, with and without an applied threshold value respectively, using Bruker's CTAn software. An obvious change in the histogram can be seen before and after staining. Stained samples show an overall change in gray scale values as well as some hard to interpret stronger changes in a spot like manner, randomly distributed inside the samples and around the periphery, which are highlighted green due to the threshold value. Stronger staining around the periphery is probably due to easier infiltration of

Die approbierte gedruckte Originalversion dieser Diplomarbeit ist an der TU Wien Bibliothek verfügbar.
The approved original version of this thesis is available in print at TU Wien Bibliothek.
TU Bibliothek Your knowledge hub WIEN

$BaSO_4$ into the tissue closer to the samples' border.

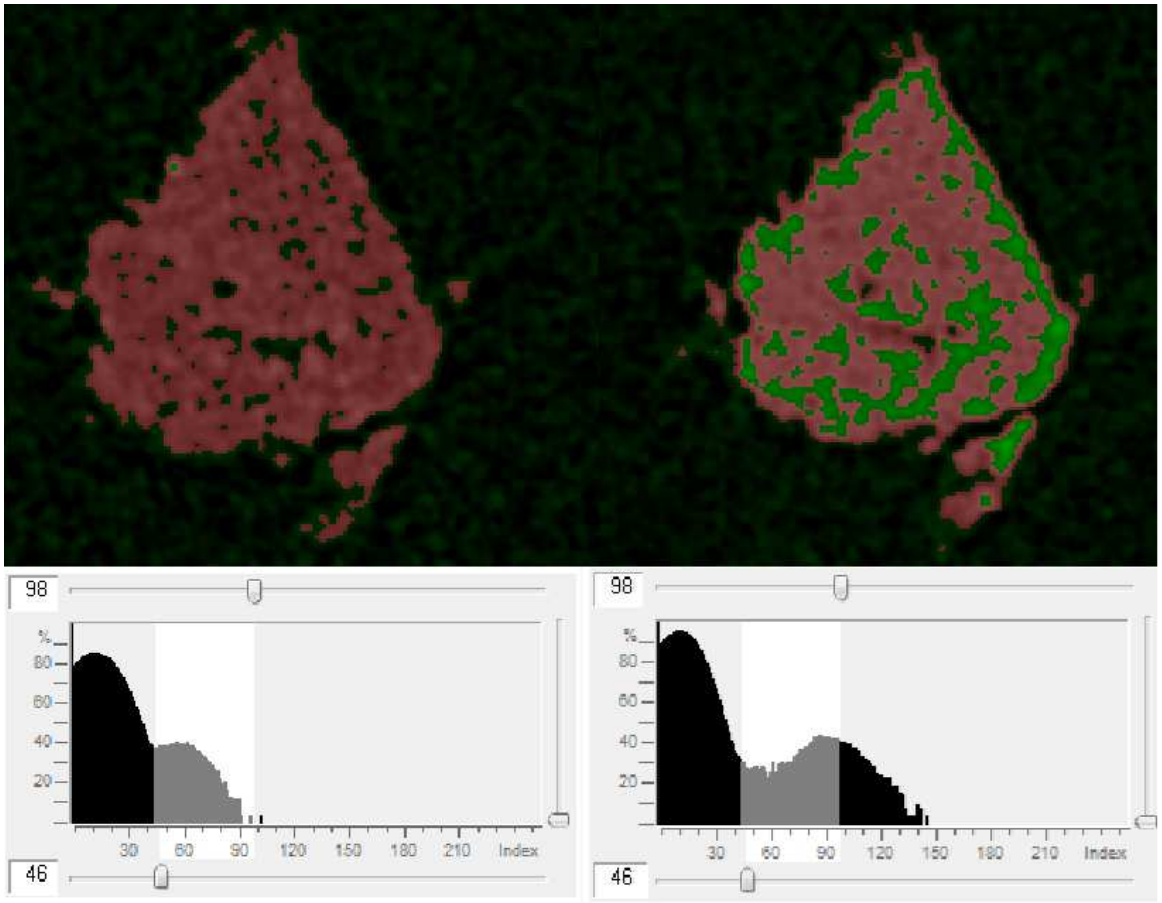

Figure 6.4: Comparison between unstained (left) and stained sample (right). The Threshold value is set to highlight brighter areas inside the bone in green. There is an obvious change in the histogram: Brighter values in the stained scan are caused by the contrast medium $BaSO_4$

However, even cracks, which were obvious before staining, were not labeled using these staining methods. Two examples thereof are shown in figures 6.5 and 6.6 depicting samples stained with the protocols according to Wang et al. and Landrigan's respectively for 48 hours and scanned with a resolution of 1.5 μm. Some obvious cracks at the unstained samples did not even show up at all at the stained samples. Thus, obtained micro-CT scans were not

Die approbierte gedruckte Originalversion dieser Diplomarbeit ist an der TU Wien Bibliothek verfügbar.
The approved original version of this thesis is available in print at TU Wien Bibliothek.
TU Bibliothek Your knowledge hub WIEN

considered trustworthy enough to be taken under consideration for microdamage assessment. The rat femur from figure 6.6 was scanned solely to test the staining protocols.

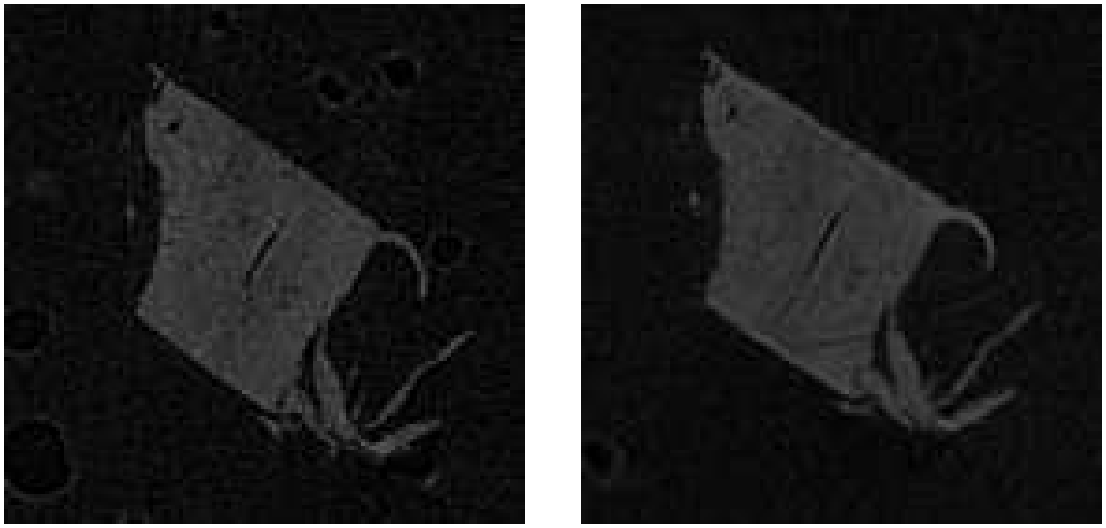

Figure 6.5: micro-CT scan of a dog trabecular cross-section before staining (left) and after staining for 48 hours (right) with a resolution of 1.5 μm. The obvious crack does not show any change in gray value, which would be expected due to staining.

Die approbierte gedruckte Originalversion dieser Diplomarbeit ist an der TU Wien Bibliothek verfügbar.
The approved original version of this thesis is available in print at TU Wien Bibliothek.
TU Bibliothek Your knowledge hub WIEN

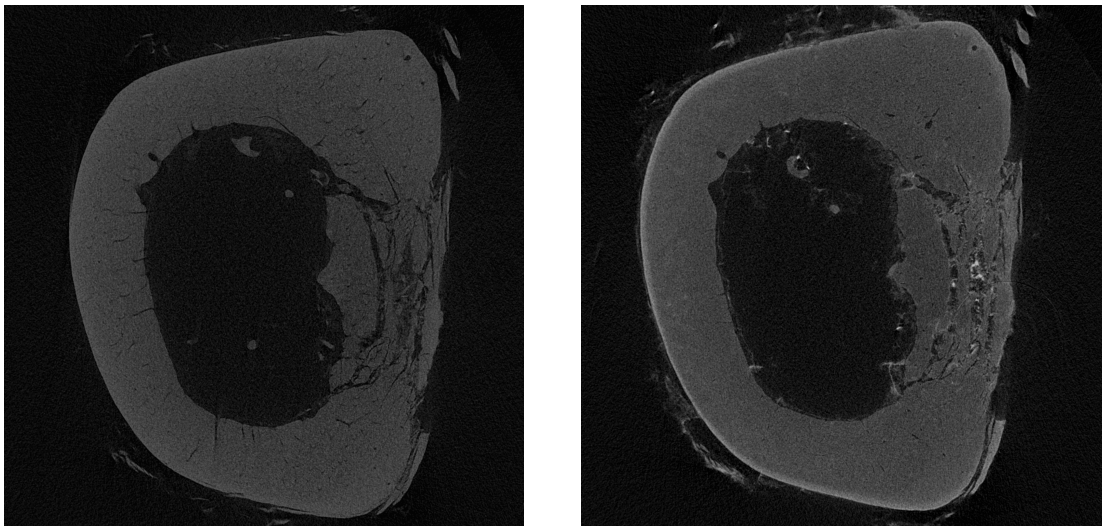

Figure 6.6: micro-CT scan of a cross-section of a rat femur before staining (left) and after 48 hours staining (right) with a resolution of 1.5 μm. This rat femur was previously tested for 2 million load cycles in 3-point bending without breaking. The shown cross-section was taken at the mid shaft of the femur since greatest damage was assumed at this region.

Die approbierte gedruckte Originalversion dieser Diplomarbeit ist an der TU Wien Bibliothek verfügbar.
The approved original version of this thesis is available in print at TU Wien Bibliothek.

7 Conclusion and Outlook

This study has shown that alendronate and raloxifene change material properties of individual trabeculae without significantly affecting microdamage accumulation at the level of individual trabeculae. Raloxifene improved the material properties and thus indicates a reduction of risk pf fracture without significantly effecting material bone mineral density (BMD). This is contrasted by alendronate, which showed a trend to increase BMD, causing significant stiffening of individual trabeculae. These results emphasize that raloxifene causes changes in the material and mechanical properties by a different mechanism that is relatively independent of BMD, and thus warrant further investigations. Thus, this study strengthens the assumption that BMD is just one of several factors that accounts only for a small degree of bone strength. Nevertheless, aBMD (which takes a whole cross section of bone, including the marrow cavity and haversian canals and BMD into account) is often used as a surrogate for bone strength that makes it stand in focus for diagnosis and treatment of osteoporosis, which is not an ideal approach.

The novel test-setup used for this research project to conduct tensile tests of individual trabeculae inside a physical environment led to new insights into the bone's mechanical properties on the material level and how anti-resorptive treatments affect them. However, since these tests are extremely sensitive, more precise and less erroneous load frames should be used in future studies. Furthermore, adopted testing profiles with slower displacement and better camera systems could make it easier to detect whitening prior to failure. Additionally, due to extreme fragility of the samples, the time-consuming harvesting and preparation of each sample, an automated approach could lead to better and faster results in the future.

Non-ovariectomized beagle dogs were used as specimens for this study, which

Die approbierte gedruckte Originalversion dieser Diplomarbeit ist an der TU Wien Bibliothek verfügbar.
The approved original version of this thesis is available in print at TU Wien Bibliothek.
TU Bibliothek Your knowledge hub WIEN

does not reflect the common circumstances shown in osteoporotic patients who usually show an absence of estrogen. This warrants further investigation of individual trabeculae from osteoporotic human bone, which are treated with anti-resorptive agents, which could lead to fundamentally different results, especially for raloxifene treated samples due to its possible estrogen dependency.

Die approbierte gedruckte Originalversion dieser Diplomarbeit ist an der TU Wien Bibliothek verfügbar.
The approved original version of this thesis is available in print at TU Wien Bibliothek.
TU Bibliothek Your knowledge hub WIEN

8 Appendix

8.1 3D Registration for Barium Staining Protocol:

- Open ‘DataViewer’
- Choose ‘Actions’ in the menu bar
- Click ‘3D Registration’
- ‘Input’ side box will appear.
- Double click ‘Reference’ and choose a pre-stained file
- Double click ‘Target’ and choose a post-stained file
- Double click ‘Fusion’ until it is set to ‘Inverted colors to show difference’
- Click ‘Options’
- Shift step (pixel) = 5.0
- Rotation step (degree) = 2.0
- Scaling step (%) = 1
- Max loading dimension = 2000
- Scaling range = 1
- Click ‘Load’
- Use the arrows in the Coronal, Transaxial, and sagittal views to adjust the Target image over the Reference image
- Once the bones are nearly-nearly aligned over each other, click on the ‘R’ in the top right corners within the transaxial, coronal, sagittal boxes.

Die approbierte gedruckte Originalversion dieser Diplomarbeit ist an der TU Wien Bibliothek verfügbar.
The approved original version of this thesis is available in print at TU Wien Bibliothek.
TU Bibliothek Your knowledge hub WIEN

- If the overlay alignment is closer, click ‘Register all’
- If the overlay alignment is not closer, continue to use the arrows to find where the alignment is off
- Click ‘Register all’ again
- Click ‘Save’
- Save “Target image”, “Reference image”, and “Difference image” in different folders
- Options:
- Save at resolution: As loaded (no resizing)
- Select region (1): No VOI (full volume)
- Data dynamic range (2): Original
- Create an ‘Output folder’. Set the ‘Output file format’ to bmp. Click target image, reference image, and difference image
- Click ‘Ok’

8.2 CTAn Threshold Protocol

- Load image of interest *either pre or post barium staining*
- Click on ‘Binary images’
  - Click ‘From dataset’
  - Click ‘Histogram’. Value should be around 70-80
- Click on ‘Custom processing’
  - Task list

Die approbierte gedruckte Originalversion dieser Diplomarbeit ist an der TU Wien Bibliothek verfügbar.
The approved original version of this thesis is available in print at TU Wien Bibliothek.
TU Bibliothek Your knowledge hub WIEN

    - ‘Filtering’ to Median, 3D space, 1 radius
    - ‘Save bitmaps’ to Image, BMP, Copy dataset log file
- Run process
- Open filtered images
- Click ‘Binary Images’
- Click ‘From dataset’
- Click ‘Histogram’. Value should be around 70-80
- Click on ‘Processed images’
- Analysis
- Click on ‘3D results’ ii. Click on ‘Basic values’ and ‘Auto save results as’
- Press ‘ok’
- Rename and save file *collect data for TV, obj. V., and obj. V/TV*
- Click ‘Binary Images’ a. Click ‘From dataset’ b. Click ‘Histogram’. Value should be around 70-80 however, change the threshold to 200
- Click on ‘Processed images’ a. Analysis i. Click on ‘3D results’ ii. Click on ‘Basic values’ and ‘Auto save results as’
- Press ‘ok’
- Rename and save file *collect data for TV, obj. V., and obj. V/TV*

8.3 Skyscan micrsoCT Settings

[System]

- Scanner = Skyscan1172

Die approbierte gedruckte Originalversion dieser Diplomarbeit ist an der TU Wien Bibliothek verfügbar.
The approved original version of this thesis is available in print at TU Wien Bibliothek.

- Instrument S/N = 065
- Hardware version = A
- Software=Version 1.5 (build 6)
- Source Type=Hamamatsu 100/250
- Camera=Hamamatsu 10Mp camera
- Camera Pixel Size (um) = 11.59
- CameraXYRatio = 1.0000
- Incl.in lifting (um/mm) = 4.3890

[Acquisition]

- Number of Files = 626
- Source Voltage (kV)= 59
- Source Current (uA)= 167
- Number of Rows = 2096
- Number of Columns = 4000
- Image Pixel Size (um) = 1.47
- Object to Source (mm) = 44.010
- Camera to Source (mm) = 346.896
- Vertical Object Position (mm) = 46.850
- Optical Axis (line) = 1042
- Filter = Al 0.5 mm
- Image Format = TIFF
- Depth (bits)=16

Die approbierte gedruckte Originalversion dieser Diplomarbeit ist an der TU Wien Bibliothek verfügbar.
The approved original version of this thesis is available in print at TU Wien Bibliothek.
TU Bibliothek Your knowledge hub WIEN

- Screen LUT = 0
- Exposure (ms) = 8246
- Rotation Step (deg) = 0.300
- Frame Averaging = ON (2)
- Random Movement = OFF (10)
- Use 360 Rotation = NO
- Geometrical Correction = ON
- Camera Offset = OFF
- Median Filtering = ON
- Flat Field Correction = ON
- Rotation Direction = CC
- Scanning Trajectory = ROUND
- Type Of Motion=STEP AND SHOOT
- Scan duration=02:51:56

8.4 NRecon Reconstruction Settings

[Reconstruction]

- Reconstruction Program = NRecon
- Program Version=Version: 1.7.4.2
- Reconstruction engine = GPUReconServer
- Engine version=Version: 1.7.4

Die approbierte gedruckte Originalversion dieser Diplomarbeit ist an der TU Wien Bibliothek verfügbar.
The approved original version of this thesis is available in print at TU Wien Bibliothek.
TU Bibliothek Your knowledge hub WIEN

- Reconstruction from batch = No
- Postalignment Applied = 1
- Postalignment = -6.00
- Reconstruction servers = IN-ANAT-DK7XTV1
- Dataset Origin = Skyscan1172
- First Section = 69
- Last Section = 2025
- Reconstruction duration per slice (seconds) = 1.499745
- Total reconstruction time (1957 slices) in seconds = 2935.000000
- Section to Section Step = 1
- Sections Count = 1957
- Result File Type = BMP
- Result File Header Length (bytes) = 1134
- Result Image Width (pixels) = 4000
- Result Image Height (pixels) = 4000
- Pixel Size (um) = 1.47016
- Reconstruction Angular Range (deg) = 187.80
- Use 180+ = OFF
- Angular Step (deg) = 0.3000
- Smoothing = 0
- Ring Artifact Correction = 12
- Draw Scales = OFF

Die approbierte gedruckte Originalversion dieser Diplomarbeit ist an der TU Wien Bibliothek verfügbar.
The approved original version of this thesis is available in print at TU Wien Bibliothek.
TU Bibliothek Your knowledge hub WIEN

- Object Bigger than FOV = ON
- Reconstruction from ROI = OFF
- Filter cutoff relative to Nyquist frequency = 100
- Filter type = 0
- Filter type description=Hamming (Alpha = 0.54)
- Undersampling factor = 1
- Threshold for defect pixel mask (%) = 0
- Beam Hardening Correction (%) = 0
- CS Static Rotation (deg) = 0.00
- CS Static Rotation Total(deg) = 0.00
- Minimum for CS to Image Conversion = 0.000000
- Maximum for CS to Image Conversion = 0.330000
- HU Calibration = OFF
- BMP LUT = 0
- Cone-beam Angle Horiz.(deg) = 7.644545
- Cone-beam Angle Vert.(deg) = 4.010056

Die approbierte gedruckte Originalversion dieser Diplomarbeit ist an der TU Wien Bibliothek verfügbar.
The approved original version of this thesis is available in print at TU Wien Bibliothek.
TU Bibliothek Your knowledge hub WIEN

References

[1] Matthew R. Allen, Ken Iwata, Roger Phipps, and David B. Burr. Alterations in canine vertebral bone turnover, microdamage accumulation, and biomechanical properties following 1-year treatment with clinical treatment doses of risedronate or alendronate. *Bone*, 39(4):872 – 879, 2006.

[2] Matthew R. Allen, Ken Iwata, Masahiko Sato, and David B. Burr. Raloxifene enhances vertebral mechanical properties independent of bone density. *Bone*, 39(5):1130 – 1135, 2006.

[3] Matthew R. Allen, Ken Iwata, Masahiko Sato, and David B. Burr. Raloxifene enhances vertebral mechanical properties independent of bone density. *Bone*, 39(5):1130 – 1135, 2006.

[4] Yuehuei An and Robert A Draughn. *Mechanical Testing of Bone and the Bone–Implant Interface*. Elsevier, 01 2000.

[5] M. F. Ashby and D. R. H. Jones. *Engineering Materials 1: An Introduction to their Properties and Applications, 3rd edition*. Elsevier, 2005.

[6] Stacyann Bailey, Atharva Poundarik, and Deepak Vashishth. Do noncollagenous proteins affect skeletal mechanical properties? *Calcified tissue international*, 97, 06 2015.

[7] Joel D Boerckel, Devon E Mason, and Anna M McDermott. Microcomputed tomography: approaches and applications in bioengineering. *Stem Cell Research and Therapy*, 5(144), 2014.

[8] David B. Burr and Matthew R. Allen (Eds.). *Basic and Applied Bone Biology*. Elsevier, 2014.

[9] D.B. Burr and M. Hooser. Alterations to the en bloc basic fuchsin staining protocol for the demonstration of microdamage produced in vivo. *Bone*,

Die approbierte gedruckte Originalversion dieser Diplomarbeit ist an der TU Wien Bibliothek verfügbar.
The approved original version of this thesis is available in print at TU Wien Bibliothek.
TU Bibliothek Your knowledge hub WIEN

17(4):431 – 433, 1995.

[10] T C Lee, Sahar Mohsin, Daisey Taylor, Raman Parkesh, Thorfinnur Gunnlaugsson, Fergal O'Brien, M Giehl, and W Gowin. Detecting microdamage in bone. *Journal of anatomy*, 203:161–72, 09 2003.

[11] A.J. Campbell, M.C. Robertson, and M.M. Gardener. Falls prevention over 2 years: a randomised control trial in women 80 years and older. *British Geriatrics Society, Age Aging*, 28:513–518, 1999.

[12] BC Campus. *Bone Tissue and the Skeletal System*. Chapter 6. Anatomy and Physiology. OpenStax CNX, 2016.

[13] B. Clarke. Normal bone anatomy and physiology. *Clinical Journal of the American Society of Nephrology*, 3:131–139, 11 2008.

[14] C. Cooper, Z. A. Cole, C. R. Holroyd, S. C. Earl, N. C. Harvey, E. M. Dennison, L. J. Melton, S. R. Cummings, J. A. Kanis, and The IOF CSA Working Group on Fracture Epidemiology. Secular trends in the incidence of hip and other osteoporotic fractures. *Osteoporosis International*, 22(5):1277, Apr 2011.

[15] Christian Crowder and Sam Stout. *Bone Histology: An Anthropological Perspective*. CRC Press Taylor and Francis Group, 2012.

[16] Steven R Cummings and L Joseph Melton. Epidemiology and outcomes of osteoporotic fractures. *The Lancet*, 359(9319):1761 – 1767, 2002.

[17] Matthew D Landrigan, John C Flatley, Travis Turnbull, Jamie Kruzic, Jack Ferracane, Thomas Hilton, and Ryan Roeder. Detection of dentinal cracks using contrast-enhanced micro-computed tomography. *Journal of the Mechanical Behavior of Biomedical Materials*, 3:223–7, 02 2010.

[18] D. Allen et al. Trackpy v.0.3.2. https://soft-matter.github.io/trackpy/v0.3.2/, 2016.

Die approbierte gedruckte Originalversion dieser Diplomarbeit ist an der TU Wien Bibliothek verfügbar.
The approved original version of this thesis is available in print at TU Wien Bibliothek.
TU Bibliothek Your knowledge hub WIEN

Accessed: 2019-06-01.

[19] Stanislas Von Euw, Tsou-Hsi-Camille Chan-Chang 1and Caroline Paquis, Bernard Haye, Gérard Pehau-Arnaudet, Florence Babonneau, Thierry Azaïs 1, and Nadine Nassif. Organization of bone mineral: The role of mineral–water interactions. *geosciences*, 32(2), 2013.

[20] Georg Fantner, Tue Hassenkam, Johannes Kindt, James Weaver, Henrik Birkedal, Leonid Pechenik, Jacqueline Cutroni, Geraldo Cidade, Galen Stucky, Daniel Morse, and Paul Hansma. Sacrificial bonds and hidden length dissipate energy as mineralized fibrils separate during bone fracture. *Nature materials*, 4:612–6, 09 2005.

[21] N. L. Fazzalari, M. R. Forwood, K. Smith B. A. Manthey, and P. Herreen. *Assessment of Cancellous Bone Quality in Severe Osteoarthrosis: Bone Mineral Density, Mechanics, and Microdamage*, volume 22. Elsevier, 4 1998.

[22] Julia-Theresa Fischer. Quantification of microdamage formation during fatigue testing of individual trabeculae. *Technische Universität Wien, Diplomarbeit*, 2018.

[23] H. Fleisch. *Bisphosphonates in Bone Disease: From the Laboratory to the Patient*. Parthenon, 1997.

[24] M. Frank, D. Marx, D. H. Pahr, and P. J. Thurner. Mechanical properties of individual trabeculae in a physiological environment. In *2017 13th IASTED International Conference on Biomedical Engineering (BioMed)*, pages 141–146, Feb 2017.

[25] Martin Frank, Dorothee Marx, Vedran Nedelkovski, Julia-Theresa Fischer, Dieter H. Pahr, and Philipp J. Thurner. Dehydration of individual bovine trabeculae causes transition from ductile to quasi-brittle failure mode.

Die approbierte gedruckte Originalversion dieser Diplomarbeit ist an der TU Wien Bibliothek verfügbar.
The approved original version of this thesis is available in print at TU Wien Bibliothek.
TU Bibliothek Your knowledge hub WIEN

Journal of the Mechanical Behavior of Biomedical Materials, 87:296 – 305, 2018.

[26] Martin Frank, Dorothee Marx, Dieter Pahr, and Philipp Thurner. Mechanical properties of individual trabeculae in a physiological environment. *13th IASTED International Conference on Biomedical Engineering (BioMed)*, 01 2017.

[27] Martin Frank, Dorothee Marx, Dieter H. Pahr, and Philipp J. Thurner. Tissue mechanical properties of bovine trabeculae in tension are different in a dry or wet environment. *Congress of the European Society of Biomechanics*, 23rd, July 2017.

[28] Bo Gullberg, O Johnell, and J.A. Kanis. World-wide projections for hip fracture. *Osteoporosis international : a journal established as result of cooperation between the European Foundation for Osteoporosis and the National Osteoporosis Foundation of the USA*, 7:407–13, 02 1997.

[29] M Hammond, J Wallace, M Allen, and T. Siegmund. Finite element models of linear microcracks in trabecular bone with simulated bisphosphonate and raloxifene treatment. *Journal of bone and mineral research*, 32, Dec 2017.

[30] Christopher J. Hernandez, Simon Y. Tang, Bethany M. Baumbach, Paul B. Hwu, A. Nico Sakkee, Frits van der Ham, Jeroen DeGroot, Ruud A. Bank, and Tony M. Keaveny. Trabecular microfracture and the influence of pyridinium and non-enzymatic glycation-mediated collagen cross-links. *Bone*, 37(6):825 – 832, 2005.

[31] IOF. International osteoporosis foundation. https://www.iofbonehealth.org, 2017.
Accessed: 2019-06-07.

Die approbierte gedruckte Originalversion dieser Diplomarbeit ist an der TU Wien Bibliothek verfügbar.
The approved original version of this thesis is available in print at TU Wien Bibliothek.
TU Bibliothek Your knowledge hub WIEN

[32] Olof Johnell. The socioeconomic burden of fractures: today and in the 21st century. *The American journal of medicine*, 103 2A:20S–25S; discussion 25S–26S, 1997.

[33] C.W. Jones, D. Smolinski, A. Keogh, T.B. Kirk, and M.H. Zheng. Confocal laser scanning microscopy in orthopaedic research. *Progress in Histochemistry and Cytochemistry*, 40(1):1 – 71, 2005.

[34] Rice Biomaterials Lab. An overview of nrecon: reconstructing the best images from your microct scan. https://bml.rice.edu/sites/g/files/bxs936/f/MN062_NRecon%20overview.pdf, 2014.
Accessed: 2019-06-021.

[35] Qing Luo, Huijie Leng, Xiaodu Wang, Yanheng Zhou, and Qiguo Rong. The role of water and mineral–collagen interfacial bonding on microdamage progression in bone. *Journal of Orthopaedic Research*, 32(2), 2013.

[36] John Maloney. Notes on true strain e vs. engineering strain ϵ. http://john.maloney.org/Papers/On%20strain%20(9-20-06).pdf, Sept. 20, 2006. Accessed: 2019-05-27.

[37] R. Bruce Martin, David B. Burr, and Neil A. Sharkey. *Skeletal Tissue Mechanics*. Springer-Verlag New York, 1 edition, 1998.

[38] Schaffler MB, Choi K, and Milgrom C. Aging and matrix microdamage accumulation in human compact bone. *Bone*, 17:521–525, 1995.

[39] Leica Microsystems. Supplemantary Instruction Manual Leica SP2600. https://drp8p5tqcb2p5.cloudfront.net/fileadmin/downloads_lbs/Leica%20SP2600%20Ultramiller/User%20Manuals/Leica_SP2600_Manual_EN.pdf.
Accessed: 2019-06-02.

[40] Stephen W. Paddock. Confocal laser scanning microscopy. *BioTechniques*,

Die approbierte gedruckte Originalversion dieser Diplomarbeit ist an der TU Wien Bibliothek verfügbar.
The approved original version of this thesis is available in print at TU Wien Bibliothek.
TU Bibliothek Your knowledge hub WIEN

27(5):992–1004, 1999. PMID: 10572648.

[41] Christina Papageorgopoulou, G Kuhn, Urs Ziegler, and Frank Ruhli. Diagnostic morphometric applicability of confocal laser scanning microscopy in osteoarchaeology. *International Journal of Osteoarchaeology*, 20:708 – 718, 11 2010.

[42] Atharva Poundarik and Deepak Vashishth. Multiscale imaging of bone microdamage. *Connective tissue research*, 56:1–12, 02 2015.

[43] Gerardo Presbitero, FergalJ.O'Brien, T.CliveLee, and David Taylor. Distribution of microcrack lengths in bone in vivo and in vitro. *Journal of Theoretical Biology*, 304:164–171, 3 2012.

[44] Bartl R., Bartl C., Frisch B., and von Tresckow E. *Bisphosphonates in Medical Practice: Actions – Side Effects – Indications – Strategies*. Springer, 2014.

[45] Jae Young Rho, Richard B. Ashman, and Charles H. Turner. Young's modulus of trabecular and cortical bone material: Ultrasonic and microtensile measurements. *Journal of Biomechanics*, 26(2):111 – 119, 1993.

[46] Stephen D. Ryan and John L. Williams. Tensile testing of rodlike trabeculae excised from bovine femoral bone. *Journal of Biomechanics*, 22(4):351 – 355, 1989.

[47] Thierry Savin and Patrick S. Doyle. Static and dynamic errors in particle tracking microrheology. *Biophysical Journal*, 88(1):623 – 638, 2005.

[48] Zeynep Seref-Ferlengez, Oran D Kennedy, and Mitchell B Schaffler. Bone microdamage, remodeling and bone fragility: how much damage is too much damage? *BoneKEy Reports*, 4(644):513–518, 2015.

[49] Thomas Siegmund, Matthew R. Allen, and David B. Burr. Can deterministic mechanical size effects contribute to fracture and microdamage

Die approbierte gedruckte Originalversion dieser Diplomarbeit ist an der TU Wien Bibliothek verfügbar.
The approved original version of this thesis is available in print at TU Wien Bibliothek.
TU Bibliothek Your knowledge hub WIEN

accumulation in trabecular bone? *Journal of Theoretical Biology*, 265(2), 7 2010.

[50] A. Synek, Y. Chevalier, S.F. Baumbach, and D.H. Pahr. The influence of bone density and anisotropy in finite element models of distal radius fracture osteosynthesis: Evaluations and comparison to experiments. *Journal of Biomechanics*, 48(15):4116 – 4123, 2015.

[51] David Taylor, Jan G Hazenberg, and T. Clive Lee. Living with cacks: damage and repair in human bone. *Nature Materials*, 6(4):263–268, 2007.

[52] P. Thevenaz, U. E. Ruttimann, and M. Unser. A pyramid approach to subpixel registration based on intensity. *IEEE Transactions on Image Processing*, 7(1):27–41, Jan 1998.

[53] Philipp J. Thurner. Atomic force microscopy and indentation force measurement of bone. *Wiley Interdisciplinary Reviews: Nanomedicine and Nanobiotechnology*, 1(6):624–649, 2009.

[54] P.J. Thurner, B. Erickson, R. Jungmann, Z. Schriock, J.C. Weaver, G.E. Fantner, G. Schitter, D.E. Morse, and P.K. Hansma. High-speed photography of compressed human trabecular bone correlates whitening to microscopic damage. *Engineering Fracture Mechanics*, 74(12):1928 – 1941, 2007. First International Conference on the Mechanics of Biomaterials and Tissues.

[55] Xiang Wang, Daniel B Masse, Huijie Leng, Kevin P Hess, Ryan Ross, Ryan Roeder, and Glen Niebur. Detection of trabecular bone microdamage by micro-computed tomography. *Journal of biomechanics*, 40:3397–403, 02 2007.

[56] Harvard Women's Health Watch. Treating osteoporotic fractures of the spine. https://www.health.harvard.edu/newsletter_article/

Die approbierte gedruckte Originalversion dieser Diplomarbeit ist an der TU Wien Bibliothek verfügbar.
The approved original version of this thesis is available in print at TU Wien Bibliothek.
TU Bibliothek Your knowledge hub WIEN

Treating_osteoporotic_fractures_of_the_spine, 2008. Accessed: 2019-06-10.

[57] Cyrus Wong and Matthew J McGirt. Vertebral compression fractures: A review of current management and multimodal therapy. *Journal of multidisciplinary healthcare*, 6:205–14, 06 2013.

[58] Q.D. Yang, Brian N. Cox, Ravi K. Nalla, and R.O. Ritchie. Fracture length scales in human cortical bone: The necessity of nonlinear fracture models. *Biomaterials*, 27(9):2095 – 2113, 2006.

Die approbierte gedruckte Originalversion dieser Diplomarbeit ist an der TU Wien Bibliothek verfügbar.
The approved original version of this thesis is available in print at TU Wien Bibliothek.